Benefits and barriers of organic Rankine cycles for waste heat recovery and deep geothermal

Alison Auld

Thesis submitted towards the
degree of Doctor of Philosophy

School of Engineering and Computing Sciences
Durham University
United Kingdom

July 28, 2016

Benefits and barriers of organic Rankine cycles for waste heat recovery and deep geothermal

Alison Auld

Abstract

This thesis describes a study to evaluate the energy recovery potential and challenges associated with the application of Organic Rankine Cycle (ORC)s. Application of ORCs for both waste heat streams and deep geothermal sources are considered.

A model which calculates the thermodynamic performance of ORCs for any source heat or sink stream and cycle configuration was developed. Simulations for three waste heat case studies showed a potential thermodynamic benefit from using zeotropic working fluids.

An experimental rig was built to explore the reported discrepancy in performance between theory and experimental observations for zeotropic mixtures. Experiments were carried out with a near azeotropic working fluid, R410a, and a zeotropic mixture R407c. Results show that the global heat transfer coefficient of the zeotropic mixture was lower than for the azeotrope.

The availability of theoretical models to accurately calculate heat transfer for zeotropic mixtures was explored. Appropriate models are available in the literature. However, to incorporate these into the ORC model is a significant bit of work beyond this project.

The thermodynamic performance, footprint and cost of an ORC plant are key parameters that will determine the feasibility or otherwise of an ORC plant. These factors are considered together and the interdependence of them is discussed. Three deep geothermal heat sources are considered, within the context of these three factors. The reasons for the feasibility or otherwise of fuelling an ORC with each of these heat sources is discussed.

Ultimately, while simulations show there is potential improvement in thermodynamic performance, by using zeotropic working fluid, experimental work shows there may be a penalty to pay in terms of the size of the system. The analysis of the deep geothermal case studies shows that finance and social factors also have a huge influence on whether a project to recover low enthalpy heat will evaluate or not.

Declaration

The work in this thesis is based on research carried out in Durham University. No part of this report has been submitted elsewhere for any other degree or qualification and it is all my own work unless referenced to the contrary in the text.

Parts of this work have been published in the following:

Journals

- A. Auld, A. Berson, and S. Hogg, *Organic rankine cycles in waste heat recovery: a comparative study*, International Journal of Low-Carbon Technologies, vol. 8, no. suppl 1, pp. i9-i18, 2013.
- A. Auld, S. Hogg, A. Berson and J. Gluyas, *Power production via North Sea Hot Brines*, Energy, vol. 78, pp. 674 - 684, 2014.
- C. Adams, A. Auld, J. Gluyas and S. Hogg, *Geothermal Energy the Global Opportunity*, Proceedings of the Institution of Mechanical Engineers, Part A: Journal of Power and Energy, vol. 229(7), pp. 747-754, 2015.

Conferences

- J. Gluyas, A. Auld, C. Adams, C. Hirst, S. Hogg and J. Craig, Getting into hot water: An opportunity for the Petroleum Industry, The Fourth London Geothermal Symposium: The Launch of BritGeothermal, London UK, 2014.
- A. Auld, M. Hilfer, S. Hogg, G. Ingram and A. Messenger, Application of an Air-Curtain Fluidic Jet Type Seal to Reduce Turbine Shroud Leakage, ASME Turbo Expo 2013: Turbine Technical Conference and Exposition, San Antonio, Texas, USA, June, 2013.
- A. Auld, S. Hogg and A. Berson, Organic Rankine Cycles in Waste Heat Recovery: A Comparative Study, Heat Powered Cycles Conference, The Netherlands, September 2012.

Acknowledgements

Supervisors, Academic and Technical Support

Firstly, thank you to supervisors Simon and Charlotte for steering me through this PhD and getting me all the way to the end! Your time, efforts and amazing amounts of patience have really been very much appreciated.

Jon Gluyas, thank you for taking the time to introduce me to the world of earth sciences and the interesting engineering challenges that come with it, especially hot brines.

Mart, Ian, Hutch, Gary your technical support to build the ground source heat pump test rig in enough time for me to collect data was invaluable, thank you.

Wayne Richardson, Revolution Power, thank you for sharing your practical understanding of heat pumps and for your amazing heat pump trouble shooting over the phone!

'Team Turbine' and the Energy CDT, thank you for all the bouncing ideas and helpful discussions which contextualised, challenged and furthered my thinking. Particularly, thank you Rich for your reliable support and much needed post-work pints.

Friends and Family

For all the friendship along the way, heartfelt thanks to: Monday Bunday Crew, Ustinov Unicorns and the Après Foot readership, Durham University Canoe Club, Sunday Night Film Club and the Micro-Adventure Crew. Also, housies and partners: Pete, Sophie, Sam, Cat, Katie and Michael. I only wish we'd had more pinata parties.

Beth Davies you deserve a special mention! Since first paddling together nearly 9 years ago as you were finishing your PhD you have been a great mentor and friend. Your wise words and support have been seen me through to the end of this life pillar!

Nina, your enthusiasm for adventures, vegetarian cooking, philosophical discussions and unique interpretation of time have created some of the best moments over the past few years. Here's to having time for more!

Sam, your unique take on life has been the source of so much fun, thank you. And Cat, thank you for all the biking, geothermal and beginners geology chat, and the rides out.

To the family, I got there in the end! Thank you Mum for the unsolicited supplies of cereal bars and onesies and Dad for always e-mailing 'Letter from Dad' every week.

Contents

List of Tables

List of Figures

Nomenclature

Constants

R	Universal Gas Constant $[kJ/kmolK]$

Dimensionless Groups

Le	Lewis Number
Pr	Prandtl Number
Re	Reynolds Number
Sc	Schmit Number

Subscripts

$_C$	Cooling fluid stream
$_g$	Referring to gas phase
$_l$	Referring to liquid phase
$_O$	Organic Working Fluid stream
$_S$	Source heat fluid stream
$_{,C}$	Cold side of heat exchanger
$_{,H}$	Hot side of heat exchanger
$_{crit}$	Referring to the critical point
$_{int}$	Referring to interface between liquid and thin film
$_i$	Inside of tube
$_{liq}$	Liquid
$_{LM}$	Log Mean
$_P$	Pump
$_{sat}$	Referring to a saturated condition
$_{TOT}$	Total

$_T$ Turbine

$_{vap}$ Vapour

I Isentropic

PP Pinch point

Variables

α Local heat transfer coefficient

$\bar{y}$ Molar fraction of vapour phase $[kg/kg]$

β Mass transfer coefficient $[m/s]$

$\dot{m}$ Mass flow [kg/s]

$\dot{n}$ Condensing molar flux $[kmol/m^2s]$

η Efficiency

ρ Density $[kg/m^3]$

ξ Gradient of vapour saturation curve $[J/kgK^2$

A Area $[m^2]$

C_t Molar concentration $[kmol/m^3]$

d Diameter [m]

DT_{min} Minimum pinch point temperature difference

h Specific enthalpy [J/kg]

L Length [m]

M Molar Mass [kg/kmol]

Q Heat energy [kW]

T Temperature $[K]$

U Global Heat Transfer Coefficient [W/m2K]

y Mass fraction of vapour phase $[kg/kg]$

d Discount Rate

FV Future Value [Euros]

H Enthalpy [J]

n Years from present

P	Pressure [Pa]
s	Specific Entropy [J/kgK]
W	Mechanical Power [kW]

Acronyms

ORC	Organic Rankine Cycle
WHR	Waste Heat Recovery
DECC	Department of Energy and Climate Change
IEA	International Energy Authority
ICE	Internal Combustion Engine
DOE	Department of Energy
HD	Heavy Duty
BTE	Brake Thermal Efficiency
HCs	hydrocarbons
HCFCs	hydrochlorofluorocarbons
CFCs	hhloroflurocarbons
PFCs	herfluorocarbons
HFEs	hydrofluroehters
CHP	Combined Heat and Power
ODP	Ozone Depletion Potential
GWP	Global Warming Potential
TFC	Trilateral Flash Cycle
SFEE	Steady Flow Energy Equation
T-H	Temperature-Enthalpy
TIP	Turbine Inlet Pressure
LMTD	Log Mean Temperature Difference

NTU	Number of Tranfer Units
EGS	Enhanced Geothermal Systems
GEA	Geothermal Energy Association
COP	Coefficient of Performance
ASHP	Air Source Heat Pump
GSHP	Ground Source Heat Pump
DSW	Durham Software for Windtunnels
AONB	Area of Outstanding National Beauty
WEC	World Energy Congress
CfD	Contracts for Difference
OLR	Offtaker of Last Resort
RHI	Renewable Heat Incentive
RGF	Regional Growth Fund
DPV	Discount Present Value
bwpd	Barrels of water per day
WOR	Water to Oil Ratio

Chapter 1

Introduction

1.1 Motivation

Meeting energy demand is framed by the need to address three main challenges, this is often described as the *'energy trilemma'*. These three challenges of energy supply are: to ensure it meets social requirements such as cost and availability; that is secure (i.e. not reliant on imports from elsewhere) and that it meets emissions requirements defined by climate change policies [1]. Conventional energy supply methods, via fossil fuels, cannot meet these challenges alone and therefore new technologies must be developed. Waste Heat Recovery (WHR) technologies, such as Organic Rankine Cycle (ORC), are important because they have the potential to make a significant contribution to meeting the energy challenges described. These technologies produce more useful energy for each unit of fuel used and offer the potential to reduce the volume and cost of carbon emissions per unit of energy produced and increase energy security by using fuel most efficiently. Similarly, some technologies developed for WHR may also be applied to deep geothermal energy. Here the heat available is renewable and indigenous, unlike most WHR scenarios, so the second two energy challenges described are fulfilled further by geothermal energy exploitation.

Waste heat is an abundant and inevitable consequence of all industrial processes and electricity generation. The amount of heat energy available is difficult to quantify as the

sources vary widely in their nature and magnitude. However studies state that 20 - 50 % of energy from raw fuels is dissipated directly as heat [2–4]. A study for the UK Department of Energy and Climate Change (DECC) in 2013 identified 11 TWh/yr of industrial waste heat which has the technical potential to be used [5]. This could offset 2.4 % of annual UK industrial energy consumption [6], therefore WHR technologies have the potential to play a significant role in UK energy supply conservation. Deep geothermal energy also has the potential to play a significant role in meeting energy demand. Deep geothermal energy is available as both a byproduct from oil production, i.e. heated production water, or as the sole product of a well. The total global potential for electricity production from geothermal sources is 148,800 MWe which translates to 10 - 100 % of today's electricity demand [7]. Gluyas et al. estimate more than 15,000 MWe may be produced from geothermal energy from oil production processes [8].

To date the uptake of heat recovery technologies in the UK is limited. In a report for the DECC written in 2013 figures for *"a best first estimate of the existing economic potential for industrial waste heat recovery"* are presented [5]. This simultaneously indicates the lack of existing WHR systems and large potential for their application. Similarly there is only one operational geothermal energy scheme in the UK [9].

Heat recovery technologies can be divided into two types, those that recover heat to be used directly as heat and those that convert the waste heat to electricity or mechanical work. Technologies that supply heat are limited due to the fact heat energy cannot be transported far without high cost, while producing electricity makes the recovered energy more easily transportable. Therefore in this study we focus on the application of ORCs, which covert low temperature heat into electricity or mechanical work. WHR technologies are well understood but not widely employed. This study seeks to evaluate and understand the lack of uptake of ORCs given the apparently favourable demand, availability of low temperature waste heat and potential to reduce carbon emissions.

To evaluate the application of ORCs in WHR and geothermal applications analytical models of the thermodynamic ORC cycle, the heat exchange processes, the economic

scenarios and physical space that the systems occupy have been developed. Various typical waste heat supplies are simulated to identify commonalities in ORC design. This analytical work is validated through experimental work carried out by collecting data on the heat exchange processes in a ground source heat pump. The study is concluded by considering the waste geothermal heat applications from the petroleum industry and the only dedicated geothermal system in the UK (Southampton). The sources of waste heat from oil and gas production come from coproduced brines, examples are identified from onshore operations in the North Sea and onshore operations at Wytch Farm.

1.2 What is Waste Heat?

1.2.1 Overview

In this study waste heat is defined as: unused heat energy generated as a by-product of energy conversion processes. It is inevitable that most industrial processes generate waste heat due largely to thermodynamic limits and equipment inefficiencies, but the heat discarded varies widely between processes. Waste heat streams are characterised by the following parameters:

- Temperature,
- Flow Rate,
- Composition.

The same parameters of the available cooling stream are also required to determine the recoverable heat potential for producing mechanical power. The difference between the heat source and sink streams determines the rate of heat transfer per unit and indicates the total heat transfer possible.

Grade or quality describes the amount of heat energy which it is possible to recover from the heat source. While the waste heat temperatures vary widely depending on the source, cooling streams tend to vary less. For example a typical available cooling stream from industrial plants is water at a temperature of 40 - 90 °C. Therefore waste heat

potential has been commonly classified according to the waste heat stream temperature. However, in a recent DECC study heat source and sink temperature bands have been defined [5]. Temperature bands for both heat sources and sinks are shown in Table 1.1. High quality means a large amount of available heat energy is recoverable per unit volume, while low quality sources have a low potential for energy recovery per unit volume. The total amount of available energy is proportional to the available volume of waste heat. Frequently, high quality sources of waste heat are available in small volumes and low quality heat is available in large volumes. Therefore often the total amount of recoverable heat may be larger from the low quality heat stream, than it is from a typical high quality stream.

High grade waste heat is available from processes such as metal smelting, hydrogen plants and fume incinerators. These waste heat sources are typically solid or gaseous. Waste heat from these processes may be used to pre-heat air entering the metal furnaces using recuperators, regenerators or pre-heaters, or to produce mechanical/ electrical work. Recovering heat from these environments can be challenging due to the high temperatures. However, heat recovery in metal smelting plants is now common. For example, the International Energy Authority (IEA) indicate several commercially viable heat recovering technologies in steel production in their 2007 study on energy efficiency indicators [10].

Medium grade waste heat sources are more commonly found in power generation applications from the exhausts of steam or gas turbines and also in heating applications such as cement kilns, drying ovens and Internal Combustion Engine (ICE)s. These medium grade waste heat sources are generally gaseous and can be used directly as heat sources.

The vast majority of available waste heat is of low quality. In a study of WHR potential in the UK, 65.6 % of waste heat sources identified were low grade [5]. Common sources of low grade waste heat are: cooling water from furnaces or power cycles and refrigeration cycles.

Quality Category	Heat Source [2, 11]	Heat Source [5]	Heat Sink [5]
High	>650 °C	>500 °C	>250 °C
Medium	230 - 650 °C	250 - 500 °C	150 - 250 °C
Low	<230 °C	<250 °C	<150 °C

Table 1.1: Waste heat quality categories defined in [2, 5] and heat sink quality as defined in [5]

1.2.2 Example Waste Heat Sources Used in the Study

Internal Combustion Engines

The use of waste heat from ICEs has been the focus of large amounts interest since the fuel crisis of the 1970s [12, 13]. Interest lapsed as oil prices recovered in the 1980s and engine design improved sufficiently so that fuel economy was no longer a critical issue. In recent years, research on WHR in ICEs has intensified due to increasing oil prices and increasingly stringent emissions regulations. A key driver for implementing WHR systems in ICEs has been the US Department of Energy (DOE) SuperTruck program [14]. This 5 year program was initiated by the U.S. government and aims to increase the Brake Thermal Efficiency (BTE) of Class-8 long haul trucks by 20 % (to 50%) and the overall freight efficiency by 50 % relative to 2010 technology.

ICEs are the most common primary power source for vehicles, freight lorries and ships. Heavy Duty (HD) ICEs are the second largest CO_2 emissions producers in the transport sector of every major economy in the world, surpassed only by air travel [14]. Therefore, improvements in fuel efficiency within this subsector represents a large potential for reduction in CO_2 emissions and operating costs. As a result research to date has focused on implementing WHR systems on HD ICEs.

There are several sources of waste heat from ICEs, the key sources of waste heat are shown in Figure 1.1. The figure shows, the two main sources of waste heat from HD diesel engines are the coolant water and the exhaust gas. Depending on the load that the engine is running at these two waste heat streams contain similar amounts of energy. However, the cooling water is a low grade heat stream as the temperature of the water

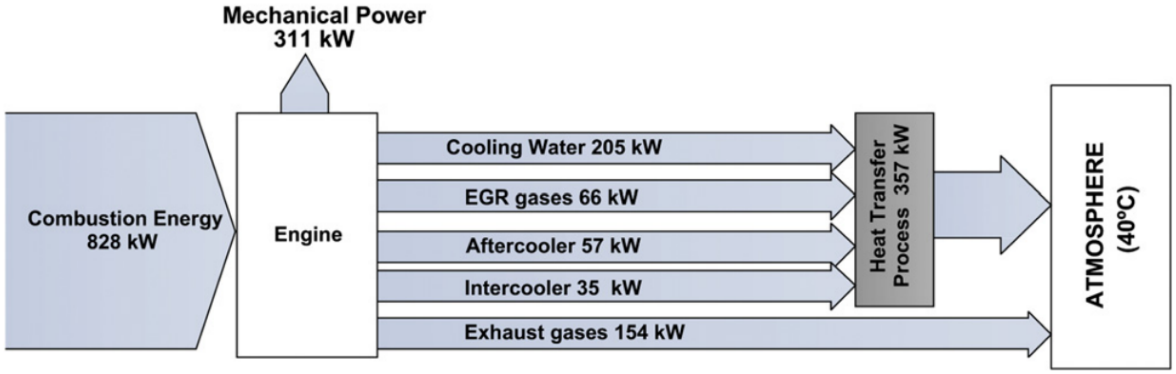

Figure 1.1: Waste heat sources from an example 12L HD Diesel Engine as published by Dolz et al. [15]

is low ($\sim$ 80°C) whereas the exhaust heat is considered medium grade with a typical temperature of 330°C. See table 1.1. Therefore research has focused on systems that recover heat from the exhaust heat streams of HD engines [12, 13, 15–17]

Hot Brines From Oil Extraction

Petroleum is typically extracted from reservoirs in the North Sea at depths between 2.5 - 5 km. Fluids extracted from these depths are hot, approximately 70 - 150 °C, due the geothermal gradient. Hot brines are coproduced from oil wells in increasing quantities as production proceeds within the Earth's crust. Water injection is a common technique used after a producing well has reached peak production in order to maintain yield. Sea water or coproduced water is pumped down the well to "sweep" the remaining residual oil from pore spaces in the reservoir whilst maintaining reservoir pressure, see Figure 1.2. As the well declines, and less oil is produced, the production water may be 20 times the volume of oil produced, at rates in some cases of approximately 100,000 barrels/day (180 kg/s) [18]. Therefore, hot brines represent a vast, low grade energy source.

Currently, at the production well head the oil and water are separated. Then the hot brine is either cleaned and discarded or reinjected into the injection well. Some studies have been carried out into the potential of using this resource, and demonstration ORCs have been installed, for example [19]. However, to date this application of WHR technology is yet to become widely adopted. In this study we examine in depth the

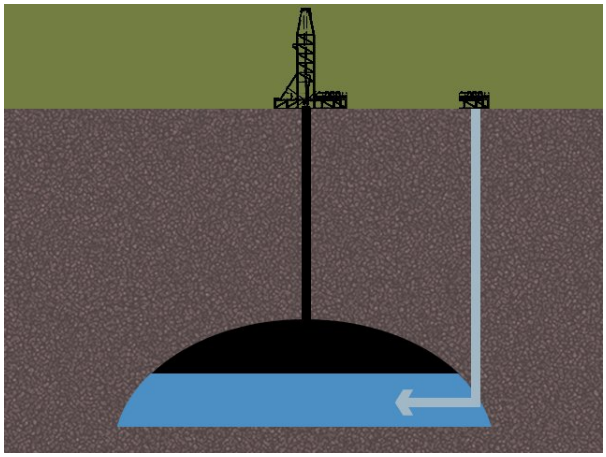

Figure 1.2: Diagram of water injection process for producing oil wells.

potential to recover and use this large energy resource economically offshore in the North Sea and onshore at Wytch Farm.

A natural progression from waste streams of geothermal heat is to consider wells dedicated solely to the extraction of geothermal heat. In the UK, geothermal temperature gradients typically range from 2 - 5.1 °C per 100 m [20]. At well depths in the region of 2 km, the hot water streams available are very similar to low temperature waste heat streams. The resource may be similar for waste heat and dedicated geothermal streams but the economic scenarios are very different. Therefore both scenarios are considered in this thesis to evaluate how this affects heat recovery technology selection.

Industrial Waste Heat

Combustion, chemical, mechanical and heat exchange processes produce unused streams of heat energy. The most energy intensive industrial processes have been evaluated for waste heat recovery systems in literature, as these represent the largest source of potentially recoverable energy. Examples of these industries are chemical, glass, metal, cement, paper and pulp [2, 3]. Temperatures and volumes of potential waste heat streams have been collated from several sources, these are shown in Figure 1.3. Liquid and solid streams, hot air and flue gases, pressurised hot water, waste water and exhaust vapour are typical waste heat mediums.

Figure 1.3 highlights characteristics of the wide array of industrial waste heat streams

available, combined with the range of energy recovery technologies available to exploit them. Energy is commonly recovered from industrial boilers as clean gaseous steams. To avoid condensation of acidic flue gases cooling is limited to the dew point of the exhaust stream (typically 100 - 130 °C). This prevents condensation of acids in the gas and therefore WHR is less common for acidic or 'dirty' exhaust streams. WHR is also less common is small scale applications and for low grade heat, as these scenarios are often more expensive per unit of energy generated. Industrial waste heat recovery applications do exist but uptake is highly dependant on local subsidies for heat recovery technologies and the specific waste heat streams.

The example of industrial waste heat used in this study is from a typical plant supplying steam and electricity to surrounding process works in Teesside, UK. In this plant, steam from a gas and a biomass fuelled boiler is used to produce thermal and electrical energy. WHR from waste steam and flue gases are explored for a number of different sources around the plant.

1.3 Heat Recovery Technologies

In order to exploit the energy from waste heat and geothermal heat streams, technologies capable of recovering this energy into a usable form of energy are required. Figure 1.3 shows there are numerous WHR technologies in existence. These are in various stages of commercial deployment and have different ranges of applications for different heat sources. Below is a brief overview of various heat energy recovery technologies. As this study focuses on ORC technology, heat recovery technologies which operate with similar waste heat conditions are described. These are in the medium and low heat quality bands. Energy recovery from high grade energy sources tends to be used directly as heat or in steam power cycles both of which are mature and well known technologies. Barriers to uptake of high grade waste heat are most commonly due to the challenges of operating equipment in such high temperatures and therefore are very different from those of low to medium grade resources. Often, high grade heat recovery generates additional low and medium quality sources of waste heat, which can be used by the technologies described

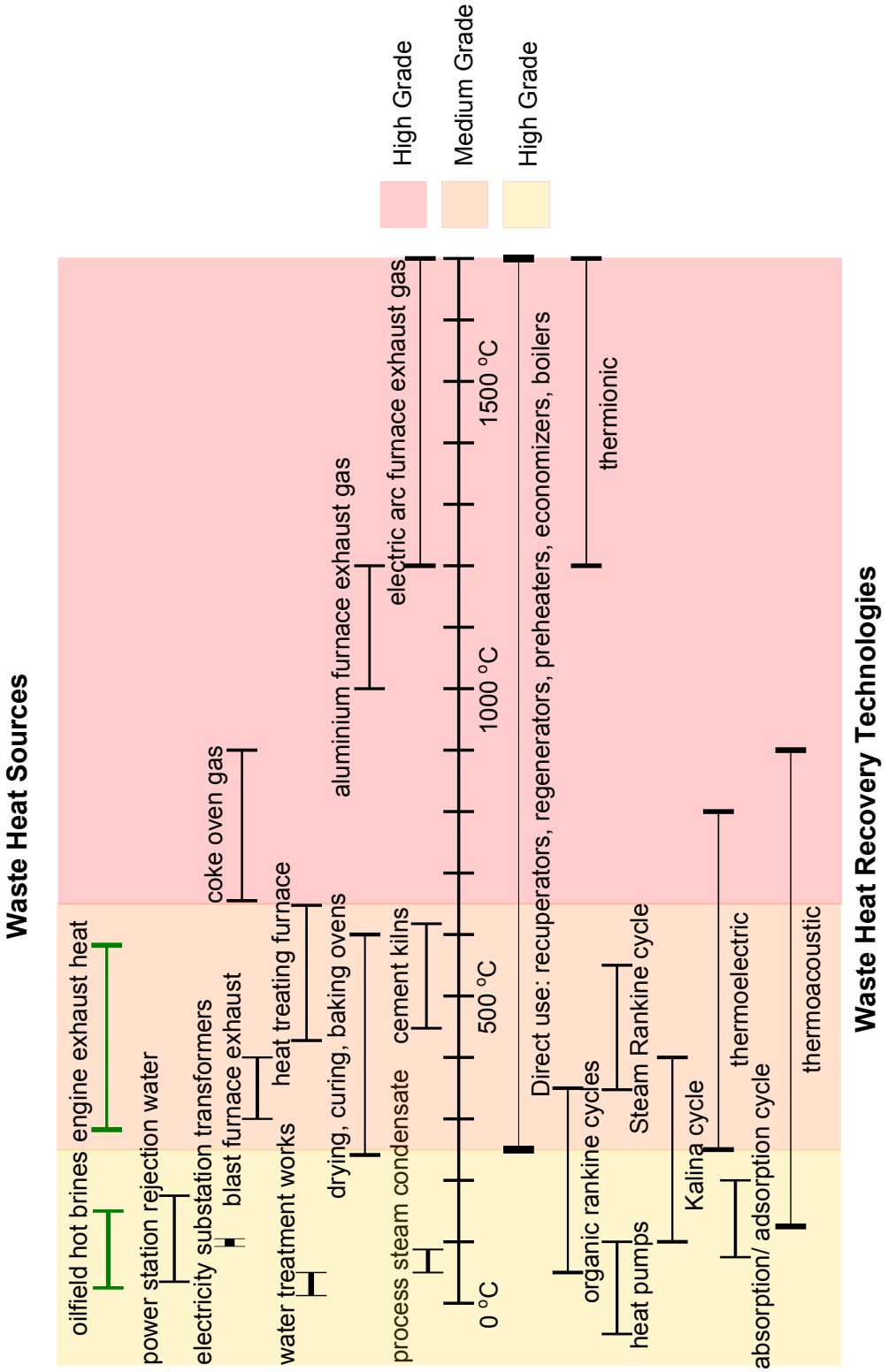

Figure 1.3: Diagram of temperature scales for Waste Heat Sources and Technologies, from references [2, 11, 21]

below, in what is known as a cascade [2].

1.3.1 Direct use as heat

The most straightforward use of a waste heat source is to recover the heat via a heat exchanger and use it to meet a heat demand. Heat exchangers are a mature technology and various types have been developed for common waste heat applications. For example, waste heat sources, usually exhaust gases, are commonly used to preheat boiler feedwater via a heat exchanger. Using waste heat to increase the temperature of water going into a boiler means less fuel is then required to vaporise the water, therefore increasing fuel economy. This type of system is usually called an economiser and is widely adopted. Other heat exchanger systems used to recover heat are: recuperators, regenerators, and waste heat boilers [2].

The applicability of these technologies is limited by having a waste heat stream that can help meet a local heat demand. Heat streams can be transported short distances via thermally insulated heat pipes to a heat demand, otherwise known as heat networks [22]. However (over significant distances, several kms) the cost of pipework means transporting the heat stream becomes prohibitively expensive.

1.3.2 Heat Upgrade Cycles

In situations where there is a local heat demand but the quality of available waste heat stream is too low quality to meet this demand, heat upgrade technologies, such as a heat pump, might be employed to use the available waste heat and fulfil the heat requirement. In these scenarios, heat exchangers are used to recover the heat to a working medium which then undergoes a thermodynamic cycle to produce either a higher grade heat or cooling stream. Typical cycles include vapour compression cycles (also known as a heat pump cycle) and absorption/adsorption cycles. The vapour compression and absorption cycles are illustrated in Figure 1.4.

Figure 1.4a shows a vapour compression cycle, the cycle operates as follows:

- The heat source vaporises the working fluid inside the cycle via the evaporator.

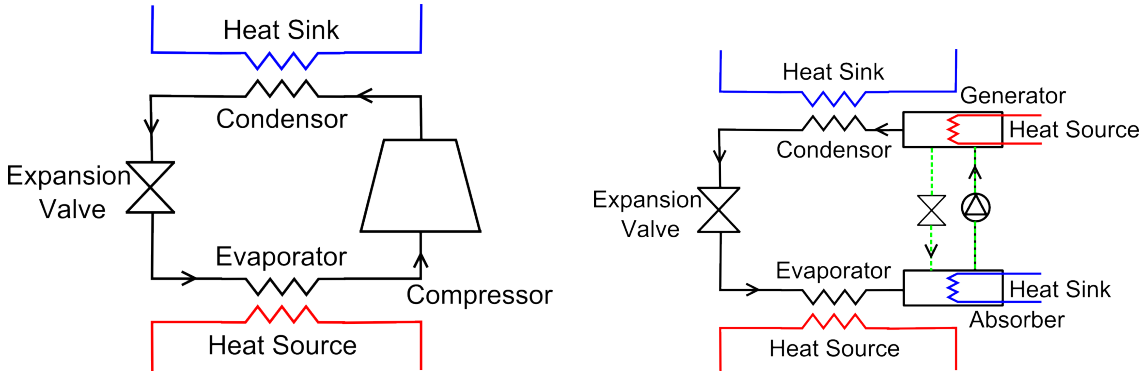

(a) Vapour compression (b) Absorbsion

Figure 1.4: Diagram of heat cycles used in WHR

- Mechanical work is added by a compressor, increasing the pressure of the working fluid causing it to become a superheated vapour.
- Heat is rejected from the working fluid, to the cooling stream in the condenser, at a higher temperature than was absorbed from the heat source.
- The working fluid is expanded through an expansion valve whereby it returns to its original state, allowing the cycle to repeat.

Thus, the waste heat has been upgraded by the additional of mechanical work in the compressor.

Absorption and adsorption systems, Figure 1.4b, are very similar cycles but the mechanical compression stage is replaced by a chemical process. In the case of the absorption cycle this is an absorbent liquid. Whereas an adsorption cycle uses a solid medium for the compression stage. Adsorption and absorption cycles require an additional heat source and sink therefore they have several possible configurations. For example if the waste heat was supplied to the generator (see, Figure 1.4) the system can then provide cooling and extracts heat to the working fluid via the evaporator.

Vapour compression cycles generally operate with low grade heat streams, approximately -20 - 100 °C, and are able to provide temperature uplifts of 20 - 50 °C. This can make them appropriate for providing domestic hot water. Absorption cycles require heat source temperatures of 100 - 200 °C and are able to provide larger temperature uplifts

than vapour compression cycles of 100 - 200 °C [23].

Absorption and adsorption cycles are complex; however they offer several advantages over mechanical compression cycles. For example the lack of moving parts with no mechanical compressor, use of environmentally benign natural refrigerants as working fluids and the ability to use higher temperature heat sources are advantageous, as a result there are many commercially available systems.

Applications for these cycles, like direct heat use, are constrained by the requirement to have a local heat demand. Furthermore, the cost of heat supply via heat pumps must be competitive with more conventional methods (i.e. burning natural gas).

1.3.3 Direct Electrical Conversion Technologies

Direct electrical conversion devices convert thermal energy into electrical energy. Traditional power generation, for example via the Rankine cycle, requires the heat to be converted to mechanical energy before it can be converted to electrical energy. Therefore, direct electrical conversion methods have the potential to be simpler and to require lower maintenance than traditional power generation.

The most common method of converting heat to electricity is via thermoelectric generators. These devices produce electricity via the Seebeck effect; this refers to how a voltage is produced when a temperature gradient is applied over two different conductors. The thermal gradient causes a heat flux and charge carriers flow from the hot to cold regions, creating a potential difference [24]. These systems operate with typical efficiencies of 2 - 5 % for low heat qualities, 80 - 175 °C. Several studies have proposed systems to recover exhaust heat [25] because it is very compact, scalable, silent and reliable, with no moving parts. But, the efficiency of thermoelectric generation must be improved and the cost reduced before it can become a commercially viable heat recovery technology. Low efficiencies are due to the difficulty of producing materials that maintain a large thermal gradient over the thermoelectric device.

Other direct electricity generation methods include piezoelectric, thermoionic and thermophotovoltaic generation. Several studies in literature propose these technologies would

be appropriate to recover heat from low and medium quality heat streams [2, 26], however this is yet to be demonstrated on an industrial scale. In general, these technologies all require significant improvements in performance/cost before commercial applications can be considered. Therefore, direct electrical conversion technologies are not realistic considerations for heat recovery at present.

1.3.4 Mechanical Conversion Technologies

The most common heat recovery technologies convert heat to mechanical work; this work may then be used or converted in to electricity via a generator. Examples of these technologies are thermodynamic cycles, such as binary cycles, and thermoacoustic engines.

Binary cycles are thermodynamic cycles that convert heat to mechanical power. The term 'binary' refers to a two stage process whereby heat is extracted from the heat source via a heat exchanger and transferred to a secondary fluid, known as the working fluid. There are several different types of thermodynamic cycles that produce mechanical work, those most commonly used in WHR are the Rankine and Kalina cycles [27].

There are several variations of the Rankine cycle and, as a result, it is used to produce mechanical work from various heat sources. The most common power generation method in the world is the steam Rankine cycle, this cycle is illustrated in Figure 1.5. In its most basic form, this cycle comprises of the following processes:

1. Water is vaporised by a heat source at constant pressure - isobaric heat addition.

2. The steam is expanded through a turbine or expander - isentropic work extraction.

3. Steam is condensed to water at constant pressure - isobaric heat rejection.

4. Water is pumped to a high pressure - isentropic work addition.

Water is an appropriate working fluid for many Rankine cycles due to its high thermal and chemical stability. Its low viscosity therefore means it requires little pump work and its high specific heat capacity means it can transfer large amount of energy. It is neither toxic or flammable, has low cost and high abundance. However, water can only be used in

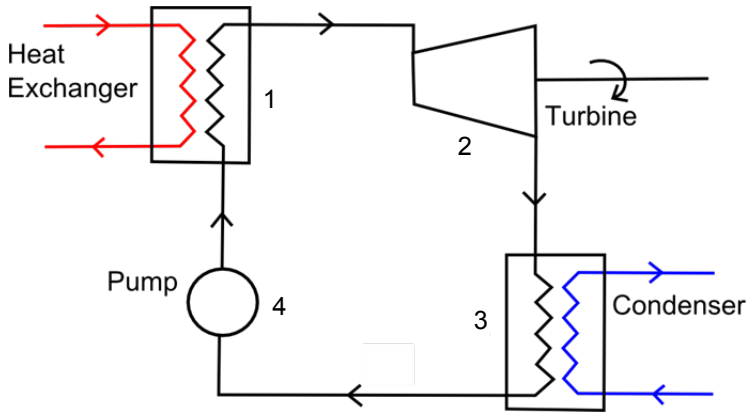

Figure 1.5: Diagram of the basic Rankine cycle

Rankine cycles with heat source temperatures above 350 °C [2], below this temperature the cycle is unlikely to be cost effective, because low pressure steam requires larger heat exchangers and the cycle is less efficient.

At temperatures of less than 300 °C (low and medium quality heat) the Organic Rankine Cycle (ORC) or Kalina cycle may be employed [28].

The ORC consists of the same processes as the regular Rankine cycle. However, the water circulating round the cycle is replaced in favour of an organic working fluid with a lower evaporation temperature. Lower evaporation temperature of the working fluid enables the ORC to operate with heat supplied from lower temperature heat sources than the steam Rankine cycle.

The Kalina cycle is a similar cycle to the ORC. In this cycle, a water/ ammonia mixture is used as the working fluid. This is more complex than the Rankine cycle, see Figure 1.6, but the same four key processes of the Rankine cycle are employed evaporation, expansion, condensation and compression, with the addition of a generator and absorber. The generator and absorber control the ratio of water to ammonia so the ratio of components differs throughout the cycle. This enables the thermal profiles of the source and sink to match that of the working fluid, thus increasing overall thermodynamic efficiency. Studies predict the Kalina cycle could be up to 30 - 50 % more efficient than the ORC but experimental results show much smaller improvements in system efficiency of just 3 % [29]. The Kalina Cycle is patented with patents owned by Global Geothermal Ltd.

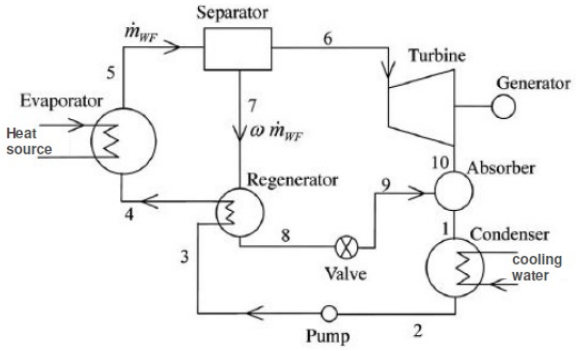

Figure 1.6: Diagram of the Kalina cycle http://rotunds.com/

This combined with only a marginal increase in efficiency means their development has been relatively limited. Currently a handful of Kalina cycles are operating, mostly in geothermal applications.

The overall thermal efficiency of the cycles described can be improved further by adding recuperator and reheat technologies as described in section 1.3.1. Addition of these technologies increase the cost and complexity of the heat recovery system which must be balanced against the improvement in performance.

Thermoacoustic heat engines use a thermal gradient applied over a thermoacoustic element, or stack, to generate a standing wave in a gas. This standing wave is manifestly a form of mechanical work and can be converted to electrical energy via a linear alternator. While the principal of thermoacoustic systems is simple, there are few operating commercially. They have been identified in literature as appropriate for waste heat applications because they have the potential to operate with low grade heat streams (<150 °C), and because they use simple materials, safe (noble) gases and have few moving parts [30]. Development has been limited because the systems are large and/or operate at very high pressures, which results in expensive systems and the linear alternators, required for electricity generation, have poor efficiency. With significant further development thermoacoustic systems could operate in the same heat supply range as ORCs for waste heat recovery applications.

Thermoacoustic technology, along with direct electrical conversion technologies, are immature technologies. Currently ORCs are the most readily available and appropriate

systems to produce electricity from low to medium grade waste heat sources. Therefore this study will focus on ORC technology.

1.4 Organic Rankine Cycles

1.4.1 Technical Introduction

The thermodynamic processes that make up an organic Rankine cycle are identical to those found in the traditional Rankine cycle. The key difference lies in the working fluid which is circulated around an ORC. In place of water, organic fluids such as hydrocarbons (HCs),hydrochlorofluorocarbons (HCFCs), hhlorofluorocarbons (CFCs), herfluorocarbons (PFCs), siloxanes, slcohols, hydrofluroehters (HFEs) and other refrigerant type compounds are are all potential working fluids [31]. The key benefit from using these fluids is that they have lower boiling points than water, so evaporation of the fluid occurs at a lower temperature and pressure. This means lower temperature heat sources can be used to supply heat to the ORC. Waste heat streams are available at a variety of temperatures, mediums and flow rates and the working fluid in an ORC can be selected to best match that of the heat source characteristics to enable most heat recovery. This makes the ORC a highly adaptable technology, appropriate for a range of heat recovery and geothermal applications.

Aside from the low boiling points, there are several other properties of organic fluids which also make them attractive for use in a Rankine cycle. Firstly, as the the evaporation of working fluids in ORCs happens at lower temperature and pressures than steam Rankine cycles, these less extreme conditions mean that the system can be designed with less expensive materials. In addition to lower evaporation temperatures, ORCs have smaller temperature differences between the evaporator and condenser than steam Rankine cycles. This means the pressure drop is smaller and single stage turbines can be used, further reducing cost and complexity of the cycles.

A further advantage of organic working fluids is that many organic fluids are dry or isentropic. Classification of a fluid as dry, isentropic or wet refers to the gradient of the

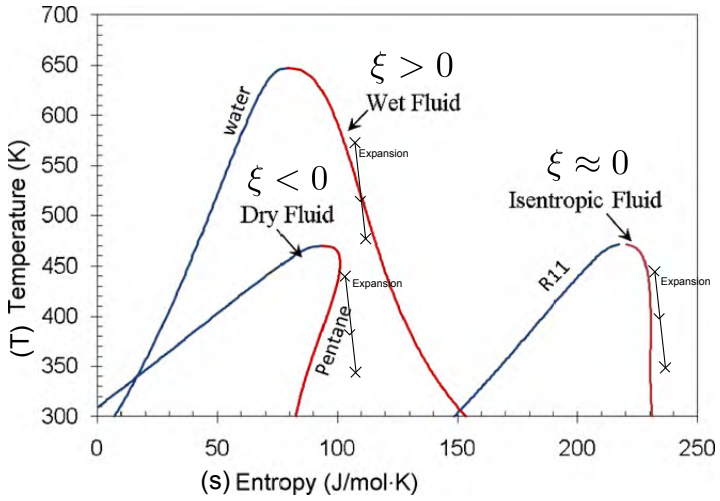

Figure 1.7: Classification of compounds via their Saturation Curve, diagram taken from [27]

vapour saturation curve, ξ, as defined by equation 1.1.

$$\xi = \frac{ds}{dT}. \tag{1.1}$$

Wet fluids, like water, have a positive saturation curve as shown in Figure 1.7. This means it is possible when a saturated or superheated vapour undergoes an expansion process for the vapour at outlet to be a mixture of liquid and gas. This condensation during expansion causes the turbine blades to be eroded consequently steam Rankine cycles must be designed with additional superheat to avoid operating turbine damage. Isentropic and dry fluids cannot undergo condensation through expansion from a saturated vapour and so these fluids offer the advantage that no additional superheating is required alongside the reduced risk of erosion to the expansion device. Behaviour of the fluids is shown in Figure 1.7 with the black lines terminated by crosses showing possible expansion processes.

The design and optimisation of ORCs is very different from that of steam Rankine cycles because they are constrained differently. For example there is no limit regarding vapour quality at outlet on the expansion device for ORCs and thus no requirement for

superheat as with steam Rankine cycles. Different limitations are placed on the expander design due to the fact that the organic fluids used are dense gases. Dense gases have a much lower speed of sound and high Mach numbers are reached at lower vapour speeds. Supersonic effects make traditional expander design inefficient and so these conditions should be avoided [32].

There are two different pathways to maximise heat recovery from ORC systems. Firstly, the cycle may be changed to improve its thermal efficiency. This is achieved by employing technologies such as recuperators, regenerators, reheat or vapour injectors. These technologies all improve cycle efficiency by maximising the average temperature between heat addition and heat rejection and therefore maximising the amount of heat in the cycle that is converted into mechanical work [33].

Secondly, the work output of the system may be increased by maximising the heat energy added to the cycles, thereby increasing the heat available to be converted into work and thus increasing the thermal efficiency of the entire system. Irreversibilities in heat transfer are reduced by matching the temperature profiles of the heat source and sink streams to the working fluid in the cycle, this is illustrated in Figure 1.8. The temperature profile of the heat stream is the change in temperature per unit of energy. To achieve closely matching temperature profiles the following cycle architectures are employed or proposed in literature: Transcritical cycles, Trilateral cycles, Cycles with zeotropic mixtures as working fluids, Cycles with multiple evaporation pressures, and Organic flash cycles (OFCs). [28, 33]. OFCs are similar to steam flash cycles found in geothermal power plants.

Transcritical cycles use evaporation pressures above the critical pressure of the working fluid [34]. This means the temperature profile of the working fluid follows a similar shape to the saturation curve and therefore may better match some heat sources. Supercritical cycles extend this idea further to include both evaporation and condensation processes occurring above the working fluid's critical pressure [34]. These cycles require very high pressures and the additional safety precautions required mean these systems are more

expensive. There are also limitations on working fluid selection as some will degrade at sufficiently high pressures and temperatures.

Similarly trilateral cycles (TLCs) use the saturation curve profile of the working fluids to match temperature profiles, through not heating the working fluid any further than a saturated liquid state. This cycle is inherently less efficient than an ORC but the increased amount of heat into the cycle, due to good thermal profile matching, means there is significant interest in these cycles. The key challenge in implementing the TLC is the development of an expander device that will allow expansion from a saturated liquid to a liquid/ vapour mixture [35].

OFCs are similar in concept to TLC cycles. In this cycle the working fluid is throttled to a lower pressure in a flash tank after heat addition from the heat source, in order to best match the temperature profiles during the heat addition. There are limited examples of their deployment as the increased heat energy into the cycle is mostly lost during the throttling process [36].

Finally, zeotropic mixtures can be used within a standard Rankine cycle configuration to improve thermal efficiency. Zeotropic mixtures have different compositions in the vapour and liquid phases in an equilibrium state. Constituent fluids in zeotropic mixtures condense/evaporate at different rates and therefore change temperature during phase change, unlike pure fluids. This means the temperature profile of a heat source or sink might be better matched by selecting an appropriate zeotropic mixture as the cycle working fluid. Fluids mixtures which do not change temperature during phase change, i.e. change phase at the sme rate, are known as azeotropic fluids. Several studies identify the potential benefit of using zeotropic mixtures [27, 37, 38] and predict significant improvements in thermal efficiency from their use but identify a lack of understanding of the phase change process for the fluids. The possibility of using zeotropic mixtures is examined later in the work described in this thesis.

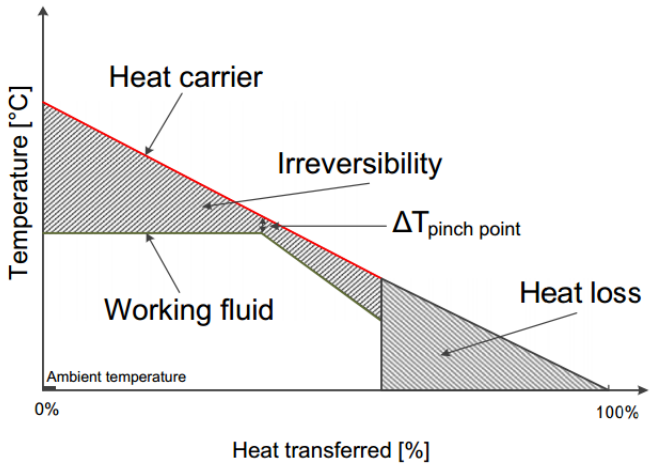

Figure 1.8: Heat transfer irreversibilities in an ORC evaporator, taken from [33]

1.4.2 Applications and Maturity of Organic Rankine Cycles

Organic Rankine cycles have existed since the 1880s, but significant research into developing ORCs did not occur until 1980s [11]. Interest in ORCs was primarily sparked by the fuel crisis in the late 70s but research has increased hugely over the last 10 years. This is shown in Figure 1.9, where the cumulative number of publications on ORCs against time is plotted.

Presently, ORCs have a variety of heat source applications including: biomass, geothermal, solar and waste heat recovery. For each of these applications, ORC technology is in a different state of commercialisation.

The most mature ORC application is for large geothermal power plants. ORCs fuelled by geothermal fluids at tempertures greater than 150 °C have been developed by ORMAT technologies since the 1980s. Systems developed are of MW scale and are commercially mature. Similarly, biomass fuelled ORCs are commercially available in MW scale units. Biomass and geothermal ORCs are commonly employed as Combined Heat and Power (CHP) units, where the condenser temperature is set to approximately 60 °C to supply domestic hot water. These systems are often driven by heat demand rather than electricity production. Solar driven ORCs are the least common application for ORC technology with only a handful of systems in operation [11].

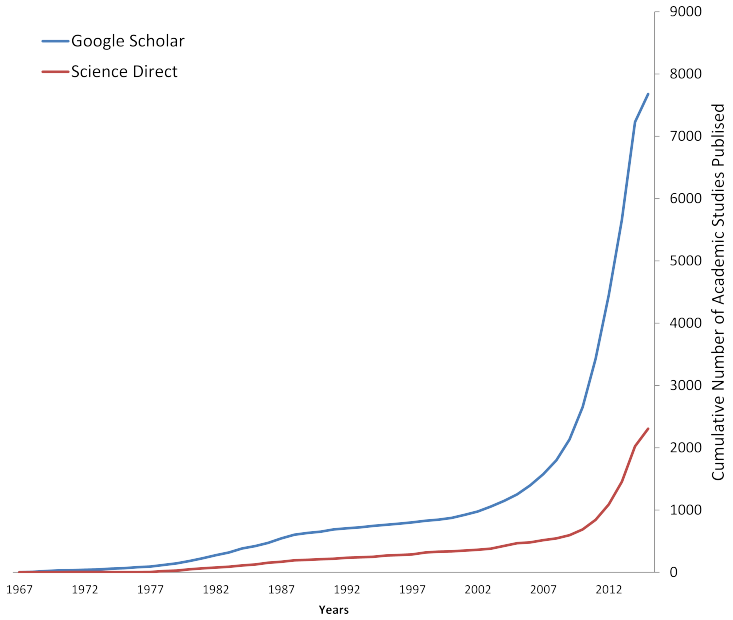

Figure 1.9: Plots of the historical volume of academic publications including the term "organic Rankine cycle" and the Brent crude oil price against time [39].

In general ORC technology on a MW scale is mature with costs of approximately €1000 - €3000 /kW. Costs of ORC systems do not scale favourably, kW scale ORC systems cost in the region of €3000 - €8000 /kW [11]. Significant development is required in small scale ORC applications for them to became as commercially mature as larger systems.

Many manufacturers produce modular ORC systems. So that a standard ORC unit may be manufactured, taking advantage of economies of production, which then may be applied with few adaptations to various heat sources. One example of this modular type of ORC is shown in Figure 1.10. In a contrast to traditional steam Rankine power generation this modular approach means ORCs can be considered for small scale and decentralised generation.

1.5 Means, Motive and Opportunity

The introduction to this chapter, highlighted the present challenges of meeting energy demand. Using waste heat to fulfil some energy demand reduces carbon emissions, improves fuel economy and further secures energy supply by generating more electricity for the same amount of fuel. Similarly using geothermal heat sources is an energy supply

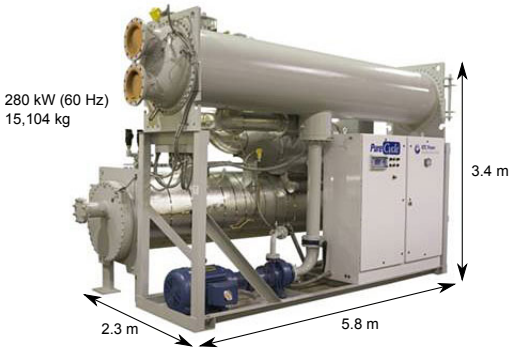

Figure 1.10: Example of a commercial ORC module manufactured by PureCycle

from a native, renewable and reliable energy source. Therefore there is strong motivation to use waste heat and geothermal energy sources.

In section 1.2 several sources of waste heat and geothermal energy have been identified which represent a vast untapped energy resource. Globally waste heat amounts to approximately 167 EJ per year of unharnessed energy [28] and for the UK's industrial sector this translates into 0.396 EJ per year (11 TWh/yr) [5]. The global geothermal resource is large, the World Energy Council estimates the thermal energy of the global low-temperature geothermal resource to be 140 EJ/yr (39,000 TWh/yr) [40]. In comparison the heat demand of the UK in 2011 was 1.7 EJ (471 TWh) [41]. This indicates waste heat streams are available for energy recovery, yet they remain largely unexploited.

Lastly, in this section WHR technologies have been identified and discussed. Existing heat recovery technologies and potential heat sources to supply them are summarised in Figure 1.3. The applicability of these technologies is determined by additional factors such as cost, size, etc.

In summary, the motivation to use waste heat and help meet global energy demand has been identified, there are abundant waste heat streams with various characteristics and there are existing waste heat recovery technologies to make use of this heat. Since uptake of these technologies is limited there are still barriers preventing widespread adoption of heat recovery systems.

One barrier to WHR uptake may simply be; capital costs and profitability of ORC

systems, which are strongly site dependent [11]. Other barriers might be the limited scalability of ORCs, small scale systems are expensive. Similarly, industrial waste heat recovery often requires some bespoke design and lack of physical space increases the cost of installing a system further. A further barrier to utilising exhaust gas steams is that they are often acidic gases, this means that they cannot be cooled below 100 - 130 °C to avoid the acid condensing out of the gas causing corrosion problems and this limits the heat recovery potential. This thesis examines the organic Rankine cycle to identify, understand and improve upon current barriers to their further use in waste heat recovery and geothermal applications.

1.6 Thesis Structure

The thesis comprises of a further 5 chapters, divided into three themes: computational modelling, experimental work and a combined assessment of ORC applicability, considering size, cost and thermodynamic performance, with a particular focus on deep geothermal heat sources.

In Chapter 2, a Rankine cycle model is introduced and used to model ORC systems for three waste heat source examples. The model has been built from scratch as part of this study and includes a novel method of computing heat exchanger pinch point analysis. Simulations are carried out for ORCs in various configurations for each of the case study heat sources presented. Conclusions are drawn concerning how ORC design might be generalised across different energy scales for both pure and zeotropic working fluids. Conclusions are also drawn on the benefit or otherwise of binary fluid mixtures for the heat exchange process in ORCs.

Chapter 3 focuses on the heat transfer processes in the ORC. An experimental test rig to measure the heat exchange across an evaporator and condenser using organic working fluids is described. The design and implementation of a test rig is reported. Results for an azeotropic and zeotropic working fluid are presented and compared.

In chapter 4 the global UA value is calculated from experimental data for an azeotropic and zeotropic working fluid. The need for an appropriate theoretical model to accurately

account for the heat transfer coefficient for zeotropic mixtures is discussed. Understanding of heat transfer coefficients would allow the calculation of the heat exchange area required by the heat exchangers. This enables prediction of the physical size of the ORC system, which can be considered alongside estimated thermodynamic performance, to understand the overall benefit or otherwise of employing an ORC system. A heat exchanger model is introduced, which aims to simulate accurately the behaviour of binary fluids during phase change.

Chapter 5, consolidates the results obtained in chapters 2 3 and 4. Results are collated for ORC thermodynamic performance, size and cost. These key factors are examined in order to understand in what situations ORCs might be most effective and to identify current barriers to further uptake.

The final chapter in this thesis examines in detail three sources of deep geothermal heat. The particulars of each scenario are examined to establish the key factors which determine the feasibility or otherwise of using ORC plant to convert this source of thermal energy into mechanical work. Factors are divided into three categories: social, physical and financial. Reasons for the success or otherwise of deep geothermal projects are discussed using these metrics.

References

[1] O. Wyman, "World energy trilemma, time to get real - the myths and realities of financing energy systems," tech. rep., World Energy Council, 2014.

[2] "Waste heat recovery: Technology and opportunities in u.s. industry," 2008.

[3] M. Z. Stijepovic and P. Linke, "Optimal waste heat recovery and reuse in industrial zones," *Energy*, vol. 36, pp. 4019–4031, 2011.

[4] G. Hammond and J. Norman, "Heat recovery opportunities in uk industry," *Applied Energy*, vol. 116, pp. 387–397, 2014.

[5] Element, Energy, Ecofys, Imperial, College, P. Stevenson, and R. Hyde, "The potential for recovering and using surplus heat from industry," version 2, Department of Energy and Climate Change, December 2013.

[6] I. MacLeay, K. Harris, and A. Annut, "Digest of united kingdom energy statistics 2014," tech. rep., Department of Energy and Climate Change, 2014. ISBN: 9780115155307.

[7] L. Welding, "United states geothermal energy market report," tech. rep., Glitnir Geothermal Research, September 2007.

[8] J. Gluyas, A. Auld, C. Adams, C. Hirst, S. Hogg, and J. Craig, "Getting into hot water: An opportunity for the petroleum industry," in *The Fouth London Geothermal Symposium: The Launch of BritGeothemal*, (The Geological Society, London), Britgeothermal, October 2014.

[9] Department of Energy and Climate Change, "Policy paper, 2010 to 2015 government policy: low carbon technologies." Updated: May 2015.

[10] Various, "Tracking industrial energy efficiency and co2 emissions," tech. rep., International Energy Authority, 2007.

[11] B. F. Tchanche, G. Lambrinos, A. Frangoudakis, and A. Papadakis, "Low-grade heat conversion into power using organic rankine cycles: A review of various applications," *Renewable and Sustainable Energy Reviews*, vol. 15, pp. 3963–3979, 2011.

[12] E. Doyle, L. Dinanno, and S. Kramer, "Installation of a diesel-organic rankine compound engine in a class 8 truck for a single-vehicle test," tech. rep., SAE Technical Paper, 1979.

[13] C. Leising, G. Purohit, S. DeGrey, and J. Finegold, "Waste heat recovery in truck engines," tech. rep., SAE Technical Paper, 1978.

[14] O. Delgado and N. Lutsey, "The u.s. supertruck program: Expediting the development of advanced heavy-duty vehicle efficiency technologies," white paper, The International Council on Clean Transportation, June 2014.

[15] V. Dolz, R. Novella, A. García, and J. Sánchez, "Hd diesel engine equipped with a bottoming rankine cycle as a waste heat recovery system. part 1: Study and analysis of the waste heat energy," *Applied Thermal Engineering*, vol. 36, pp. 269–278, 2012.

[16] D. Koeberlein, "Cummins supertruck program: Technology demonstration of highly efficient clean, diesel powered class 8 trucks," in *Directions in Engine-Efficiency and Emissions Research Conference*, U.S Department of Energy, 2011.

[17] C. Katsanos, D. Hountalas, and E. Pariotis, "Thermodynamic analysis of a rankine cycle applied on a diesel truck engine using steam and organic medium," *Energy Conversion and Management*, vol. 60, pp. 68 – 72, 2012.

[18] J. G. Gluyas and H. M. Hichens, *United Kingdom oil and gas fields: commemorative millennium volume*, vol. 20. Geological Society, 2003.

[19] D. Zabek, J. Penton, and D. Reay, "Optimization of waste heat utilization in oil field development employing a transcritical organic rankine cycle (orc) for electricity generation," *Applied Thermal Engineering*, vol. 59, pp. 363–369, 2013.

[20] P. L. Younger, J. G. Gluyas, and W. E. Stephens, "Development of deep geothermal energy resources in the uk," *Proceedings of the Institution of Civil Engineers*, vol. 164(EN0), pp. 1–14, 2011.

[21] Buro Happold Ltd and The Greater London Authority, "London's zero carbon energy resource, secondary heat," summary report, Mayor of London, July 2013.

[22] C. Adams, A. Auld, J. Gluyas, and S. Hogg, "Geothermal energy the global opportunity," *Part A Journal of Power and Energy*, vol. 0, no. 0, pp. 1–8, 2015.

[23] C. J. Roos and Northwest, CHP and Center, Application, *An overview of industrial waste heat recovery technologies for moderate temperatures less than 1000 F*. Northwest CHP Application Center, 2009.

[24] L. E. Bell, "Cooling, heating, generating power, and recovering waste heat with thermoelectric systems," *Science*, vol. 321, no. 5895, pp. 1457–1461, 2008.

[25] M. Karri, E. Thacher, and B. Helenbrook, "Exhaust energy conversion by thermoelectric generator: Two case studies," *Energy Conversion and Management*, vol. 52, no. 3, pp. 1596–1611, 2011.

[26] K. Ebrahimi, G. F. Jones, and A. S. Fleischer, "A review of data center cooling technology, operating conditions and the corresponding lowow-grade waste heat recovery opportunities," *Renewable and Sustainable Energy Reviews*, vol. 31, pp. 622–638, 2014.

[27] H. Chen, D. Y. Goswami, and E. K. Stefanakos, "A review of thermodynamic cycles and working fluids for the conversion of low-grade heat," *Renewable and Sustainable Energy Reviews*, vol. 14, pp. 3059–3067, 2010.

[28] B. F. Tchanche, M. Pétrissans, and G. Papadakis, "Heat resources and organic rankine cycle machines," *Renewable and Sustainable Energy Reviews*, vol. 39, pp. 1185–1199, 2014.

[29] X. Zhang, M. He, and Y. Zhang, "A review of research on the kalina cycle," *Renewable and Sustainable Energy Reviews*, vol. 16, no. 7, pp. 5309–5318, 2012.

[30] S. Spoelstra, "Thermoacoustic heat pump for upgrading industrial waste heat," tech. rep., Energy research Centra of the Netherlands (ECN), 2007.

[31] B. F. Tchanche, G. Papadakis, G. Lambrinos, and A. Frangoudakis, "Fluid selection for a low-temperature solar organic rankine cycle," *Applied Thermal Engineering*, vol. 29, no. 11, pp. 2468–2476, 2009.

[32] A. P. S. Wheeler and J. Ong, "The role of dense gas dynamics on orc turbine performance," in *ASME Turbo Expo 2013: Turbine Technical Conference and Exposition Volume 2: Aircraft Engine; Coal, Biomass and Alternative Fuels; Cycle Innovations*, (San Antonio, Texas), June 2013.

[33] S. Lecompte, H. Huisseune, M. van den Broek, B. Vanslambrouck, and M. De Paepe, "Review of organic rankine cycle (orc) architectures for waste heat recovery," *Renewable and Sustainable Energy Reviews*, vol. 47, pp. 448–461, 2015.

[34] J. Harnick, *Super- and Transcritical Fluid Expansions for Next-Generation Energy Conversion Systems*. PhD thesis, T U Delft, 2010.

[35] H. Öhman and P. Lundqvist, "Theory and method for analysis of low temperature driven power cycles," *Applied Thermal Engineering*, vol. 37, pp. 44–50, 2012.

[36] T. Ho, S. S. Mao, and R. Greif, "Increased power production through enhancements to the organic flash cycle (ofc)," *Energy*, vol. 45(1), pp. 686–695, 2011.

[37] F. Heberle, M. Preissinger, and D. Bruggemann, "Zeotropic mixtures as working flu-

ids in organic rankine cycles for low-enthalpy geothermal resources," *Energy*, vol. 37, pp. 364 – 370, 2012.

[38] M. Chys, M. van den Broek., B. Vanslambrouck., and M. D. Paepe, "Potential of zeotropic mixtures as working fluids in organic rankine cycles," *Energy*, vol. 44, pp. 623–632, 2012.

[39] "Spot prices, crude oil in dollars per barrel, products in dollars per gallon," April 2015.

[40] R. Bertani and J. Lund, "World energy resources: 2013 survey," Tech. Rep. 23rd Edition, World Energy Council, October 2013.

[41] U. D. of Energy and C. Change, "The future of heating: A strategic framework for low carbon heat in the uk," March 2012.

Chapter 2

Modelling Organic Rankine Cycles, The Thermodynamic Perspective

2.1 Introduction

The first step in establishing the feasibility, or otherwise, of an Organic Rankine Cycle (ORC) Waste Heat Recovery (WHR) system is to quantify the energy recovery possible for a given application. A huge amount of literature has been published that uses theoretical models of ORC systems, the key findings of these studies are summarised in a literature review in section 2.2.

An analytical model capable of modelling the thermodynamic performance of ORC systems is developed and described in section 2.3. The model was developed in order to calculate heat recovery and performance of ORCs between the available heat source and sink streams, as in a practical WHR scenario. The model is then used to evaluate the potential heat recovery from three waste heat sources. The calculations are used to further understand the operation and optimal design of ORC systems by identifying common features for optimal ORC design over a range of energy scales.

The model is used to compute possible ORC configurations given bounding heat source and sink streams. Calculations are carried out for pure fluids and then fluid mixtures to asses their potential to improve ORC system performance, section 2.4.

Much of the work presented in the chapter has also been published as a peer reviewed paper [1].

2.2 Literature Review

In this chapter the thermodynamic performance of organic Rankine cycles are modelled with the aim of understanding how ORCs are best designed to optimise heat recovery. A representative selection of the available literature on modelling and optimising the thermodynamic performance of organic Rankine cycles will be reviewed.

The salient difference of the ORC compared to the conventional steam Rankine cycle is the working fluid. While steam Rankine cycles use water (steam), ORCs might use one of a number of potential organic working fluids, or even a mixture of several. Each organic fluid has different thermophysical properties and therefore yields different cycle performances. This has led to numerous studies on fluid selection for organic Rankine cycles, [2–8].

Hung et al. [7] published one of the first studies to try and identify the most appropriate organic Rankine cycle working fluid. Subcritical Rankine cycle calculations are carried out with the fluids R11, R12, R134a, R113, benzene and ammonia. The thermodynamic properties of the working fluids are used to define the range of operating temperatures and pressures of the Rankine cycle. No heat source or sink conditions are defined or calculated. A parametric study of condenser outlet temperature, turbine inlet temperature and turbine inlet pressure is carried out. Hung et al. recommend isentropic fluids as being most appropriate to recover low temperature waste heat, in a later publication by the same author, this recommendation is altered to wet fluids with a steep vapour saturation curve [8]. It is shown that cycle efficiency increases for wet fluids and decreases for dry fluids with an increase in turbine inlet temperature. A trend of increase in irreversibility and increase in efficiency with turbine inlet temperature is identified. Increase in condenser exit temperature reduces the cycle efficiency so, Hung et al. concluded atmospheric conditions have an important influence on cycle performance.

Maizza and Maizza [5] investigated the potential of 21 organic fluids for use in WHR

ORCs. The authors identify the following properties as desirable in an ORC fluid: high latent heat, low liquid specific heat, an ability to operate in a moderate pressure range (0.1 - 2.5 MPa) and is isentropic, these properties align with those identified in other studies in Table 2.1. In contrast to Hung et al. [7], this study uses heat source and sink temperature to provide thermodynamic boundaries for ORC operation. The study produces a set of graphs which show the thermal efficiencies for ORCs at a variety of condensing and vaporisation temperatures for each fluid. The authors suggest these might provide a quick reference to optimal cycle parameters. R123 and R124 are recommended as working fluids because they allow high efficiencies to be achieved over a large range of operating conditions. However, this type of analysis is only appropriate for the vaporisation and condensation temperatures considered.

Publications [5, 7] refer to ORCs in WHR applications, yet only consider the performance of the cycle via thermal efficiency. In WHR situations, where fuel economy is not a consideration, cycles should be optimised for maximum work output and therefore additional analysis is required to verify the value of the working fluids these studies recommend. Similarly the studies do not fully define the heat source and condensing streams. This means that the thermal recovery from the available heat source is not evaluated, this is important as in a realistic WHR scenario, the system would be designed for optimal power output using the available source and sink heat streams.

Saleh et al. [3] screen 31 fluids in ORC which operate between 30 - 100 °C with a maximum pressure of 20 MPa . The combined thermal efficiency is calculated for a variety of ORC configurations, cycles are defined by the vaporisation process and gradient of the vapour saturation line. Pinch point analysis is carried out for the heat source stream and the heat source is limited to 120 °C. The analysis shows that the inclusion of an internal heat exchanger may increase the thermal efficiency of the cycle where the working fluid is superheated at the turbine exit. Despite running calculations for many different fluids general conclusions from these simulations are limited. The authors identify fluids with a low critical temperature as being more suited to supercritical cycles, while higher critical

temperatures yield higher cycle efficiencies with superheated subcritical cycles.

Similaly Tchanche et al. [4] present a study where 20 fluids are simulated in ORCs for low-temperature solar applications . Efficiencies, volumetric flow rate, mass flow rate, pressure ratio, environmental and safety variables are compared to select the most appropriate fluid. Tchanche et al. conclude that no fluid fulfils all of the desired criteria but recommend R134a as most suitable followed by R152a, R290, R600 and R600a for use in ORC systems with heat source <90 °C. No general conclusions about fluid selection are made in this study.

Chen et al. [2] present a screening study of working fluids and propose criteria for ORC fluid selection . The value of 35 potential fluids are analysed based on the identified criteria without requiring full ORC simulations. Chen et al. also identify that there is no single fluid which meets all the criteria they define for different source heat temperatures. Critical temperature and gradient of the vapour saturation line are identified as the most important parameters that might indicate the most appropriate operating temperature and cycle configuration for a working fluid. Plots of critical temperature vs the inverse gradient of the vapour saturation curve are presented. These are then used to categorise fluids into groups according to their position in the plot. However, given vapour saturation lines are curved, the method by which this is calculated would alter the result and Chen et al. [2] do not define the method by which inverse vapour saturation gradient is calculated in their study. Therefore this variable should be used cautiously.

Stijepovic et al. [6] model subcritical ORCs with just two working fluids, n-Butane and n-Pentane. The study produces maps of the working fluid properties against ORC performance criteria of thermal efficiency, exergy efficiency and heat exchanger size. Stijepovic identify molecular mass, compressibility ratio, specific heat capacity and density as working fluid properties that are most important to the performance of the cycle.

Key fluid properties for optimal ORC performance, as identified in [2, 5, 6], are shown in Table 2.1. Conclusions are generally in agreement with the exception of latent heat. Chen et al. acknowledge this disagreement in literature and conduct analysis by deriving the

Property	Chen et al.[2]	Stijepovic et al.[6]	Maizza and Maizza[5]
Latent Heat	high	low	high
Density	high (smaller equip)	high*	high
Specific Heat	low	either*	low
Wet/Dry/Isen?	Isentropic / dry	Isentropic / dry	Isentropic
critical temp	low for condensation	-	low
Molecular Mass	-	high*	-
compressibility	-	high*	-
critical pressure	-	low	low
viscosity	-	-	low
Cp liq	-	low	-
conductivity	-	high	high

Table 2.1: Table of desirable fluid properties for ORCs from literature

enthalpy change through the expansion stage to conclude higher latent heat is favourable [2]. The three studies all recognise the following as key parameters for fluid selection:

- gradient of the vapour saturation line
- specific heat
- density
- latent heat

However, Stijepovic and Maizza state fluid selection should be based on additional properties as well [5, 6]. These studies show there is no consistent method for fluid selection in ORCs. There is no one fluid that can fulfil all ideal criteria and that the heat source characteristics and optimal working fluid are strongly coupled.

Given the inherent link in performance between heat source and working fluid, numerous studies present thermodynamic modelling and analysis for specific applications. The following studies investigate the feasibility and optimal configuration of ORCs in a variety of applications, [9–12]. In general the studies characterise the heat source and other practical constraints to provide boundaries for computational analysis.

Roy et al. [9] carry out performance analysis for an ORC system with heat supplied from flue gas exhausts of boilers from a coal fired power station. The heat source is taken as 140 °C and 312 kg/s, temperature decrease is limited to 55 °C to prevent corrosive

compounds condensing out of the stream. The study assumes a supply of 20 °C water is available for the condenser and the mass flow rate required is calculated as part of the analysis. Standard thermodynamic relations are used to calculate the work output, thermal efficiency and second law efficiency of a subcritical ORC with and without superheat. Turbine inlet pressure is optimised for both thermal efficiency and work output for 3 working fluids, R-12 (isentropic), R-123 (dry) and R134a (wet). Roy et al. recommend R-123 as the most appropriate working fluid for low-grade heat sources as it yields the largest work output and efficiencies of the fluids modelled. This is not surprising given R-12 and R-134a have critical temperatures of 112.04 °C and 101.06 °C respectively, these are lower than the critical temperature of R123 (183.79 °C). This means that the optimised cycles have a large amount of superheat, which as previous studies note, leads to inefficient cycles, or a very large pinch point temperature difference, meaning less waste heat is recovered from the heat source stream. R-123 is the optimal fluid for this study but further simulations with additional fluids is likely to give different results. Therefore R-123 may not be suitable for all low-grade heat source power generation applications.

Another theoretical study investigates the application of ORC systems in recovering energy from diesel Internal Combustion Engine (ICE) exhausts. Katsanos et al. [11] compare the operation of a Rankine cycle with water and R245ca as working fluids. It is found that heat recovered into the ORC decreases while the efficiency of the ORC increases with turbine inlet pressure. The Rankine cycle system at full load can produce 34 kW additional power using R245ca and 30 kW using water. The study concludes that the installation of a Rankine cycle system is valuable. The advantages of cycle configuration and working fluids are discussed but no optimal solution is proposed.

In a study by Jung et al. [10] eight different ORC fluids are used to determine the feasibility of an ORC supplied by heat from a stream of kerosene in a refinery. In this study the work output of the ORC is fixed at 250 kW. The kerosene heat source has a temperature of 115 °C, pressure of 8.4 bar, the temperature drop of the kerosene was fixed at 45 °C. A stream of cooling water was assumed to be available at 24 °C and

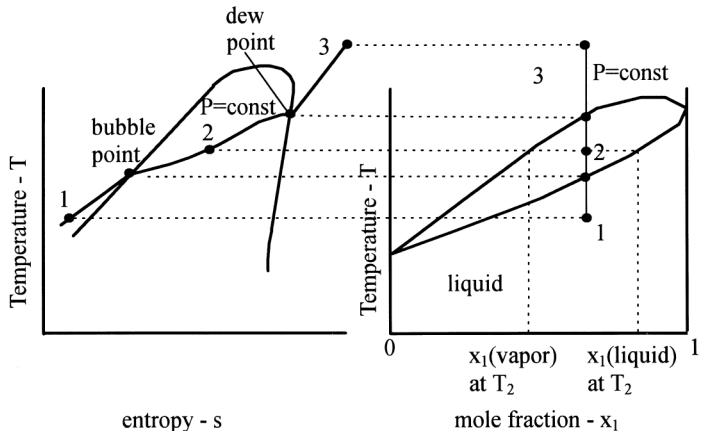

Figure 2.1: Isobaric phase change of a zeotropic mixture, after Angelino and Paliano [13]

5.6 bar. The mass flow rate of the kerosene is varied to control the heat available to the ORC. Isobutane is found to be the pure working fluid that give the greatest overall cycle efficiency of 6.8 %, while simulations show a butane/pentane mixture may allow a cycle efficiency of 7.6 % to be achieved. Both of these scenarios use less than half of the available mass flow rate of kerosene. An initial economic analysis suggests a payback period of 6.8 years would apply for a capital outlay of 3000 $/kW. However, given no fuel economy constraints apply, selection of the ORC design based on efficiency may not give the optimal system. Results show 5 of the fluids selected give similar work output performance, therefore the next stage in analysis would be to asses the impact of working fluid selection on size of ORC system and cost.

The previous studies cited all show ORC have the potential to increase the overall efficiency of various systems, however their uptake is in general low as discussed earlier in Section 1.5. One way to increase the heat recovered in the ORC is the use of zeotropic mixtures as working fluids. The definition of a zeotropic mixture is that the vapour and liquid compositions are never equal, as explained in section 1.4. This results in the temperature of a zeotropic mixture changing during phase change, this is known as a glide and is illustrated in Figure 2.1.

The use of working fluid mixtures in thermodynamic cycles has been proposed many times in literature previously. Rachermacher published a study in 1989 [14] showing how

mixed working fluids might influence Rankine cycle performance. Radermacher evaluated the influence of zeotropic fluid mixtures on various Rankine cycles. Zeotropic mixtures reduce the difference between the temperature profile in a heat exchange process, so the amount of heat recovered into and out of the cycle is larger and the overall cycle efficiency is increased. However, Radermacher identified that experimental results do not match those predicted in literature. This is due to the fact that zeotropic mixtures have non-linear temperature profiles, which is not captured in theoretical analysis, and that the heat transfer coefficient is reduced in comparison to the pure components. The reduction in heat transfer coefficient is attributed to decreased thermal conductivity due to diffusion as the local concentration of the mixture changes during phase change. This means a larger heat exchange area, with economic implications, is required to achieve the same heat transfer as with a pure fluid.

Angelino and Colonna [13] present theoretical simulations of zeotropic mixtures in ORCs. The Wong and Sandler mixing rules are used to calculate thermodynamic properties of siloxane and hydrocarbon mixtures. Angelino and Colonna demonstrate that zeotropic mixtures appear beneficial from their theoretical ORC model, but state it is only useful for initial estimates and suggest that more accurate models are required. This study also notes the potential practical issues associated with fluid mixtures, for example, fractionation in heat exchangers which would further complicate system design.

Herberle et al. [15] published a study on implementing zeotropic mixtures in ORCs using heat supplied from low-enthalpy geothermal resources, 80 - 180 °C at 65.5 kg/s. The mixtures R227ea/ R245fa and isobutane/isopentane were modelled in subcritical ORCs and compared to the performance of the pure working fluids. Second law efficiency of the cycle is calculated as a function of fluid composition and source temperature. This study found that zeotropic mixtures offer second law efficiency increase in comparison to pure fluids, and are of largest benefit in the condensation process.

Aside from cycle performance benefits, Herberle et al. suggest further benefits may come from adjusting cycle composition for environmental, safety or chemical reasons and

that fluid mixtures permit a larger variation in ORC systems.

In a similar study Chrys et al. [16] use first law analysis to investigate zeotropic mixtures in subcritical Rankine cycles. Eleven zeotropic mixtures were simulated as working fluids for heat sources of between 150 - 250 °C. The study showed that maximum power output occured for the concentration with the largest temperature glide. Chrys et al. concluded that zeotropic mixtures have a positive effect on ORC performance; for example an increase of 15.7 % in cycle efficiency and 12.3 % in power output, was calculated for a heat source of 150 °C. Zeotropic mixtures are shown to be less beneficial for higher temperature heat sources; e.g. for a heat source of 250 °C an increase of only 6 % for cycle efficiency and 5.5 % power output was calculated.

The lack of existing tools to model zeotropic mixtures theoretically with any accuracy and data from experiments to validate simulations are highlighted by Angelino, Radermacher and Chrys, [13, 14, 16]. Radermacher, Hereberle and Chrys all acknowledge the heat transfer coefficient is known to decrease for fluid mixtures. However no study has captured this effect and investigated to what extent in may impact on the potential benefits from using fluid mixtures.

2.3 ORC Analytical Model

A thermodynamic model of the organic Rankine cycle has been developed in the present study. The model is designed to accept source and sink heat stream parameters as inputs. Possible organic Rankine cycles are then calculated bounded by heat source and sink conditions. The ORC cycle parameters of turbine inlet pressure, working fluid mass flow rate, degree of superheat and working fluid, are all variables that can be changed.

The model is written in MATLAB using fluid thermodynamic and transport properties databases to calculate fluid properties as required. Standard thermodynamic relations are used to calculated the ORC cycle, as described in section 2.3.2. A novel method of pinch point analysis is used to quantify the amount of heat transferred into and out of the cycle as described next in, section 2.3.1.

2.3.1 Novel Pinch Analysis Method

This study uses pinch analysis as a method to calculate the heat exchange possible in the condenser and evaporator. A realistic estimation of the heat transfer is calculated from defined heat source and heat sink streams and a minimum temperature difference between the external heat source and heat sink streams and the cycle working fluid.

Pinch Analysis was initially developed by Bodo Linhoff [17] in 1977 as a method of optimising process heat integration in industrial applications. The use of process-to-process heat recovery is maximised by this method, with the aim of minimising the fuel requirement of industrial systems and therefore saving money. Today pinch analysis is commonly used in thermodynamic analysis of heat recovery systems, to predict the quantity of heat that can be recovered given physical limits. This information is then used to design heat exchanger networks.

Pinch analysis is applicable to counter flow heat exchangers. By assuming no heat is lost to surroundings, the governing equation of the heat transfer for two counter current streams is given by the the Steady Flow Energy Equation (SFEE) [18] as:

$$Q_{TOT} = \Delta H_1 = \Delta H_2 = \dot{m}_1 \Delta h_1 = \dot{m}_2 \Delta h_2. \tag{2.1}$$

Subscripts 1 and 2 indicate different streams and Q_{TOT} indicates the total heat energy transferred between the two streams. Equation 2.1 shows that the total enthalpy exchanged across both heat streams must be equal. In pinch analysis this is often represented on T-H plots, for example as in Figure 2.3. The smallest difference in temperature between the external flows and the cycle working fluid is called the pinch point temperature difference. This cannot be less than zero as this would reverse the heat flux between the fluids exchanging the heat.

The pinch point temperature difference is the limiting point in heat exchanger design. Practically it represents cost and heat exchanger area. A pinch point temperature of

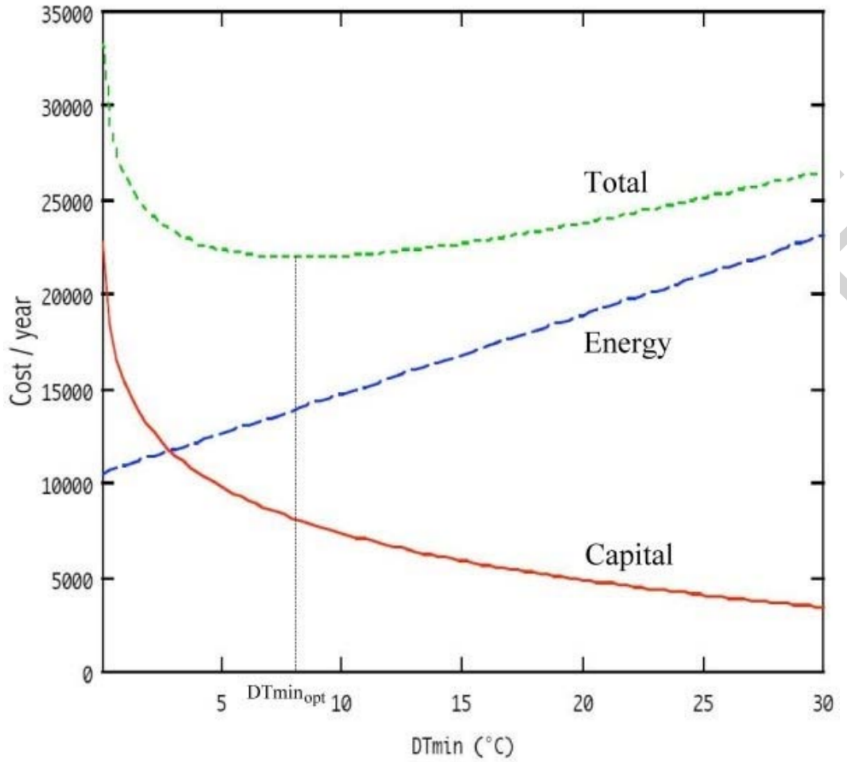

Figure 2.2: Graph of total cost, capital cost and energy transferred against pinch point temperature difference [17]

zero represents infinite heat exchange area, and therefore infinite cost. The influence of the pinch point temperature difference is shown in Figure 2.2. This figure also shows that pinch point temperature differences of 5 - 10 °C offer the best compromise between energy recovery and heat exchanger size/cost. This is corroborated by Quoilin in a report on ORC design [19]. Therefore, a pinch point temperature difference of 5 °C is chosen throughout this study.

The ORC model has been designed to allow cycle optimisation within the boundaries defined by the available operating conditions. The waste heat source and heat sink conditions are inputs to the model and the heat exchange problem solved using the model. An example of heat exchange in an evaporator caluclated using the model is shown in Figure 2.3.

The working fluid, mass flow rate and input temperature and pressure of each stream are known. Negligible pressure drop in the heat exchanger is assumed. Identifying the position of the pinch point allows the changes in enthalpy and temperature along the fluid

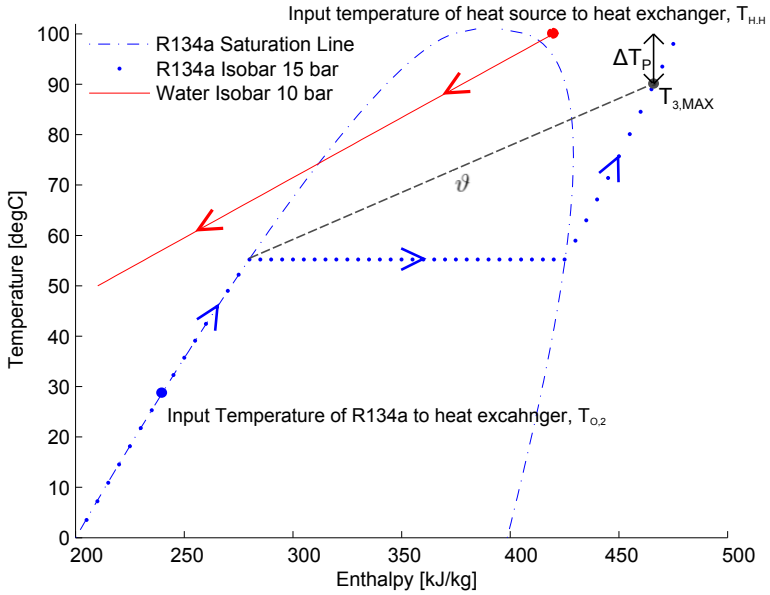

Figure 2.3: Example pinch analysis, mass flow rate of each stream is 1 kg/s

streams in the heat exchanger to be predicted.

An automated method for directly calculating the location of the pinch point from the Temperature-Enthalpy (T-H) profiles of the fluid streams has been developed. This novel approach is advantageous as it is computationally fast. The pinch analysis is carried out using straight line approximations of both fluid streams for the temperature-enthalpy profiles. For the evaporator, the maximum temperature of the working fluid is (using the Nomencalture from Figure 2.4):

$$T_{3,MAX} = T_{S,H} - \Delta T_{PP,Evap}. \tag{2.2}$$

The difference between $T_{3,MAX}$ and $T_{sat,liq}$ divided by the enthalpy change between these two points define a gradient,ϑ. This is shown in Figure 2.3 and calculated from:

$$\vartheta = \frac{T_{3,MAX} - T_{liqsat}}{\dot{m}(h_{3,MAX} - h_{liqsat})} \tag{2.3}$$

Gradient, ϑ, is used in a series logical statements to identify the location of the pinch point. For example, should the T-H gradient of the hot stream, $\frac{dT}{dH}$, be shallower than ϑ, then the pinch point must be at the inlet of the hot stream, $T_{H,H}$. Similarly, if the

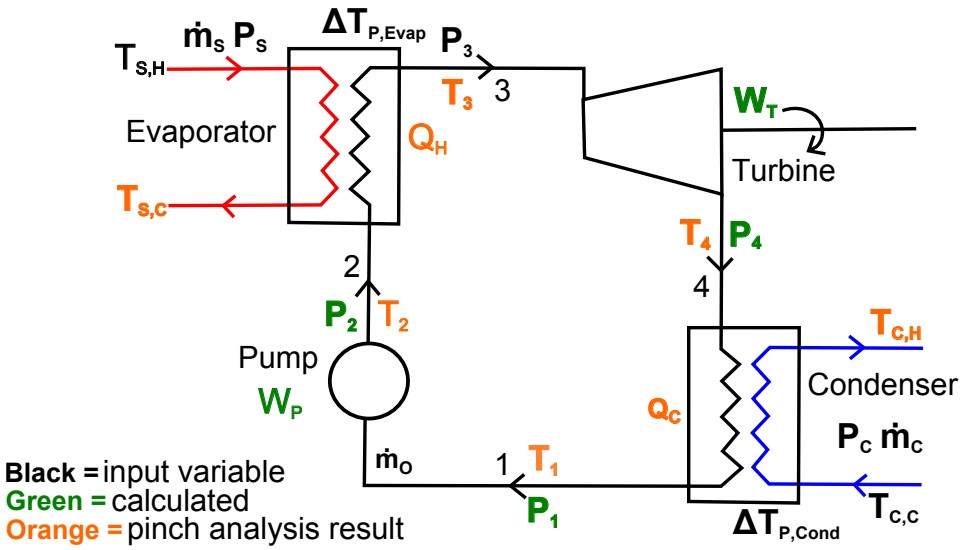

Figure 2.4: Schematic diagram of Rankine cycle showing variables using in analytical model

T-H profile of the hot stream is steeper than ϑ, the location of the pinch point is at the coolest point or liquid saturation point of the working fluid. The gradient of the liquid saturation curve of the working fluid is then compared to the T-H gradient of the source heat to determine the location of the pinch point.

After the process of gradient comparison is carried out. The adjusted T-H profiles are compared to check the pinch constraint is upheld. In some scenarios, for example where the liquid saturation curve is very curved, the pinch point may need to be adjusted.

An identical method is used to calculate the condenser heat exchange process. The temperature changes of the fluids over the heat exchangers are not fixed in this analysis. Rather, the pinch point analysis determines the maximum temperature drop and, thus, the amount of heat transfer possible, for the specified pinch point temperature differences.

2.3.2 Thermodynamic Model Relations

A model has been developed to evaluate ORC performance for any waste heat source and heat sink combination. A schematic diagram of a Rankine cycle is shown in Figure 2.4. The model is capable of simulating organic cycles of any type, ranging from Trilateral Flash Cycle (TFC)s through to subcritical cycles operating with superheated vapour

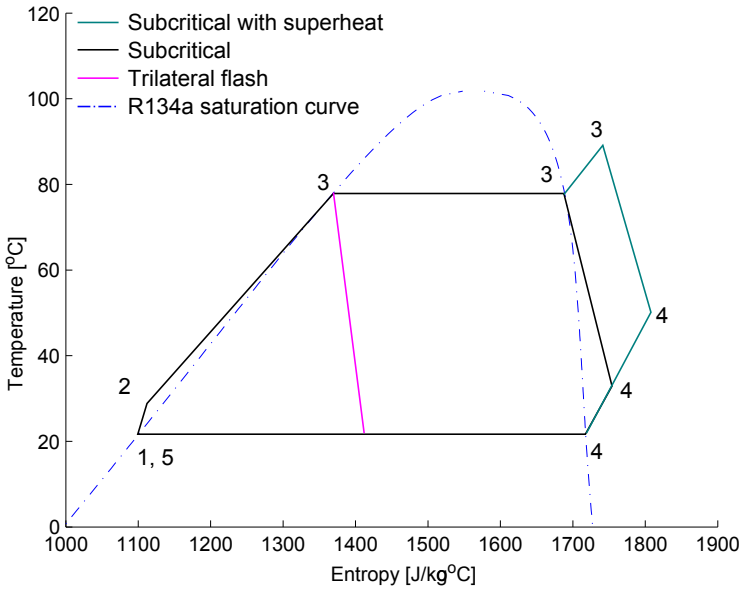

Figure 2.5: Temperature Entropy plots of different Rankine cycles modelled in this study

throughout the expansion through the turbine (Figure 2.5). The model has been designed for maximum flexibility. Therefore, any heat sink and source flow stream can be specified and any ORC cycle can be simulated within user prescribed operating limits. Standard thermodynamic heat-balance relations have been used to describe the pump, and turbine.

Pump work (W_P) is calculated from the pressure rise across the pump, ΔP. It is related to the specific enthalpy increase of the working fluid passing through the pump, by the steady flow energy equation:

$$W_P = \dot{m}_O \frac{\Delta P}{\eta_P \rho} = \dot{m}_O (h_2 - h_1). \tag{2.4}$$

The subscripted numbers refer to a location in the cycle, as indicated in Figure 2.4. The work output from the turbine W_T is related to the isentropic enthalpy rise across the turbine according to:

$$W_T = \eta_T \dot{m}_O (h_3 - h_{4,I}). \tag{2.5}$$

Where η_T is the isentropic efficiency of the turbine. The specific enthalpy at exit of the turbine, h_4 is then calculated by:

$$h_4 = h_3 - \frac{W_T}{\dot{m}_O}. \tag{2.6}$$

This study is focused on ORC in WHR and geothermal applications where fuel economy is not a consideration. Therefore, from a thermodynamic perspective, the optimal cycle is that which produces the most work output. This is in contrast to applications where fuel economy is relevant and the most thermally efficient cycle is the most appropriate. Therefore, the initial analysis considers the net work output, heat input and thermal efficiency as calculated by equations 2.1, 2.7 and 2.8.

$$W_{NET} = W_T - W_P. \tag{2.7}$$

$$\eta_t = \frac{W_{NET}}{Q_{TOT}} \tag{2.8}$$

2.3.3 Cycle Algorithm and Constraints

The pinch method and thermodynamic relations, as described in sections 2.3.1 and 2.3.2 respectively, are implemented in the model as shown in the flow chart in Figure 2.6. Initially the condenser pressure of the working fluid is estimated. Pinch point analysis is performed in an optimisation function to find the condenser pressure which satisfies the cooling stream characteristics. The working fluid is defined as a saturated liquid at output of the condenser.

The cycle calculations assume steady state conditions of all components. Additionally heat loss to the surroundings and pressure drops through the heat exchangers are neglected. Within the model some variables must be defined or constrained to bound the number of possible solutions. The isentropic efficiency of the turbine and the pump are fixed at 0.8 and 0.65, respectively, as reasonable estimates of component efficiencies in accordance with [15]. The dryness fraction of the working fluid at the exit of the turbine is limited to a minimum of 75 %. At lower vapour qualities, the vapour is considered too wet to ensure the mechanical integrity of the turbine. Turbine exit vapour quality

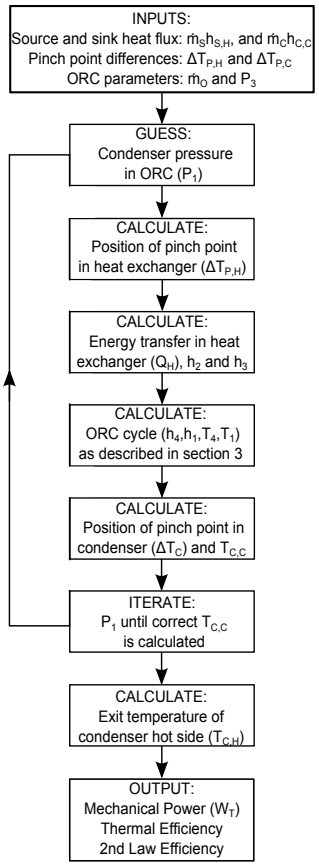

Figure 2.6: ORC Thermodynamic Model Algorithm

is therefore one of the parameters that defines the design space within which meaningful cycle simulations can be carried out using the model.

The mass flow rate and Turbine Inlet Pressure (TIP) of the ORC must be constrained to provide practical limits for the ORC configurations. An upper limit for TIP of $0.8P_{crit}$, where P_{crit} is the critical point pressure, was set in order to limit the uncertainty associated with thermodynamic properties calculated at the critical point, in accordance with Herberle at al. [15]. A lower limit of 5 % of the critical pressure was also selected to ensure that the condenser vacuum always remained within practically achievable limits. Therefore, cycle calculations were only carried out for TIP values in the range of $0.05P_{crit} > TIP < 0.8P_{crit}$.

Parameter	Aneke et al. [12]	Present Model	Relative Error %
Geothermal fluid mass flow rate (kg/s)	33.39*	33.39*	-
Geothermal fluid temperature (°C)	73.33*	73.33*	-
Cooling water mass flow rate (kg/s)	101.68*	101.68*	-
Cooling water source temperature (°C)	4.44*	4.44*	-
Working fluid	R134a*	R134a*	-
Turbine Isentropic efficiency	0.8*	0.8*	-
Turbine inlet pressure (bar)	16.95*	16.95*	-
Turbine outlet pressure (bar)	4.39*	4.39	0
Gross generator power (kW)	250*	249.15	-0.34
Pump power (kW)	40*	39.27	-1.83
Pump efficiency	0.305* inferred	0.305*	-
Generator Efficiency	0.96* inferred	0.96*	-
Geothermal exit temperature (°C)	54.94	55.16	+0.40
Cooling water exit temperature (°C)	9.91	9.78	+0.20
Working fluid mass flow rate (kg/s)	11.99	11.99*	-
Net plant power (kW)	210	209.88	-0.48
Thermal efficiency	0.08	0.083	+3.75
Evaporator heat transfer rate (kW_{th})	2570.38	2540.9	-1.15
Condenser heat transfer rate (kW_{th})	2327.1	2282.5	-1.92
Evaporator pinch size (°C)	1* inferred	1*	-
Condenser pinch size (°C)	2* inferred	2*	-

Table 2.2: Cycle properties from the model used by Aneke et al., [12] and the model used in this study

2.3.4 Validation of Model

Aneke et al. [20] compared the performance of a model written using IPSEpro, with REFPROP 7.0 to calculate fluid properties, with real data from the Chena binary geothermal power plant. The cycle parameters used in their simulations have been input into the model developed in this study. The results of both the simulations are shown in Table 2.2.

The net power output and thermal efficiency of the cycles differ by -0.48 % and +3.75 % respectively. Indicating that the results from both models agree closely despite very different modelling approaches. The original method by Aneke et al. requires the power produced by the ORC to be defined as an input to fully define the thermodynamic cycle. While pinch point analysis is used in this study, the model developed allows the power output and heat available to the ORC to be calculated.

The results presented in Table 2.2 show results from the latest version of the ORC

model developed in the study. This model uses REFPROP 9.0 to calculate the fluid properties. When the original study [1] was published, the fluid properties calculator FluidProp was used in the model [21]. The fluid properties calculator was changed to REFPROP part way through the study to allow the calculation of properties of fluid mixtures, [22]. The original model developed using FluidProp, also agreed closely with results from the model of Aneke et al. The net power and thermal efficiency agreed within +2.03 % and +3.22 %.

2.3.5 Fluids Modelled

A limited range of fluids have been selected to use as working fluids in the cycle calculations. The selection has been purposely constrained in order not to become a study on the optimal working fluid. This study aims to look at the trends in ORC performance with change in ORC configurations.

Tchanche et al., [23] grouped fluids according to the temperature of heat source that they are appropriate for use with. Given that heat sources with a range of energy scales are modelled, a few fluids appropriate for each heat band have been selected for this study. R32, Propane, R134a, and n-Butane were selected as they are appropriate for low temperature heat sources. Fluids appropriate for medium heat sources are R123 and n-Pentane. Cyclo-hexane, n-octane and toluene are appropriate for high temperature heat sources. The saturation curve for each of these fluids is shown on Figure 2.7.

The molecular mass, critical point data and inverse gradient of the vapour saturation line for each of the fluids used in the calculations are shown in Table 2.3. A negative inverse vapour saturation curve indicates a wet fluid, positive indicates a dry fluid and zero is isentropic. The inverse gradient of the vapour saturation line is calculated using REFPROP between 5 % and 80 % of the critical pressure for each fluid. There is some discrepancy with the calculated values and those published by Chen et al. [2] due the the vapour saturation line being curved.

In accordance with the literature discussed above, dry fluids and wet fluids with a steep gradient are used.

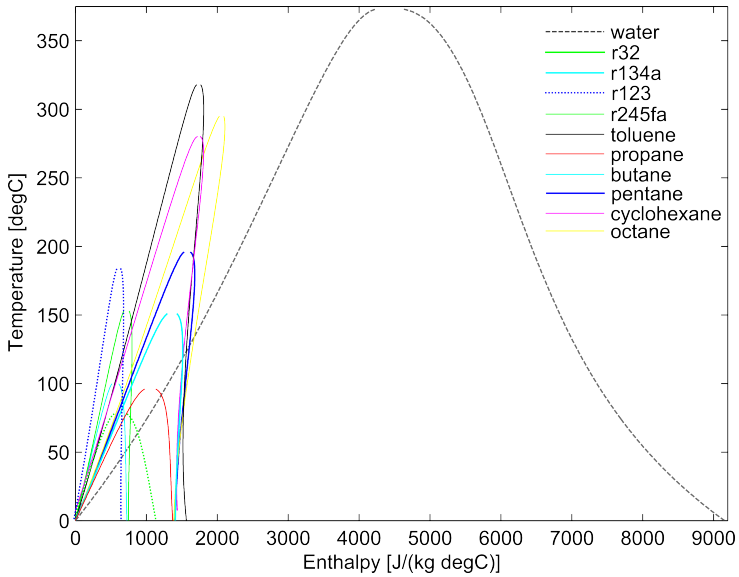

Figure 2.7: T-S saturation plots of fluids modelled

Fluid	Molecular Mass [g/mol]	Critical Temperature [°C]	Critical Pressure [bar]	Inverse Vapour Saturation Gradient ($\frac{ds}{dT}$) [kg°C^2/J]	Classification
Water	18.0153	373.95	220.64	-8.29	wet
R32	52.0240	78.1050	57.82	-4.16	wet
R134a	102.0320	101.06	40.59	-0.67	isentropic
R123	152.9310	183.68	36.62	0.22	dry
R245fa	134.0479	154.01	36.51	0.36	dry
Pentane	72.1488	196.55	33.70	1.70	dry
Octane	114.2290	296.17	24.97	2.92	dry
Toluene	92.1384	318.60	41.26	1.40	isentropic
Cyclohexane	84.1595	280.45	40.81	1.98	dry
Butane	58.1222	151.98	37.96	0.74	dry
Propane	44.0956	96.74	42.51	-1.34	wet

Table 2.3: Fluid properties of working fluids used in this study

2.3.6 Heat Sources and Sinks

The three heat source used as case studies in the work described in this chapter are exhaust heat from Heavy Duty (HD) ICEs, coproduced hot brine from petroleum wells and industrial process waste heat. These sources have been introduced in section 1.2.2. The precise waste heat characteristics used as inputs to the ORC cycle model, are shown in Table 2.5.

In the case of waste heat from engine exhausts, the characteristics of the exhaust heat steam are taken from a study by Katsanos et al. [24]. This study uses data from a six-cylinder heavy-duty two stage turbocharged truck diesel engine, which is downsized from a full sized truck engine. The exhaust gas is modelled as a gas mixture with a composition

Fluid	Composition %
Nitrogen	74.2
Carbon Dioxide	9.1
Oxygen	9.3
Water	9.1

Table 2.4: Composition of flue gas mixture by mass

Case	Mass Flow Rate, $\dot{m}_S$ [kg/s]	Temperature, $T_{S,H}$ [°C]	Pressure, P_S [bar]	Condenser Temperature $T_{C,C}$ [°C]
Fully Loaded Diesel Engine, exhaust	0.4945	397.8	1	40
Ninian oil field, coproduced brine	1231.3	102	3	8
Industrial Processing Plant, saturated steam	31.94	140	2.3	20

Table 2.5: Characteristics of waste heat sources used in this study

as shown in Table 2.4 in accordance with that used by Vaja et al. [25]. The temperature of the heat source is decreased from 397.8 °C to 326 °C to be within that allowable by the fluid property database, REFPROP. This is in agreement with a study by Vaja et al. [25]. The condenser temperature is set at 40 °C in accordance with both the Vaja and Katsanos studies [24, 25].

Data for hot brines extracted as a byproduct from petroleum production was available for a large number of fields in the Brent Province in North Viking Graben. Mass flow rate raw data is available from Department of Energy and Climate Change (DECC) and temperature data was taken from a study by Gluyas and Hitchens [26]. The Ninian field has been taken as an representative field for this section. The condenser temperature has been set at 8 °C, the average temperature of the North Sea. The case of implementing ORCs in the North Sea is revisited in more detail in Chapter 6.

The example of industrial waste heat is taken from a typical plant supplying steam and electricity to surrounding large chemical processing units on the Wilton site in Teesside. In this plant, steam from a gas and biomass fuelled boiler is used to produce thermal and electrical energy. Several streams of waste heat are available on the site, including flue gas, low pressure and intermediate pressure steam. The potential power production from an ORC fed by a single stream of low pressure waste steam is explored in this section.

The fluid in the cool side of the condenser is water in all the calculations presented in

this chapter. The mass flow rate was fixed at 5 times the mass flow of the ORC working fluid in all cases, as an arbitrary but reasonable definition of the cooling stream mass flow rate in line with the assumptions used by other workers.

2.4 Results and Discussion: Pure Working Fluids

2.4.1 Results and Discussion for Pure Working Fluid Simulations

Simulation results were obtained using the cycle model described in Section 2.3 for each waste heat stream presented in Table 2.5. In order to understand the influence of TIP, the mass of rate of ORC working fluid was constrained to 60 % of that of the heat source stream. The quantity of heat input into the cycle, cycle efficiency and work output for each TIP is examined. There is no data for pressures where there is not a calculable cycle within the constraints described in section 2.3.3, or outside the physical limits of the working fluids imposed by REFPROP.

Figure 2.8 shows thermal efficiency, heat input and mechanical work output against TIP for geothermal brines produced from the Ninian oil field. By comparing the figures it is clear the maximum heat into the cycle, thermal efficiency and work produced by the cycle all occur at different TIPs. In general the thermal efficiency of the ORC increases with TIP, with a peak in efficiency for R134a and R245fa at 26.15 bar and 8.35 bar respectively. Conversely, heat taken into the cycle decreases with TIP with significant increase in gradient for R123, R245fa and R134a at 3.45 bar, 5.94 bar and 23.78 bar respectively. Figure 2.8c shows there are distinct maxima for the following fluids R123 at 4.25 bar, R134a at 20.06 bar and R245fa 5.94 bar. Butane and Pentane show an increase of work output with TIP while propane decreases slightly.

The existence of the work output maxima relates to the amount of heat that can be input into the cycle as the operating conditions change. The study by Aneke et al. [12] also shows similar results.

Figure 2.8a shows temperature against change in enthalpy plotted for the heat source

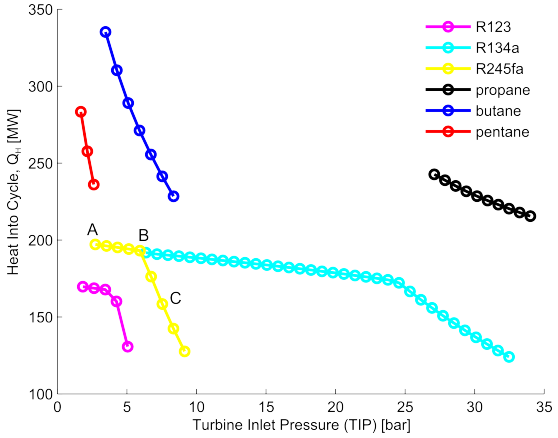

(a) Heat into ORC vs TIP

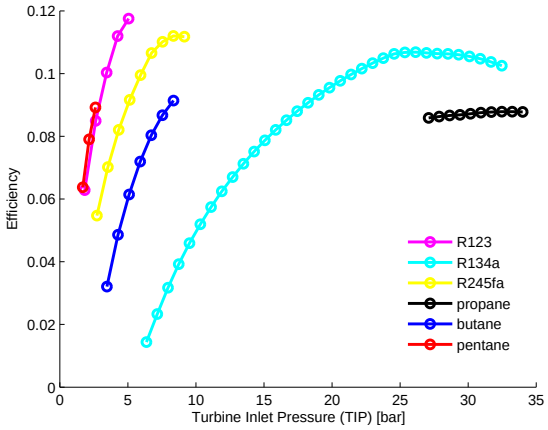

(b) Efficiency of ORC vs TIP

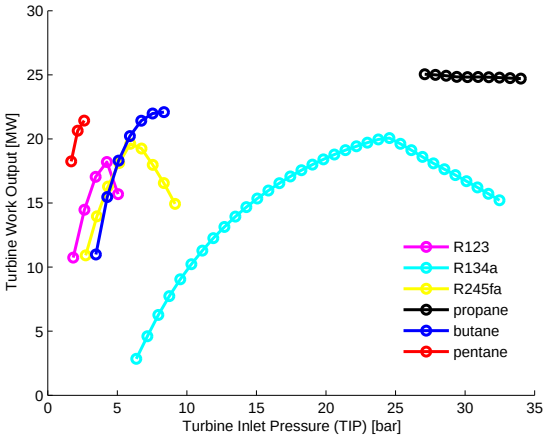

(c) Work Output of ORC vs TIP

Figure 2.8: Ninian oil field cycle simulations with mass flow rate constrained to $0.6\dot{m}_O$

and working fluid through the evaporator for the Ninian heat case with working fluid R245fa. The three plots shown, labelled A, B and C are from different TIP conditions as labelled in Figure 2.8. The heat exchange process is examined at TIPs below the maximum work output, cycle A, at the maximum work output, cycle B and at a TIP which is above the value for maximum work output, cycle C. These plots show that heat input decreases with increases in TIP, because a smaller temperature difference is achievable across the heat source steam. Heat into the cycle decreases more rapidly from cycle B to C than from A to B because the pinch point location has moved. In cycles A and B the pinch location is at the hot end of the heat exchanger, but as the TIP rises, the pinch point is forced to move to the liquid saturation point of the organic working fluid (cycle C in Figure 2.9). While heat into the cycle decreases with TIP, the thermal efficiency of the

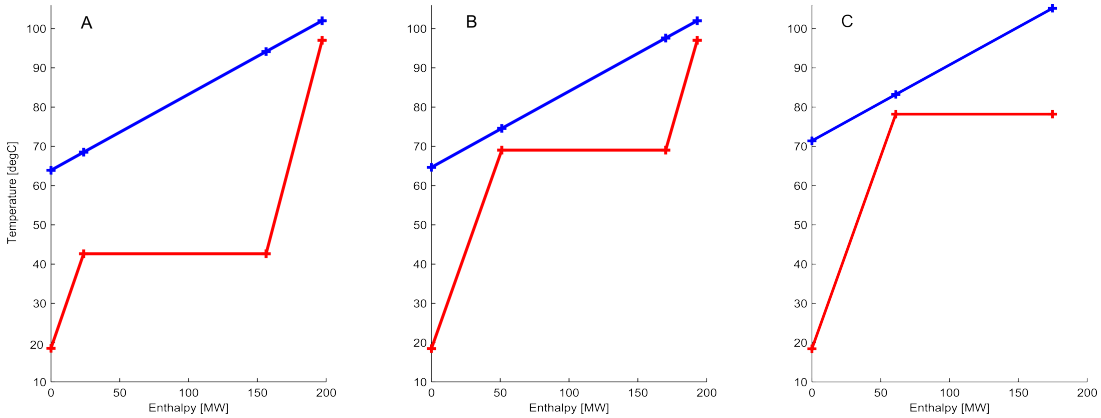

Figure 2.9: T-H Plots of Ninian Evaporator R245fa for cycles A, B and C as labelled on Fig 2.8c

cycle increases as the amount of superheating decreases, from cycle A to B. Cycle C is the most thermally efficient as it is in a subcritical cycle with no superheat.

A larger amount of work is produced by Cycle B compared to Cycle A, because the increase in efficiency outweighs the decrease in heat energy into the cycle. Work output is a trade-off between thermal efficiency and heat input into the cycle.

Figure 2.9, demonstrate that an optimum balance between heat input into the cycle and thermal efficiency of the cycle must be achieved, in order to maximise the work output.

Trends in cycle performance can be compared by considering Figures 2.8, 2.10 and 2.12. Some of the working fluids modelled in the hot brine and industrial waste steam cases show a curve that has an optimum TIP, where work output reaches a maximum. For example in the hot brines case the maximum mechanical work output is achieved at 25.59 bar for R134a and at 6.19 bar with R245fa as the working fluid. In the case of the diesel engine, Figure 2.12c, work output increases with TIP for all of the working fluids simulated. In all cases, the ORC configuration varies from subcritical or trilateral to superheated, but the optimum cycle configuration, with respect to work output, is not common in all cases.

The trend of these plots can be explained by examining the location of the pinch point and the effect this has on the heat input to the cycle, in each case. The pinch point analysis uses the T-H gradient of the heat source fluid compared with the gradient of

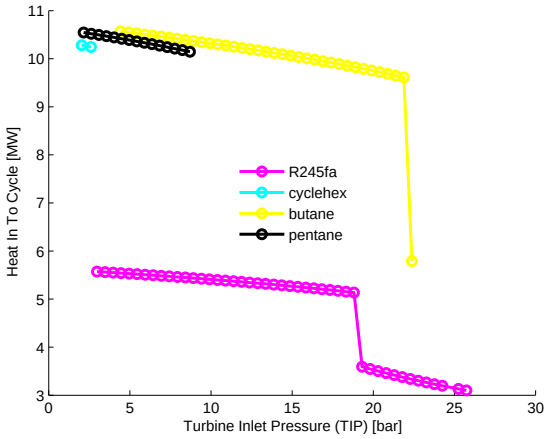

(a) Heat into ORC vs TIP

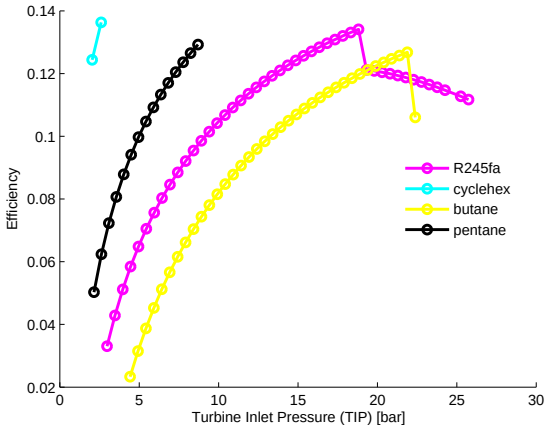

(b) Efficiency of ORC vs TIP

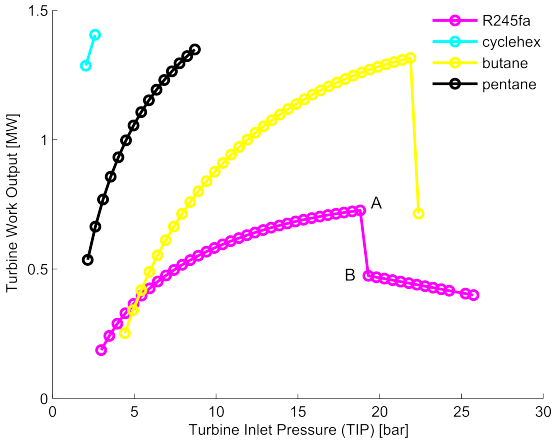

(c) Work Output of ORC vs TIP

Figure 2.10: Industrial steam case cycle simulations with mass flow rate constrained to $0.6\dot{m}_O$

the ORC working fluid, (Equation 2.3), to determine the location of the pinch point (see Section 2.3.1). In the case of the hot oil field brines with R245fa as the ORC working fluid, the gradient of the source heat fluid is less steep than the ORC working fluid gradient, as seen from Figure 2.9. This results in the pinch point being initially located at the highest temperature point of the ORC working fluid (i.e. heat exchanger exit/turbine inlet). The change in the location of the pinch point changes the rate at which the heat input to the cycle decreases with TIP, as seen in Figure 2.8a.

Similarly, in the case of industrial steam with R245fa ORC working fluid there is an optimum TIP for maximum work output after which the work output decreases, that is 18.81 bar for R245fa (Figure 2.10c) and for butane at 22 bar, while for the other fluids work output increases with TIP. Figure 2.10a shows how the rate of heat input into the

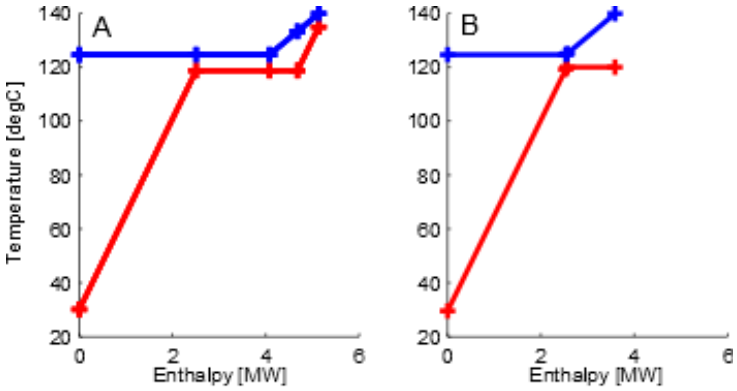

Figure 2.11: T-HPlots of Industrial case evaporator with R245fa working fluid for cycles A and B as labelled in Figure 2.10c

cycle decreases at the optimum TIP, 18.81 bar, in the same way as it did for the Ninian hot brines results (see Figure 2.8a). However, there is a significant discontinuity in both the plots of heat input and work output against TIP at the optimum TIP (Figure 2.10). This is not seen in the Ninian hot brine results. The change in the gradient of workout with TIP is due to the change in location of the pinch point in the same way as previously described for the hot brines case. The discontinuity is a result of the phase change of the heat source fluid. The phase change means that when the location of the pinch point moves from the hot end of the heat exchanger, Cycle A, (in Figure 2.11 and noted on Figure 2.10c) to the liquid saturation point of the ORC working fluid in Cycle B, much less heat can be taken into the cycle, see Figure 2.11. This is because for Cycle B, the heat input into the cycle is limited by the enthalpy change between the pinch point and hot temperature of the working fluid, which is quite small. Cycle B is close to a trilateral flash cycle and so may not be possible to implement practically. However, for this test case the results do show that it would be extremely detrimental to cycle performance if the TIP is taken above 18.81 bar with R245fa.

The remaining cases show an increase in work output with TIP. These cases are firstly, all the ORC working fluids simulated in the diesel engine case (Figure 2.12). Secondly, the ORC working fluids cyclohexane and pentane in the industrial steam case (Figure 2.10) and finally, pentane, butane, propane and R123 in the hot brines case (Figure 2.8).

As previously shown, the change in pinch point location can cause the rate of change

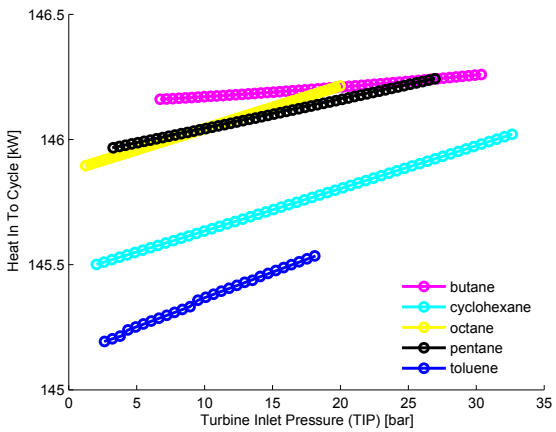

(a) Heat into ORC vs TIP

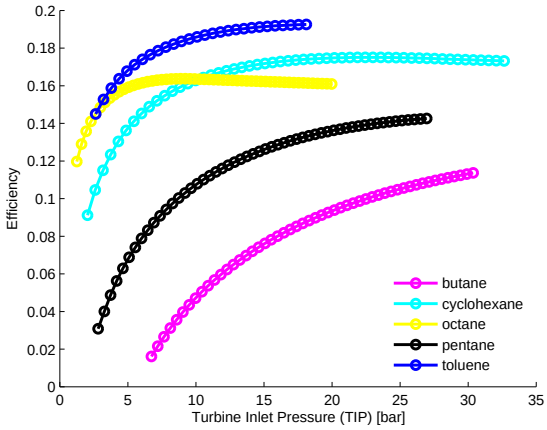

(b) Efficiency of ORC vs TIP

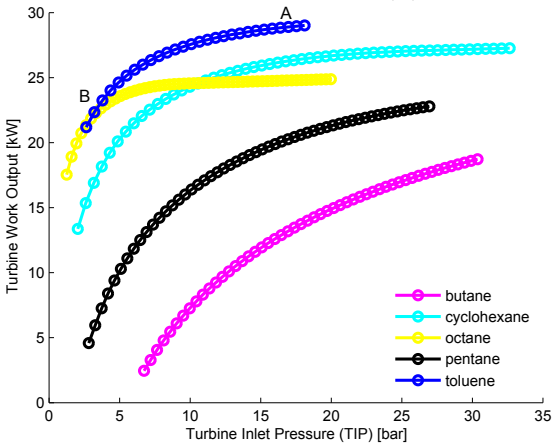

(c) Work Output of ORC vs TIP

Figure 2.12: Engine case cycle simulations with mass flow rate constrained to $0.6\dot{m}_O$

of heat input into the cycle to fall more quickly with TIP, causing work output of the cycle to also decrease. For these cases, the pinch point and therefore the rate at which the heat input to the cycle decreases with TIP does not change, as shown by the T-H plots, in Figures 2.13, relating to cycles A and B labelled on Figure 2.12.

This means that the change in work output of the cycle with TIP is primarily influenced by the thermal efficiency of the cycle. In all cases, the cycle thermal efficiency increases with TIP. Therefore, in cases where the heat input does not change significantly with TIP, the cycle work output will increase with TIP.

Overall, Figures 2.8c, 2.10c and 2.12c show that a similar maximum work output is achieved with several different ORC fluids in each case. The exceptions are pentane in the engine and hot brine case and R245fa in the industrial steam case. These results indicate

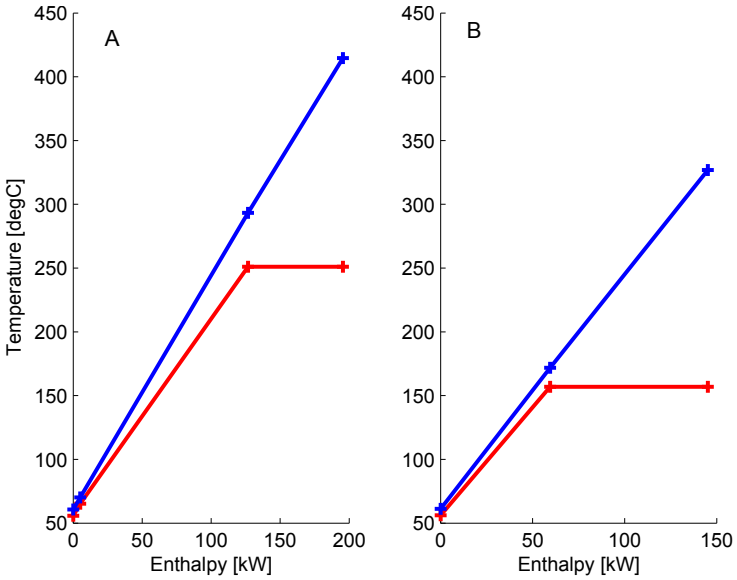

Figure 2.13: T-H Plots of Engine Case with working fluid toluene

that, under the constraints imposed in this work, i.e. $\dot{m}_O = 0.6\dot{m}_S$, the choice of ORC working fluid does not strongly influence the cycles ability to recover work. Although, the choice of working fluid does influence the TIP at which maximum energy recovery is achieved.

2.4.2 Releasing the Mass Flow Constraint

The calculations described in Section 2.4.1 were constrained by an ORC working fluid mass flow rate of 60 % of the source heat stream. This constraint was applied in order to analyse the behaviour of the ORCs with varying TIP and multiple working fluids. The simulations described in this section were carried out for mass flow rates of ORC working fluid varying from 60 % to 160 % of the heat source stream in increments of 10 %. These limits were defined in order to give a wide enough range to see the trends in ORC performance for different ORC working fluid mass flow rates. TIP was bounded between 5 % and 80 % of the critical pressure for each fluid as in the previous calculations.

Figures 2.14, 2.15 and 2.16 show contour plots of work output, heat input and cycle efficiency for varying TIP and working fluid mass flow rate on the x and y axis respectively for each heat source case.

In the case of the hot brines from the Ninian field, the figures show that maximum heat

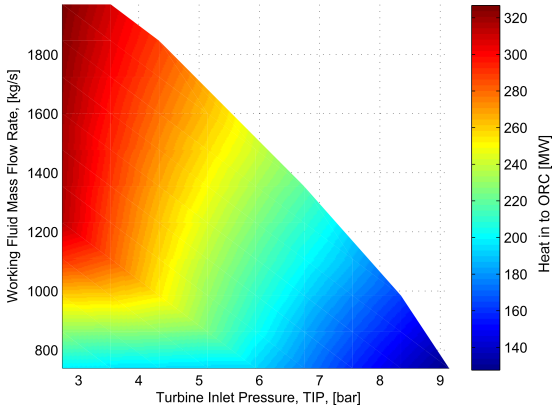

(a) Heat into ORC vs TIP and $\dot{m}_O$

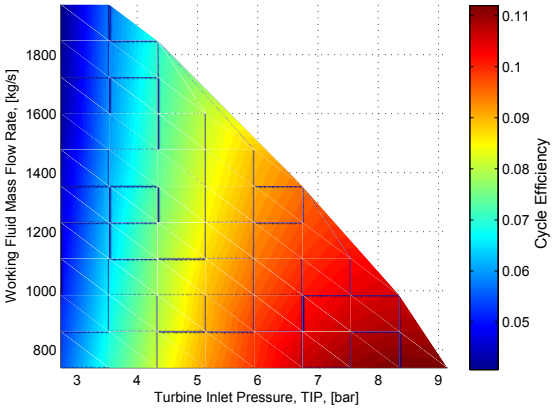

(b) Efficiency of ORC vs TIP and $\dot{m}_O$

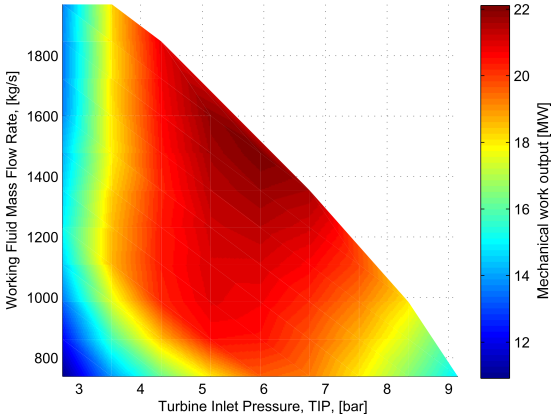

(c) Work Output of ORC vs TIP and $\dot{m}_O$

Figure 2.14: Results of Ninian oil field simulations, with working fluid R245fa. Hot brine temperature is 102 ° and mass flow rate 1231.1 kg/s

input, efficiency and work output occur at completely different values of TIP and working fluid mass flow rate, see Figure 2.14. The maximum heat into the ORC occurs at low TIP and at working fluid mass flow rates equal to the mass flow rate of the source fluid or greater, Figure 2.14a. Conversely, maximum cycle efficiency is achieved at high TIP and low mass flow rates. Maximum work output, therefore is a balance between heat in and cycle efficiency, with respect to both TIP and working fluid mass flow rate, as shown in Figure 2.14c. Figure 2.14c also shows TIP has a greater influence than working fluid mass flow rate, there is little change in work output for a fixed TIP.

Very similar trends are seen in the industrial steam case, shown in Figure 2.15. The maximum work output was achieved at the largest flow rate simulated, 49.6 kg/s, and 16 bar TIP. While maximum cycle efficiency occurred at a TIP of 18.81 bar and was relatively insensitive to ORC working fluid mass flow rate. The discontinuity in the results shown

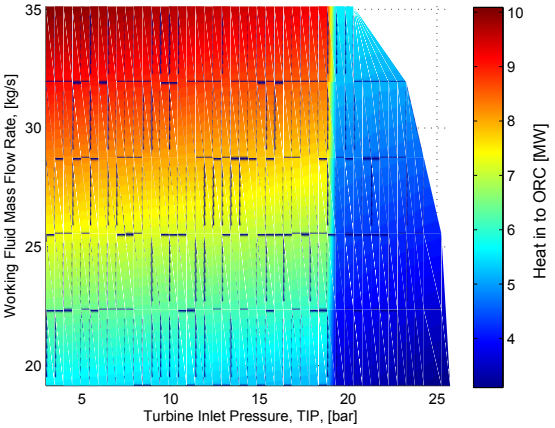

(a) Heat into ORC, [MW], vs TIP and $\dot{m}_O$

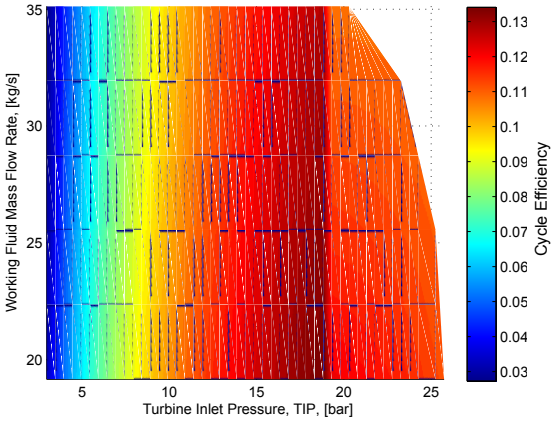

(b) Efficiency of ORC vs TIP and $\dot{m}_O$

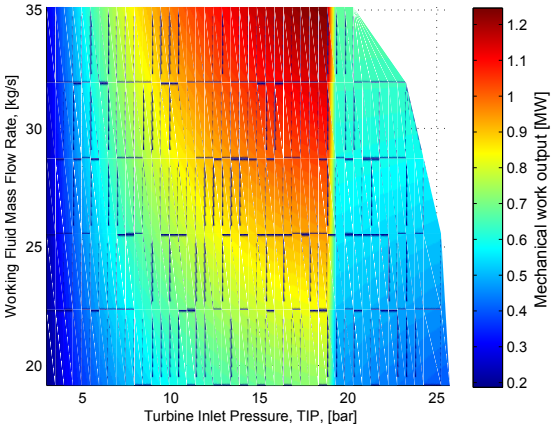

(c) Work Output, [MW], of ORC vs TIP and $\dot{m}_O$

Figure 2.15: Results of Industrial Steam case simulations with working fluid R245fa. Steam is 140 ° and mass flow rate 31.94

in Figure 2.15 is due to the pinch point location change, as explained earlier in section 2.4.1.

For the diesel engine test case, the plots show work output is dominated by the trend in cycle efficiency for both TIP and working fluid mass flow rate, see Figures 2.16b and 2.16c. Although Figure 2.16a shows the heat taken into the cycle decreases with working fluid mass flow rate this effect is very small, with an increase of only ≈2 kW over the mass flow rate range. While for efficiency, a maximum efficiency of 14.26 % is achieved at 26.96 bar and 0.2967 kg/s, i.e. maximum TIP and working fluid mass flow rate modelled. Therefore, the maximum work output is also achieved at minimum mass flow rate and maximum TIP, as shown in Figure 2.16c.

Given both the Ninian and industrial steam cases involve a trade off between heat into

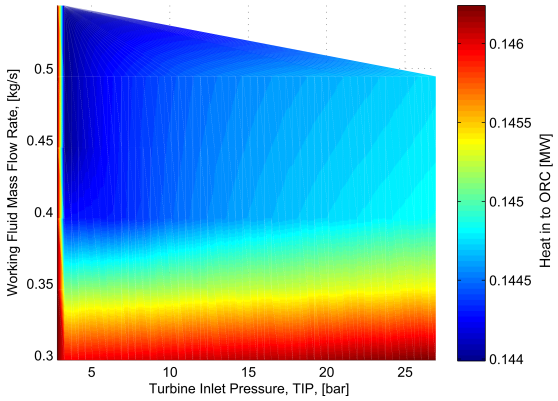

(a) Heat into ORC, [MW], vs TIP and $\dot{m}_O$

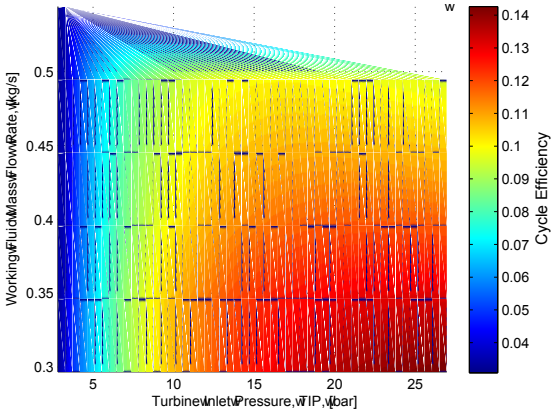

(b) Efficiency of ORC vs TIP and $\dot{m}_O$

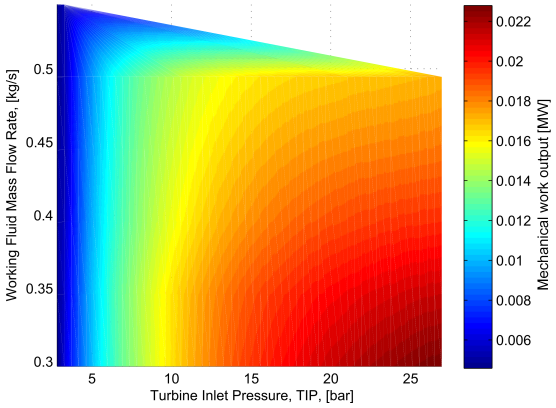

(c) Work Output, [MW] of ORC vs TIP and $\dot{m}_O$

Figure 2.16: Results of Engine simulations with working fluid Pentane. Engine exhaust is 326 ° and mass flow rate 0.4945 kg/s

the cycle and thermal efficiency, these cases may be able to benefit from increasing the heat into each cycle. For example by using fluid mixtures. However, in the case of the diesel engine, introducing fluid mixtures is unlikely to have a large effect on the cycle performance as this is dominated by the efficiency of the cycle.

2.5 Working Fluid Mixtures

Following the calculations with pure working fluids, calculations were also carried out for the following fluid mixtures:

- Ninian case - Butane/ Pentane
- Ninian case - R245fa/ Pentane

- Engine case - Butane/ Pentane
- Engine case - Toluene/ Cyclohexane
- Industrial case - Butane/ Pentane
- Industrial case - R245fa/ Pentane

Simulations were run for mixture concentrations from 0.1 to 0.9 mass fraction of each of the component fluids, in steps of 0.1. The mass flow rate of the working fluid was constrained to 60 % of the heat source fluid, in order to constrain calculations. TIP was varied with the same limits as imposed in the previous calculations. For each concentration the maximum work output possible given the ORC configuration is recorded

The results are summarised in Table 2.6. The results from the mixture calculations are compared to the maximum work output possible from each of the pure fluid that are constituents of the mixtures simulated. In the Ninian case the Butane/ Pentane mixture, with 0.5/0.5 concentration, gave a maximum work output increase of +14.26 % relative to the largest output calculated for the pure constituent fluids. While for a 0.6/0.4 mixture of R245fa/ Butane an increase of +12.74 % in work output was calculated .

Similarly, in the case of industrial steam, a potential increase on 4.44 % was calculated for a 0.5/0.5 Butane/ Pentane mixture. However, the R245fa/ Pentane mixture offers no improvement over using pure Pentane.

In the case of the diesel engine mixtures of Butane/ Pentane and Toluene/Cyclohexane were used to calculate possible ORC cycles. As predicted, the calculations show no improvement in work output for either of these mixtures, due to the dominance of cycle efficiency on work output as discussed earlier.

Figure 2.17 shows temperature against enthalpy plots of the ORC cycles which result in maximum work output for: 100 % Butane, 100 % Pentane and a mixture of 50 % Butane 50 % Pentane. This shows that the cycle configurations are the same, all subcritical with no superheat. But in the case of the 0.5/0.5 mixture, significantly more heat is taken into cycle than is the case for the pure fluids, shown by the upper solid blue line. Both heat

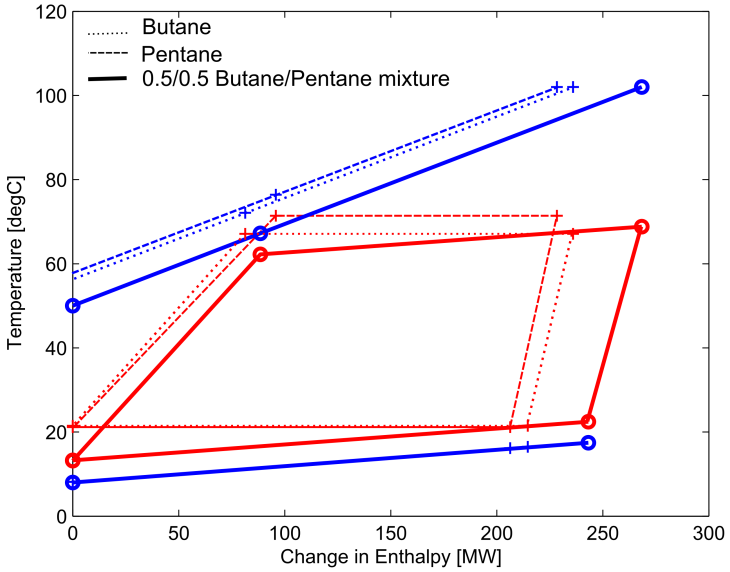

Figure 2.17: T-H Cycle Plots of Butane, Pentane and 0.5/0.5 Butane Pentane Mixture at maximum work output configuration for the Hot Brines test case

stream profiles in the condensation process, lower solid blue and red lines, are very well matched. This results in the temperature at inlet to the evaporator being 8 ° lower and therefore more heat can be absorbed into the cycle.

Figures 2.18a and 2.18b show the mixtures in more detail for the Butane/ Pentane mixture in the case of hot brines for the Ninian oil field. It is clear from the figures that the maximum work output occurs at the maximum glide for both the evaporator and condenser. The heat into the cycle can be seen in Figure 2.18, to increase with temperature glide as expected. Cycle efficiency remains approximately constant at about 9 % for all mixture concentrations calculated.

Temperature glides, heat energy input, work output and efficiency are also plotted for the engine case in Figure 2.19. Figure 2.19b shows that the heat input to the cycle increases by just over 1 % for the mixture concentrations examined. However, in contrast to the Ninian case where the efficiency remained almost constant, for the engine case shown in Figure 2.19a, the efficiency increases gradually from 11.3 % to 14.3 % as the amount of Butane in the mixture is increased. The small increase in heat input due to the fluid mixture does not outweigh the increase in efficiency with increase in concentration of Butane and thus the maximum work output is produced with 100 % Butane.

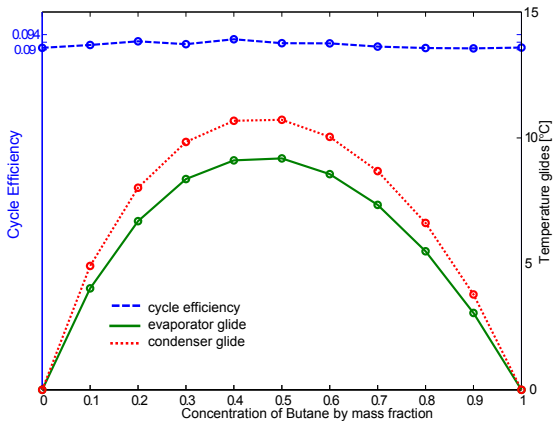

(a) Efficiency, Condenser and Evaporator Glides against Concentration

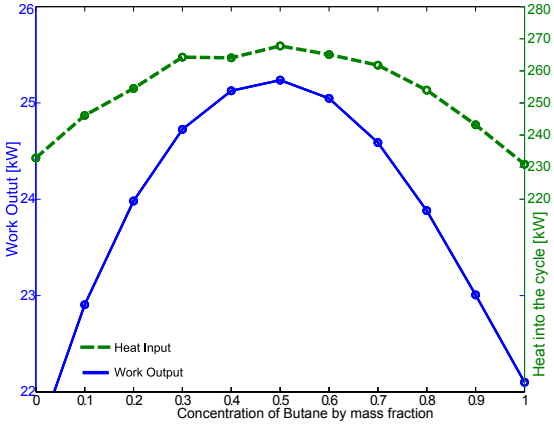

(b) Work output and Heat input against concentration

Figure 2.18: Hot Brines Case with Butane/ Pentane working fluid mixture

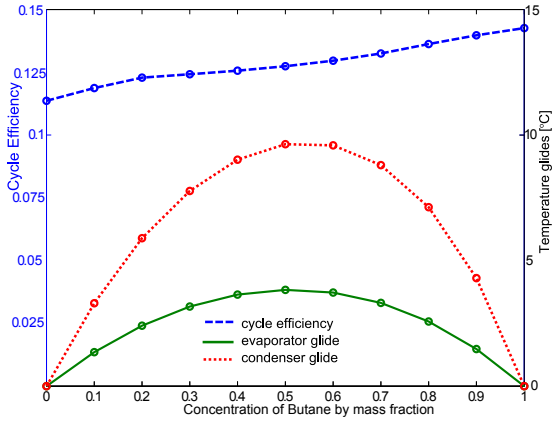

(a) Efficiency, Condenser and Evaporator Glides against Concentration

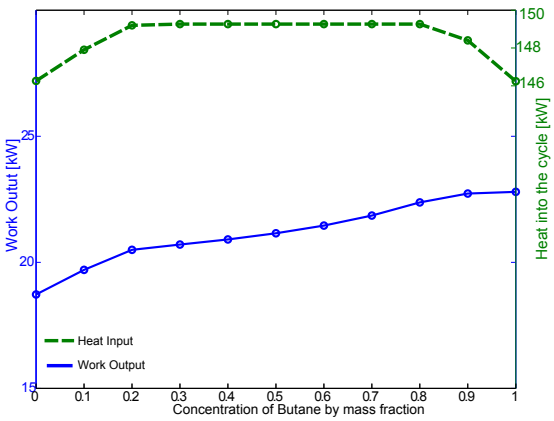

(b) Work output and Heat input against concentration

Figure 2.19: Engine Case Engine Case with Butane/ Pentane working fluid

These results show that in terms of thermodynamic behaviour, fluid mixtures have the potential to improve the work output from organic Rankine cycles, in certain circumstances. The potential benefit was largest for the Ninian hot brines case, +14.26 % with a 0.5/0.5 Butane/ Pentane mixture. For the same mixture in the industrial steam case, a smaller improvement of 4.44 % is calculated and in the diesel engine case no benefit from using fluid mixtures at all was found.

2.6 Summary and Conclusions

The thermodynamic performance of the ORC has been explored in this chapter. An ORC modelling tool has been developed in order to assess possible energy recovery at different energy scales. The model is capable of calculating ORC performance with various configurations of working fluid mass flow rate, TIP and working fluid composition between defined heat source and heat sink stream. The model is described in section 2.3. It is computationally efficient, with a typical execution time for one set of cycle constraints, of less than 5 seconds. This is achieved in part via a novel method of pinch analysis for the heat exchangers as described in section 2.3.1. The model was validated against resultls from a model developed by Aneke et al. [12].

The model was used to investigate the ORC performance for three heat source case studies: exhaust heat from a ICE, industrial waste steam and hot brine coproduced from oil production. Cycles using both pure and working fluid mixtures were calculated for a range of working fluid mass flow rates and TIPs, the results of which are shown and discussed in section 2.4. The conclusions from these ORC simulations are summarised below.

It is desirable to optimise mechanical work output (not cycle efficiency) when designing ORC systems to recover useful power from waste heat. It has been shown that the optimal cycle configuration (subcritical, superheated or TFC) for recovered work output is strongly dependent on the T-H profile of the heat source fluid. General design principles can be drawn by comparing the gradient of the ORC working fluid, with the gradient of the heat source fluid T-H profile as defined by equation 2.3. When the gradient of the source heat fluid T-H profile is steeper than that of the working fluid, the cycle work output will increase with an increase in TIP. However, care should be taken when the gradient of the source T-H profile is shallower than that of the ORC working fluid. Under these conditions, too large a TIP can result in a decrease in work output from the cycle. The results show that the conditions for optimising mechanical work output from an ORC are different from those for optimum thermal efficiency of the cycle. The maximum work

output is achieved under conditions where there is the best balance between the heat input to the cycle (decreases with TIP) and thermal efficiency (increases with TIP). ORC cycles powered by waste heat should be designed to operate in the region of the maximum work output, if possible, but avoiding conditions that might cause the pinch point location to change and therefore the rate of heat taken into the cycle to decrease. This is particularly significant for cases where the source heat fluid changes state. For these heat sources, changes in pinch point location can cause a sudden step decrease in work output from the cycle.

The results indicate that, for a fixed ORC working fluid mass flow rate, fluid selection does not have a strong influence on the ORCs ability to recover waste heat. But ORC working fluid choice does influence the TIP at which the maximum work output is achieved.

Contour plots of the cycle parameters with respect to TIP and working fluid mass flow rate show similar ORC configurations for maximum work output in the case of the Industrial steam and the Ninian oil field. However in the case of the ICE the performance is dominated by the effect of the thermal efficiency of the cycle, which is most dependant of the TIP. These results show it is not possible to adopt the same design strategy across all of the energy scales investigated in this study.

Simulations were carried out using zeotropic fluid mixtures; two mixtures for each heat source were tested. It is clear from the simulations using fluid mixtures in the Ninian and industrial steam cases that there is a potential thermodynamic benefit for using fluid mixtures to increase heat input into the cycle. A potential increase of +14.26 % was calculated using a 0.5/0.5 Butane/ Pentane fluid mixture in the Ninian case. However, no benefit was predicted from using Butane/ Pentane or Toluene/ Cyclohexane mixtures in the ICE case. This is due to cycle performance being dominated by the cycle efficiency.

References

Case	Working Fluid	Concentration	Max Work Out [kW]	Cycle Efficiency	Heat In [kW]	Evaporator Glide [°C]	Condenser Glide [°C]	Pressure Ratio
Ninian	Butane	-	22.09	0.09	228.38	0.00	0.00	3.88
	Pentane	-	21.43	0.09	236.01	0.00	0.00	4.38
	R245fa	-	19.62	0.10	193.09	0.00	0.00	5.12
	Butane/Pentane	0.5 -0.5	25.24	0.09	268.41	9.19	10.71	4.21
	R245fa/Pentane	0.6-0.4	24.16	0.10	237.20	10.91	11.11	4.94
Industry	R245fa	-	0.73	0.13	5.14	0.00	0.00	10.45
	Pentane	-	1.35	0.13	10.15	0.00	0.00	8.83
	Butane	-	1.32	0.13	9.61	0.00	0.00	6.65
	R245fa/Pentane	0.1-0.9	1.28	0.12	9.98	8.37	10.69	8.82
	Butane/Pentane	0.5-0.5	1.41	0.13	10.39	7.07	10.37	8.28
Engine	Butane	-	22.79	0.14	146.24	0.00	0.00	14.63
	Pentane	-	18.73	0.11	146.26	0.00	0.00	5.47
	Toluene	-	30.46	0.20	148.19	0.00	0.00	151.88
	Cyclohexane	-	27.26	0.17	146.02	0.00	0.00	73.10
	Butane/Pentane	0.9-0.1	22.73	0.14	148.40	1.48	4.30	13.67
	Toluene/Cyclohexane	0.9/0.1	29.27	0.19	146.34	0.91	3.50	175.41

Table 2.6: Summary of results for fluid mixtures calculations

[1] A. Auld, A. Berson, and S. Hogg, "Organic rankine cycles in waste heat recovery: a comparative study," *International Journal of Low Carbon Technology*, vol. 8 (suppl 1), pp. i9–i18, 2013.

[2] H. Chen, D. Y. Goswami, and E. K. Stefanakos, "A review of thermodynamic cycles and working fluids for the conversion of low-grade heat," *Renewable and Sustainable Energy Reviews*, vol. 14, pp. 3059–3067, 2010.

[3] B. Saleh, G. Koglbauer, M. Wendland, and J. Fischer, "Working fluids for low-temperature organic rankine cycles," *Energy*, vol. 32, pp. 1210 – 1221, 2007.

[4] B. F. Tchanche, G. Papadakis, G. Lambrinos, and A. Frangoudakis, "Fluid selection for a low-temperature solar organic rankine cycle," *Applied Thermal Engineering*, vol. 29, no. 11, pp. 2468–2476, 2009.

[5] V. Maizza and A. Maizza, "Unconventional working fluids in organic rankine-cycles for waste energy recovery systems," *Applied Thermal Engineering*, vol. 21, pp. 381 – 390, 2001.

[6] M. Z. Stijepovic, P. Linke, A. I. Papadopoulos, and A. S. Grujic, "On the role of working fluid properties in organic rankine cycle performance," *Applied Thermal Engineering*, vol. 36, pp. 406–413, 2012.

[7] T.-C. Hung, T. Shai, and S. Wang, "A review of organic rankine cycles (orcs) for the recovery of low-grade waste heat," *Energy*, vol. 22, no. 7, pp. 661–667, 1997.

[8] T. Hung, S. Wang, C. Kuo, B. Pei, and K. Tsai, "A study of organic working fluids

on system efficiency of an orc using low-grade energy sources," *Energy*, vol. 35, no. 3, pp. 1403–1411, 2010.

[9] J. Roy, M. Mishra, and A. Misra, "Parametric optimization and performance analysis of a waste heat recovery system using organic rankine cycle," *Energy*, vol. 35, pp. 5049–5062., 2010.

[10] H. Jung, S. Krumdieck, and T. Vranjes, "Feasibility assessment of refinery waste heat-to-power conversion using an organic rankine cycle," *Energy Conversion and Management*, vol. 77, pp. 396–407, 2014.

[11] C. Katsanos, D. Hountalas, and E. Pariotis, "Thermodynamic analysis of a rankine cycle applied on a diesel truck engine using steam and organic medium," *Energy Conversion and Management*, vol. 60, pp. 68 – 72, 2012.

[12] M. Aneke, B. Agnew, and C. Underwood, "Performance analysis of the chena binary geothermal power plant," *Applied Thermal Engineering*, vol. 31, pp. 1825–1832, 2011.

[13] G. Angelino and P. C. di Paliano, "Multicomponent working fluids for organic rankine cycles (orcs)," *Energy*, vol. 23(6), pp. 449 – 463, 1997.

[14] R. Radermacher, "Thermodynamic and heat transfer implications of working fluid mixtures in rankine cycles," *International Jounral of Heat and Fluid Flow*, vol. 10(2), pp. 90–102, 1989.

[15] F. Heberle, M. Preissinger, and D. Bruggemann, "Zeotropic mixtures as working fluids in organic rankine cycles for low-enthalpy geothermal resources," *Energy*, vol. 37, pp. 364 – 370, 2012.

[16] M. Chys, M. van den Broek., B. Vanslambrouck., and M. D. Paepe, "Potential of zeotropic mixtures as working fluids in organic rankine cycles," *Energy*, vol. 44, pp. 623–632, 2012.

[17] B. Linnhoff and et al., "Introduction to pinch technology," *available from Linnhoff March Ltd, UK*, vol. 1, pp. 1 – 63, 1998.

[18] G. F. Rogers and Y. R. Mayhew, *Engineering Thermodynamics Work & Heat Transfer*. Longman Group Limited, 1980.

[19] S. Quoilin, "An introduction to thermodynamics applied to organic rankine cycles," tech. rep., Leige Universiity, 2008.

[20] "SGT-500 Industrial Gas Turbine," 2011. accessed 27/01/14.

[21] P. Colonna and T. P. van der Stelt, "Fluidprop: a program for the estimation of thermo physical properties of fluids." Software, 2004. Energy Technology Section, Delft University of Technology.

[22] E. Lemmon, M. Huber, and M. McLinden, "Nist standard reference database 23: Reference fluid thermodynamic and transport properties-refprop," 2013. Version 9.1, National Institute of Standards and Technology, Standard Reference Data Program,.

[23] B. F. Tchanche, G. Lambrinos, A. Frangoudakis, and A. Papadakis, "Low-grade heat conversion into power using organic rankine cycles: A review of various applications," *Renewable and Sustainable Energy Reviews*, vol. 15, pp. 3963–3979, 2011.

[24] C. Katsanos, D. Hountalas, and E. Pariotis, "Thermodynamic analysis of a rankine cycle applied on a diesel truck engine using steam and organic medium," *Energy Conversion and Management*, vol. 60, pp. 68 – 72, 2012.

[25] I. Vaja and A. Gambarotta, "Internal combustion engine (ice) bottoming with organic rankine cycles (orcs)," *Energy*, vol. 35, p. 1084ÃćâĆňâĂIJ1093, 2010.

[26] J. G. Gluyas and H. M. Hichens, *United Kingdom oil and gas fields: commemorative millennium volume*, vol. 20. Geological Society, 2003.

Chapter 3

Experimental Investigation of Heat Exchangers

3.1 Introduction

In chapter 2 it was shown that zeotropic working fluid mixtures have the potential to create thermodynamic benefit. But the literature also indicates that zeotropic mixtures suffer a degradation of the heat transfer coefficient during phase change. The work described in this chapter aims to experimentally measure the difference in heat recovered by heat exchangers where a zeotropic mixture is used compared with an azeotropic fluid.

The experimental test rig, based on a Ground Source Heat Pump (GSHP), described in this chapter was funded through an EPSRC Impact Acceleration Account project, as part of an investigation into ORCs for diesel engine applications. The project was a collaboration involving Newcastle University and JCB. The funds available to build a rig to validate the ORC thermodynamic model and heat exchange model were £15,000.

Previous research (for example [1] and [2]) has identified potential thermodynamic improvement and degradation of heat transfer coefficient from using zeotropic mixtures in thermodynamic cycles. Some studies also state that the observed improvement for a zeotropic mixture in comparison to a pure fluid is smaller than the theoretical prediction [1–4]. These studies also indicate that a lack of experimental work limits further

understanding of the use of zeotropes. The construction and commissioning of a new experimental facility, capable of measuring heat exchange across heat exchangers with both azeotropic and zeotropic fluid mixtures is described in this chapter. This enabled investigations into deviations of experimental data from theoretical predictions for zeotropic mixtures in literature to be carried out.

In this chapter, existing literature detailing experimental studies into the use of zeotropic mixtures is briefly reviewed to contextualise and inform the experimental facility design. Next the design of the experimental facility is discussed and the instrumentation described. The working fluid selection is discussed, then the experimental programme and data reduction method are presented. Data from the commissioning tests using the conventional, azeotropic, refrigerant are presented and are used to deduce the heat exchange across the heat exchangers at a variety of operating conditions. Finally, a zeotropic working fluid mixture is introduced into the heat pump and experiments are conducted over a range of operating conditions. Data are presented showing how introducing the fluid mixture affects the performance of the heat exchangers in the heat pump system.

3.2 Literature Review

Herberle, Chyrs and Lecompte have all published studies identifying the theoretical benefit of zeotropic mixtures in Organic Rankine Cycle (ORC)s [1–3]. Each of these studies acknowledges that previous research has shown that the heat transfer coefficient of zeotropic mixtures is less than the linearly interpolated value between values for the pure fluid constituents. However, none of the theoretical models quantifies either the thermodynamic cost of using the same size heat exchange area, as for a pure fluid, or the economic cost of designing an ORC which requires larger heat transfer area. The studies all identify the lack of existing experimental data as a barrier to validating the theoretical results.

There are very few experimental studies using zeotropic working fluids in ORCs. Wang et al. [5] examine the influence of two different blends of R245fa/R152a in a low-temperature solar ORC and compare results to the same cycle operating with pure R245fa. A small scale experimental prototype ORC was instrumented with thermocouples

at key points round the cycle, two pressure transducers and a flow meter. The flow rate was kept constant for all of the working fluids tested and the cycle performance was simply measured from the product of the solar collector and cycle efficiency. Wang et al report improved performance over R245fa for both mixtures. However, the pump work and expansion work were calculated from constant assumed isentropic efficiencies, no pressure drop over the heat exchangers or pipes was considered and the circulating composition of the mixture was assumed to be constant, all of which contributes uncertainty to the results. Nonetheless, this study experimentally shows cycle performance can be improved through the use of zeotropic mixtures.

Wu et al. [6] further investigated the use of R245fa/R152a mixtures and also R290/R600 mixtures in ORCs. In their study, experimental data for the maximum temperature difference (MTD) and pinch point (PP) in a tube-in-tube evaporator was collected and compared with theoretical models. The results showed that assuming a linear temperature change during evaporation leads to inaccurate PP or MTD location predictions. Therefore this study showed that there is a need for more accurate theoretical models of the phase change process for zeotropic mixtures.

The study of zeotropic mixtures may be relatively new to ORC research but it has been the subject of research for other types of thermodynamic cycle for some time. Initially, interest in zeotropes as working fluids arose from the need to find new refrigerants. Those with particularly high Global Warming Potential (GWP) and Ozone Depletion Potential (ODP) have been phased out, but pure refrigerants that meet legislative requirements are rare [7].

The use of hhloroflurocarbons (CFCs), like R12, was banned in the 1990s. hydrochlorofluorocarbons (HCFCs) have been phased out since 2001, with transitional HCFCs (with a lower GWP than other HCFCs) banned from 2001. Virgin (i.e not recycled or reclaimed) HCFCs were banned in 2010 and the use of any type of HCFC has been illegal since January 2015 [8]. This is UK legislation in response to the Montreal protocol, so similar restrictions on the use of refrigerants are found globally. This restricts the range

of working fluids that are available for use in ORCs.

Chandr [7] describes how fluid mixtures were considered in order to reduce the flammability, toxicity or working pressure of thermodynamically appropriate pure fluids. Only in later work were zeotropic mixtures identified as also having potential thermodynamic benefit.

For example, R22 is a transitional HCFCs which was common in heat pump and air conditioning applications. The need to find a replacement has resulted in several studies on potential replacement mixtures being published [9–11].

Pannock et al. [11] measured the performance of a heat pump designed for use with R22, using working fluid mixtures of R23, R32, Rl25, R134a, R143a, and Rl52a. The results showed that a mixture of R32/R152 increased the Coefficient of Performance (COP) by up to 24 %. This is an important result because the heat exchange area was the same for the pure R22 and the R32/R152a mixture in the tests, suggesting that for the conditions tested any degradation in heat transfer coefficient was outweighed by the better thermodynamic performance of the replacement mixture. Pannock et al. also compared their experimental results with those from a theoretical model of the cycle and reported poor agreement between the two.

Similarly Yimaz et al. [9] investigated mixtures of R12, R22 and R114 in a heat pump. Their study used an Air Source Heat Pump (ASHP), instrumented with thermocouples and manometers, joined to a mixture unit which enabled control of the working fluid composition and flow rate. It was concluded from the study that improvements in thermodynamic performance can be made with fluid mixtures whilst meeting ODP and GWP restrictions.

However, not all studies report improvement in heat pump performance. Lee et al. [10] replace R22 with R407c, a zeotropic mixture of 23 % R32, 25 % R125, and 52 % R134a by mass, in a 100kW refrigeration system. Pressure transducers and thermocouples at inlet and exit of each cycle component in combination with a flow meter for each fluid steam allowed the heat duty on each side of the heat exchangers to be determined and

a full thermodynamic cycle analysis to be carried out. Lee et al. found that the cooling capacity decreased by 10 - 20 % and the COP decreased 20 - 30 % when depending on the temperature conditions of the heating and cooling streams. Each cycle component is examined and the primary cause of the loss in performance was found to be due to the decrease in the heat transfer coefficient in the heat exchangers. The decrease in performance was found to be twice as large in the evaporator, the lower pressure side of the cycle, compared with the drop in performance of the condenser.

Similarly, Garbrielii and Vamling [12] report decreases of up to 70 % in the overall heat transfer coefficient of heat exchangers using zeotropic mixtures in place of pure fluids in a refrigeration unit. The heat exchangers used in this study were a cross flow configuration, which has increased the performance penalty from using a zeotropic mixture compared with the experience of other work using counterflow heat exchanger designs. Sajjan et al. have published two studies investigating the reasons for the decrease in performance when zeotropic mixtures are used [13, 14]. These studies found that mass transfer resistance in the liquid phase was the reason for the drop in heat exchanger performance. A theoretical model was developed to model condensation on the outside of the tubes in the heat exchanger. The model predicted the heat and mass transfer values to within 7 % for pure R22, however over predicted the heat and mass transfer for R407c, a fluid mixture. The use of finned and enhanced tubes in heat exchangers is proposed to increase mixing of the working fluid components. This study shows further work is required to understand the physical processes involved in the condensation of mixtures, in order to produce analytical models capable of accurately predicting the heat transfer rates measured in the experiments.

The studies described above show that there is a need to quantify the heat transfer degradation by measuring the local heat transfer coefficient during phase change of a mixture. Fronk [15] describes how there are significant challenges with measuring heat transfer without incurring large uncertainty. Several efforts have been made to instrument heat exchangers with thermocouples capable of measuring both the wall and bulk

temperature of the working fluid mixture, for example [16, 17]. Smit et al. [16] found that the heat transfer correlation of Dobson and Chato [18] coupled with the correction method of Silver [19], Bell and Ghaly [20] predicted the mixture heat transfer within 20 to 30 %. They used a section of a condenser, a tube in tube arrangement 1.6 m long divided in to eight sections with thermocouples at the inlet and exit of each section.

Better agreement between experimental data and analytical modelling was found by Cavallini et al. [17]. Condensation of a mixture of R125/R236ea was carried out in a similar 2m long tube in tube heat exchanger arrangement to that used by Smit et al. [16]. Rather than calculating an average heat transfer coefficient however, data of the total heat duty versus outlet vapour quality was presented to validate a condenser model based on the Colburn and Drew non-equilibrium film model for the condensation. This method avoids the large uncertainty associated with quantifying local heat transfer coefficient, whilst enabling some comparisons to the calculated values for local heat transfer to be made.

In the work described in this chapter, the aim is to show the effect on the performance of the heat exchangers in a ground source heat pump from a zeotropic mixture, not previously used in literature, compared with the performance using the manufacturers near-azeotropic working fluid mixture.

3.3 Experimental Test Facility

There are several commercially available ORC units which are a small size (<15 kW) and which are appropriate for a laboratory experiment of this type. For example, those produced by Terocycle and Enogia. However, after collecting quotes all the commercially available ORCs proved to be prohibitively expensive for use in this project.

Many thermodynamic cycles use the same organic working fluids as ORCs. By using an alternative thermodynamic cycle, which uses the same working fluids and has similar heat exchange processes, the heat exchange process can be examined without requiring the whole organic Rankine cycle hardware to be procured. Examples of cycles which use the same working fluids as ORCs are vapour compression cycles such as those used in

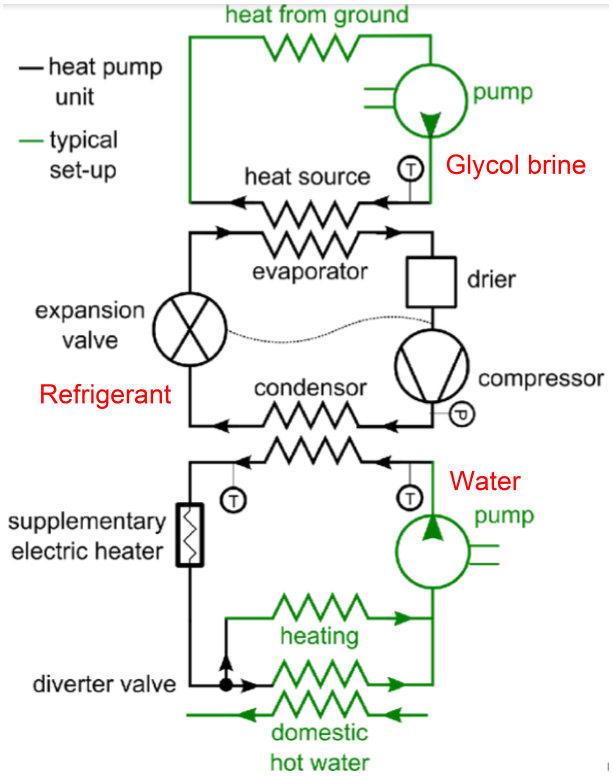

Figure 3.1: Schematic diagram of the Steibel Eltron WPF 5, a 5kW ground source heat pump

refrigeration or heat pumps. These have been available commercially for decades and therefore are much cheaper than a similar scale ORC cycle.

After consultation with Revolution Power [21], a local company specialising in the supply of domestic scale heat pumps, a ground source heat pump was selected. The heat pump is rated at 5 kW output and was manufactured by Stiebel Eltron. The heat pump was configured for use with working fluid R410a. This fluid was developed as a replacement for R22 which has been phased out on environmental grounds due to the Montreal protocol [8].

The ground source heat pump, in standard configuration, is shown in figure 3.1. A heat exchanger is used to extract heat from the ground; this is upgraded with additional work from a compressor to produce a heat supply to a domestic heating system and hot water supply.

The refrigerant is circulated around the heat pump through a series of processes, as

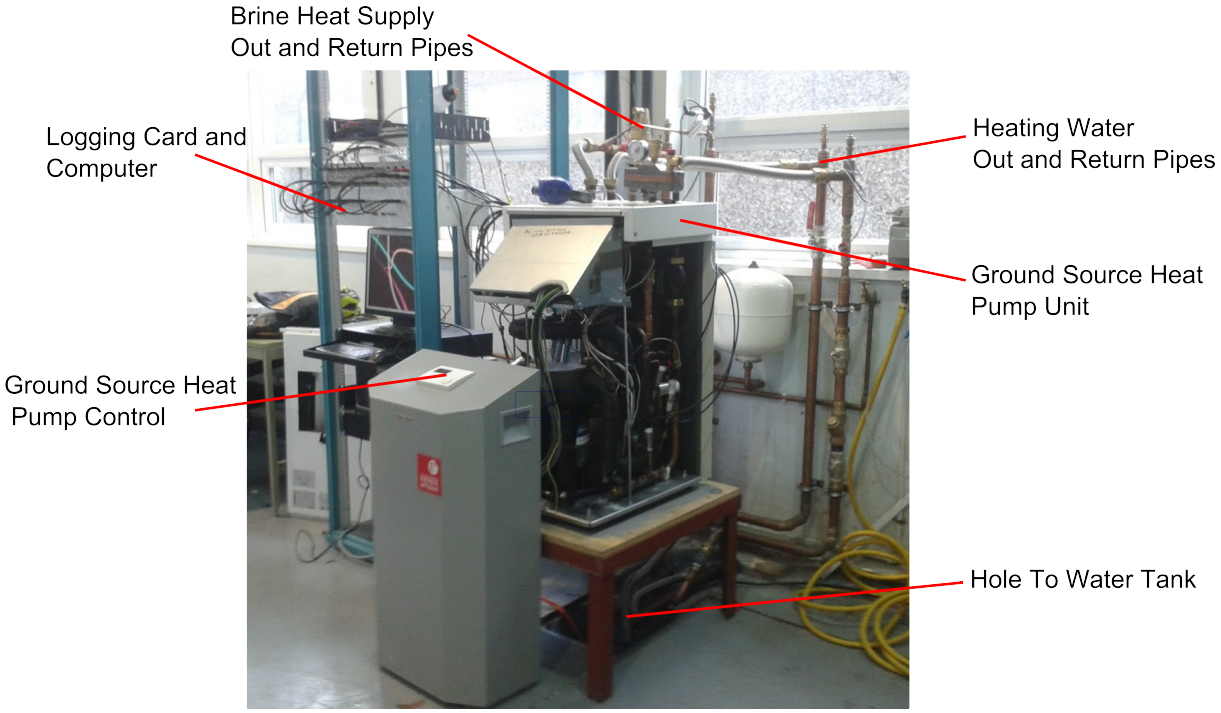

Figure 3.2: Photo of GSHP experimental rig

depicted in Figures 3.1 and 3.3:

- Firstly, heat from the ground is extracted via a heat exchanger to glycol brine. The brine is used as an intermediate loop to prevent freezing inside the heat exchangers.
- Heat from the brine is transferred to the refrigerant fluid, and the thermodynamic cycle, in the evaporator. This causes the organic fluid to vaporise. The refrigerant is then passed through a drier to ensure no liquid is present in the gas. The evaporation process occurs from points 1 to 2 labelled in Figure 3.3.
- The gaseous refrigerant is then compressed, points 2 to 3. This increases the temperature and pressure of the refrigerant.
- Heat is then transferred to the domestic heating system in the condenser, points 3 to 4. During this process the refrigerant returns to a liquid state.
- Finally an expansion valve is used to drop the pressure and return the refrigerant fluid to its original state at entry to the evaporator, points 4 to 1.

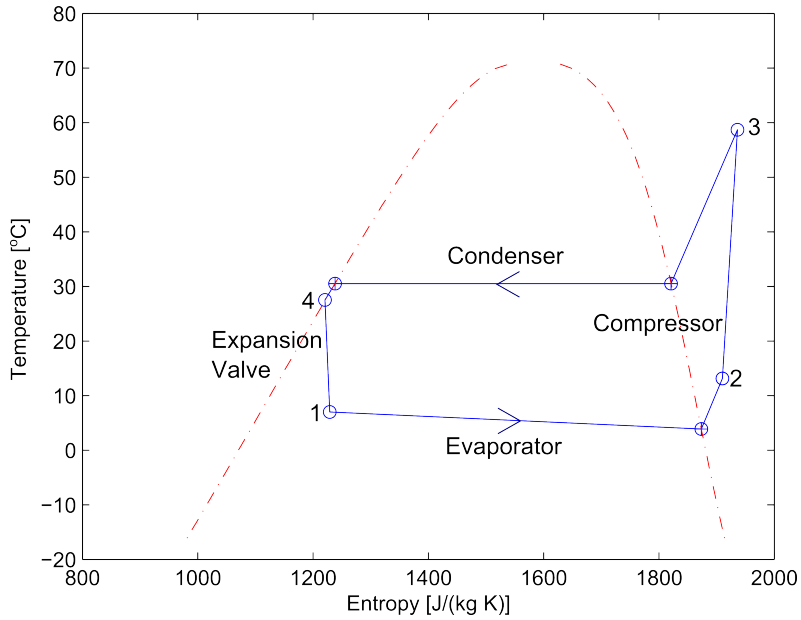

Figure 3.3: Temperature against entropy plot of a heat pump cycle

An organic Rankine cycle consists of similar evaporation, compression, condensation and expansion processes with the cycle operating in reverse.

By selecting instrumentation for the heat pump which is capable of measuring the heat transferred across the heat exchangers and allowing each point in the thermodynamic cycle to be determined, the heat transfer process can be compared with that estimated by the model described in Chapter 2 and the performance of the heat pump can be calculated.

The heat pump was installed as shown in figure 3.2. A 30 cm diameter hole, drilled at 45° through the floor allowed access from the lab into an underground tank immediately below heat pump. The tank has a footprint of approximately 6 m by 3.5 m and is 1.5 m deep. The position of the heat pump (at location 3), water tank, tank access hatch and hole are shown in the lab floor plan, Figure 3.4a. Figure 3.4b shows the inside of the tank, the black pipes, fixed to the floor are the pipes for the glycol to circuit. Heat is extracted from the tank water into the glycol as the heat source for the heat pump. The water heated by the heat pump is taken from and returned to the water tank directly in an open circuit via flexible pipes near the hole. The inlet/outlet water pipes are separated as much as possible inside the tank, to avoid returning hot water directly back into the heat pump system.

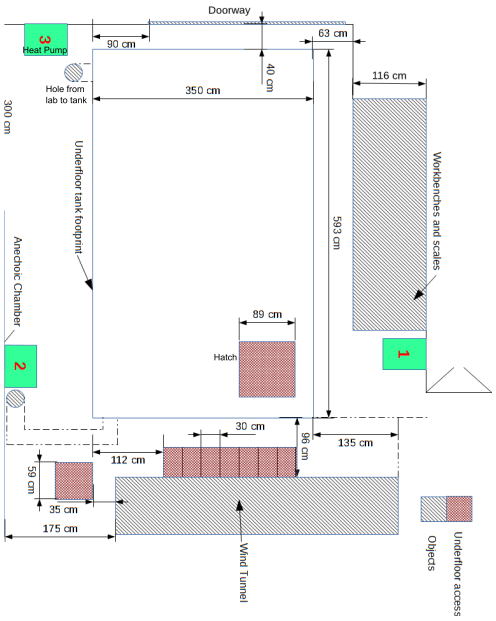

(a) Lab floor plan showing location of equipment

(b) Inside of the tank, black pipes contain the glycol

Figure 3.4: Physical layout of experimental rig

3.3.1 Instrumentation

Figure 3.5 shows how the 5 kW GSHP was modified to accommodate pressure, temperature and mass flow rate instrumentation. The working fluid temperatures and pressures were measured at the inlets and outlets of the evaporator and condenser heat exchangers. The temperature and pressure of the condenser cooling water was also measured at the inlet and outlet of the condenser. Temperatures and pressures of the glycol brine were measured at the inlet and outlet of the evaporator. Flow meters were used to measure the flow rate of the brine and water flows.

K-type chrome-nickel thermocouples were used to measure the temperatures all of the fluid streams. The outputs from the thermocouples were logged and converted into temperatures via a picoscope TC-08, an 8 channel thermocouple data logger.

Details of the pressure transducers used are given in Table 3.1. In general, a gauge pressure transducer is located at one side of each stream in each heat exchanger and a differential pressure transducer is connected between the inlet and outlet of each stream

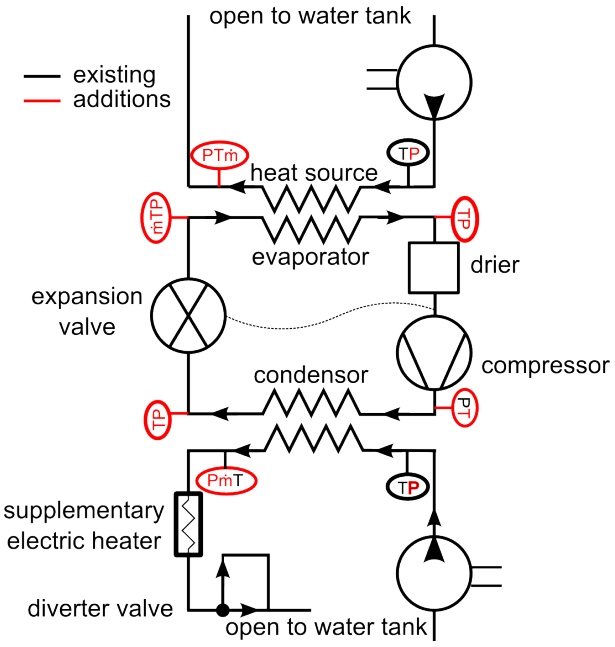

Figure 3.5: Schematic diagram of the Steibel Eltron WPF 5, 5kW ground source heat pump adapted with instrumentation

to measure the change in pressure across the heat exchanger. In the case of the refrigerant stream in the condenser, a high accuracy gauge pressure replaced the differential pressure transducer due to failure of the original differential transducer during commissioning.

Two brass turbine meters were used to measure the flow rate in the water and brine streams. These flow meters generate a pulsed output, the frequency of which is proportional to the flow rate. Frequency to voltage converters were constructed to allow the flow rate to be logged in the same manner as the voltage signals from the pressure transducers. Initially, a turbine meter was specified and purchased for the refrigerant stream. However, this failed during commissioning. As there was a long lead time and significant expense in replacing this piece of instrumentation, the decision was taken to proceed without a flow meter to directly measure the refrigerant flow rate. The mass flow rate of the refrigerant was deduced from heat balances over each of the heat exchangers, although this adds uncertainty to the refrigerant flow rate it is a reasonable estimate of refrigerant mass flow rate. The method of calculating refrigerant mass flow rate is discussed in section 3.4 and the value of including a flow meter in the future is discussed in section 3.6.

A logging script was written, for use with Durham Software for Windtunnels (DSW).

Instrumentation	Model	Location	Accuracy
Pressure Transducers:			
0 - 16 bar guage	Sensor Tecnics CTE8016GY1N	Evaporator Outlet	$\pm 0.1\% FSO$
0 - 35 bar guage	Sensor Tecnics CTE8035GY1N	Condenser Inlet	$\pm 0.1\% FSO$
0 - 5 bar guage	Sensor Tecnics CTE8005GY1N	Water Inlet, Brine Inlet	$\pm 0.1\% FSO$
0 - 35 bar guage	Omega PXM459-035BG10V	Condenser Outlet	$\pm 0.08\% FSO$
0 - 350 mbar	Sensor Tecnics BTEM50350D1AX	Brine Outlet	$\pm 0.2\% FSO$
0 - 100 mbar	Sensor Tecnics BTEM50100D1AX	Water Outlet	$\pm 0.2\% FSO$
0 - 200 mbar	Sensor Tecnics BTEM50200D1AX	Evaporator Inlet	$\pm 0.2\% FSO$
Thermocouples:			
-270 - 1370$^\circ C$	K Type	All	$\pm 0.2\% + \pm 0.5^\circ C$
Flow Meters:			
$0.003\dot{3}e^{-3}$ - $0.6\dot{6}e^{-3}m^3/s$	Omega FTB371B	Water Outlet Brine Outlet	$\pm 1\% FSO$

Table 3.1: Instrumentation used on GSHP rig

This software allowed the voltages from the pressures transducers and flow meters in addition to the temperatures measured by the picoscope to be logged by the same logging script, which was not previously possible with DSW. The script was flexible, allowing the user to select the number of readings, samples per reading and length of time between samples via a National Instruments USB-6218 logging card and PC running Windows XP.

3.3.2 Working Fluid Selection

The GSHP used is designed to operate with refrigerant R410a. This is a near azeotropic mixture of 50 % R32 / % R125, by mass. This means the mixture has a small change in temperature during phase change, of approximately 0.11 °C at 10 bar, as shown in Figure 3.6. The components of the mixture condense/evaporate at a very similar rate and therefore can be considered in a similar manner to a pure fluid. A set of tests were conducted with R410a to gather baseline data before changing refrigerant.

Simulations have been run to select a fluid mixture that has a significant glide and is capable of operating at similar pressures as the heat pump operating with R410a, i.e. in the range 9 - 25 bar. These showed that varying the composition of the R32/ R125 mixture yields a maximum glide of 0.45 °C at 9 bar with 0.16 % R32 / 0.84 % R125 mixture. This temperature glide was too small to carry out meaningful measurements of the effect of glide on heat exchanger performance and so an alternative fluid mixture was

sought.

R410a was developed as a replacement for R22 together with R407c. R407c is a ternary refrigerant mixture consisting of 23 % R32, 25 % R125, 52 % R134a. In order to limit the possible combinations of binary zeotropic mixture to try in the heat pump to sensible combinations, the remaining possible binary combinations of R407c components are considered. These are mixtures of R32/ R125 and R125/ R134a. REFPROP predicts maximum temperature glides at 9 bar of 4.5 °C and 6 °C at 50 % R125 / 50 % R134a and 35 % R134a / 65 % R32 respectively. Following discussions with a refrigerant supplier a mixture of R125/ R134a was selected, as R32 was difficult to procure.

However, while initially assured by the supplier that it would be possible for them to deliver the mixture of R125/ R134a, it became apparent this would have to be mixed specially by another supplier. This process became very time consuming and the lead time extended beyond the project timescale. It was therefore decided to replace R410a in the heat pump with R407c. R407c is a zeotropic mixture so the change in heat exchange due to this mixture can be measured. Figure 3.6 shows R407c has a glide of 5.13 $°C$ at 15 bar, which is sufficient to measure with the equipment available. The limitation of using R407c is that it is a ternary mixture making it more difficult to model the heat exchange process in detail with three working fluid components. However, this is an area of potential future work, and R407c is sufficient for the current project.

3.4 Data Analysis and Reduction

The pressure and temperatures measurements were used to establish the state of the working fluid at each point in the thermodynamic cycle. REFPROP was used to check the state of the refrigerant (i.e. subcooled, vapour/ liquid mixture or superheated). At entry to the evaporator the refrigerant was usually a vapour/ liquid mixture. If this was the case, for R410a working fluid, the vapour quality of the working fluid was determined by assuming a constant enthalpy throttling process through the expansion valve. REFPROP was then used to calculate the enthalpy, entropy and specific volume at each point in the cycle. In the case of R407c, the temperature change during the phase change allows

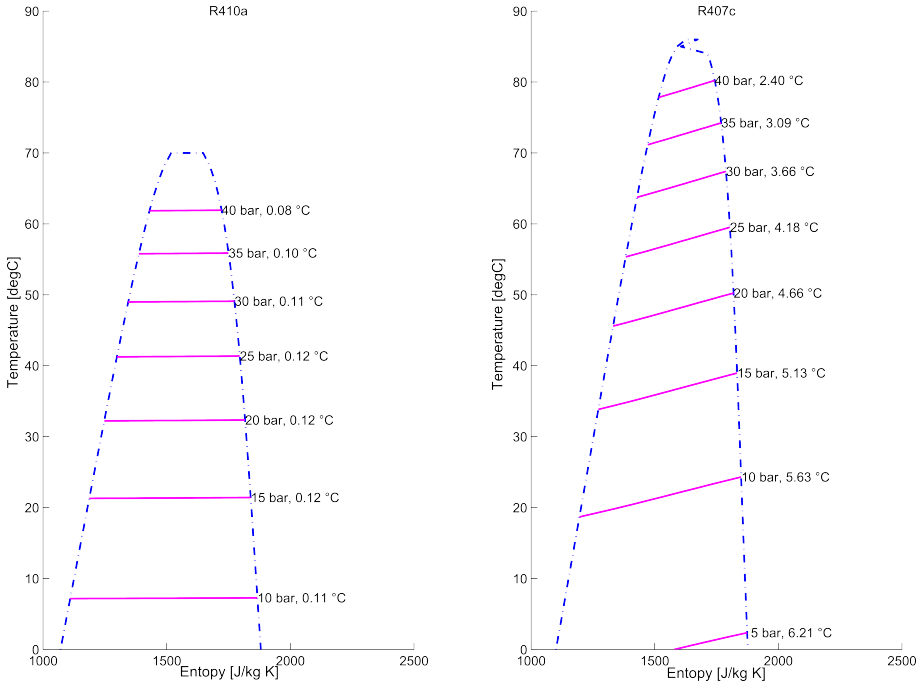

Figure 3.6: Plots of Temperature against Entropy showing temperature glides at various pressures for R410a and R407c.

the enthalpy and entropy to be directly calculated with REFPROP using the measured pressure and temperature data.

Mass flow rates of the brine and water flow are required to calculate the heat duty of the heat exchangers. In order to calculate the mass flow rate the volumetric flow rates measured must be multiplied by the density of each fluid. The density of water at the pressure and temperatures logged is calculated from REFPROP. The density of the glycol mixture was measured directly because the precise composition of the glycol/ water mixture is unknown.

To measure the density of the brine, a sample was taken from the evaporator inlet. The sample was decanted into a specific gravity bottle, of 25 ml and the density was calculated to be 1061 kg/m^3 at 1.00525 bar and 15.34 °. Glycol mixtures are not available in REFPROP, however the composition of the glycol mixture was deduced using an alternative fluid properties calculator, COOLPROP [22]. The brine was found to have a composition of 33 % Monoethylene glycol / 77 % water.

The rate of heat transfer for both heat exchangers was calculated using the following

equations:

$$Q_{evaporator} = \dot{m}_{brine}(h_{brine,in} - h_{brine,out}) \tag{3.1}$$

$$Q_{condenser} = \dot{m}_{water}(h_{water,out} - h_{water,in}) \tag{3.2}$$

Heat balances are then conducted across both the evaporator and condenser in order to determine the mass flow rate of the working fluid in the heat pump. For example the equation 3.3 was used together with equation 3.2 for $Q_{condenser}$ to determine the working fluid mass flow rate from the condenser data.

$$\dot{m}_{refrig} = \frac{Q_{condenser}}{h_{refrig_in} - h_{refrig,out}} \tag{3.3}$$

Heat loss to atmosphere was neglected. The heat exchanger is lagged and the area exposed to the atmosphere is small so the heat loss is expected to be small.

The COP was calculated using both working fluids. For a heat pump, COP is defined as heat energy output from the cycle divided by the mechanical work input to the cycle:

$$COP = \frac{Q_{condensor}}{W_{compressor}} \tag{3.4}$$

In order to compare the performance of two different heat pump cycle configurations COP is often expressed as a fraction of the maximum possible cycle performance. For a pure fluid the maximum COP of the heat pump cycle is calculated from the Carnot cycle, see Figure 3.7 The Lorenz cycle accommodates the change in temperature during phase change when using a zeotropic mixture. Therefore maximum COP for a zeotropic mixture is calculated from the Lorenz cycle, see Figure 3.7 and the following equations:

$$COP_{CARNOT} = \frac{1}{1 - \frac{T_{cond,in}}{T_{evap,out}}} \tag{3.5a}$$

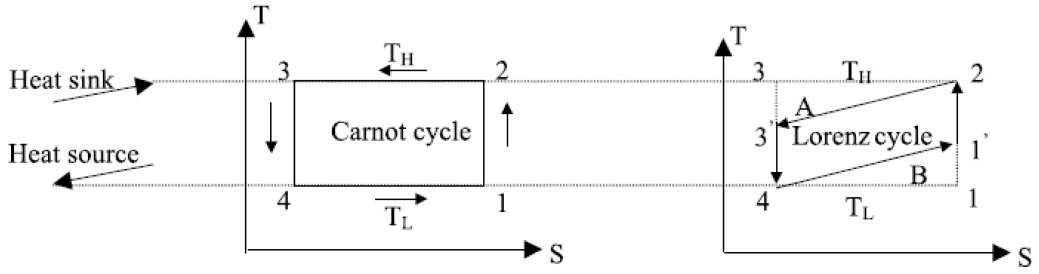

Figure 3.7: T-s diagrams of different COP calculations for pure and zeotropic mixtures

$$COP_{LORENZ} = \frac{1}{1 - \frac{T_{cond,in}+T_{cond,out}}{T_{evap,in}+T_{evap,out}}} \tag{3.5b}$$

Instrumentation errors are shown in Table 3.1. Standard uncertainty relations were used to combine the instrumentation errors and calculate the error associated with each calculation. Where a fluid property calculator is used, and the precise mathematical manipulation of the raw data are difficult to find, errors are calculated by finding the maximum and minimum bounds of a calculation from the uncertainty of the input data.

3.5 Results and Discussion

3.5.1 Azeotropic Working Fluid

The GSHP was run at a range of different brine inlet temperatures which results in different cycle performance. The change in brine inlet temperature is due to the tank water heating up over time. The results of the heat pump performance are dicussed below.

Raw Data

Figures 3.8 and 3.9 show the pressures, temperatures and flow rate data logged in the evaporator and condenser respectively, for a typical test. The data were logged over a period of approximately 1 hour, for a steady brine inlet temperature of 16.1 +/- 1.03 $°C$ in the case shown. The change in temperatures over the first 2000 seconds and initial discontinuity in pressures is due to the heat pump being switched on and the cycle reaching a steady state operation.

Figure 3.8 shows the evaporator data. This figure shows, once the GSHP, has reached a steady state operation, the temperature difference of the refrigerant at inlet and outlet of the evaporator is 7.31 $°C$ with a small pressure drop of 0.39 bar (measured at 3500 seconds). The volumetric flow rate of the brine is measured as 0.000201 +/- 6.23×10^{-6} m^3/s.

Figure 3.9 shows the data logged for the condenser. At 3500 seconds, in steady state operation, the refrigerant undergoes a 34.26 $°C$ temperature drop and 0.0933 bar pressure decrease. The water flow rate is measured to be 0.000316 +/- 6.23×10^{-6} m^3/s.

Thermodynamic Cycle

A Temperature-Entropy plot for the heat pump cycle was produced, using the approach described in Section 3.4 and is shown in Figure 3.10. This plot was produced using the data shown in Figures 3.8 and 3.9. Saturation points are calculated using measured pressures at the nearest point in the cycle using REFPROP. This plot shows that the cycle is as expected. Evaporation starts with the working fluid as a liquid/vapour mixture and the evaporation process ends in a superheated state. The compression stage increases the temperature and pressure of the refrigerant further and then the condensation process ends with the fluid in a subcooled state. The green dashed lines shows isobars calculated at the inlet pressure to each heat exchanger. This shows that the effect of the small pressure drop measured in the condenser is negligible. Conversely, the larger pressure drop across the evaporator, causes the temperature to drop during the evaporation process, before entering the superheated zone and increasing again. This pressure drop means that more heat input is required to reach saturated vapour than would be the case if the phase change occurred at a constant pressure.

Heat Exchange

Figures 3.11b and 3.11a are temperature against enthalpy plots for the evaporator and the condenser respectively. In the evaporator, the inlet temperature of the refrigerant was recalculated using the measured pressure and the assumed enthalpy (the condenser outlet enthalpy) because of the constant enthalpy throttling assumption. For all other

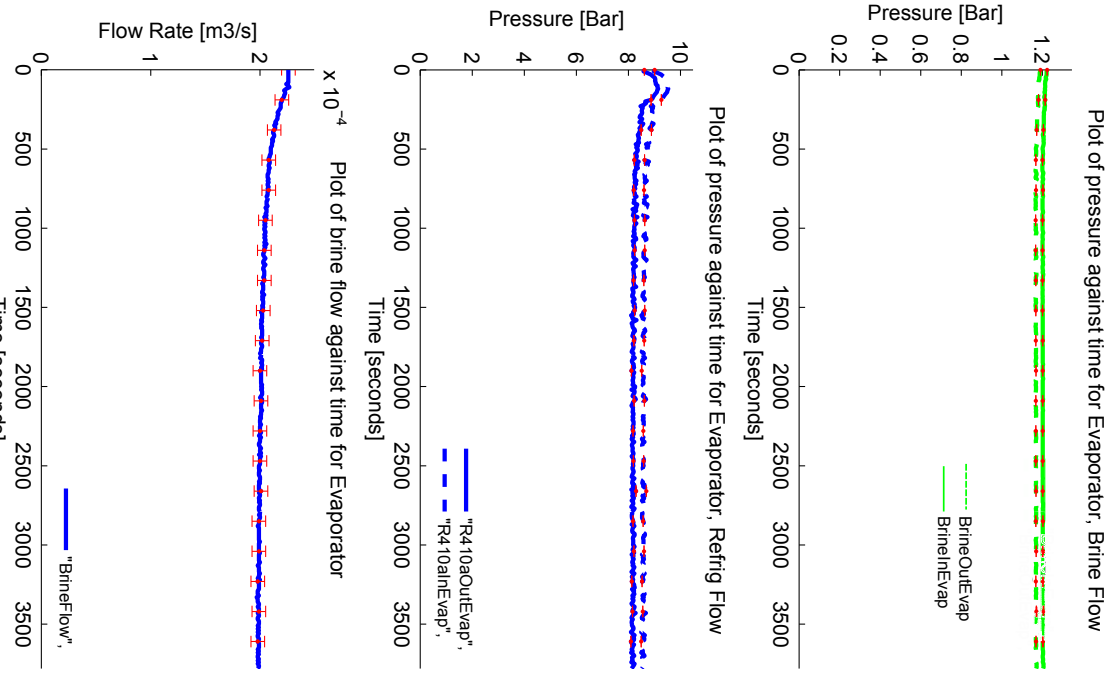

Figure 3.8: Evaporator data from GSHP with R410a working fluid. Error bars are shown in red

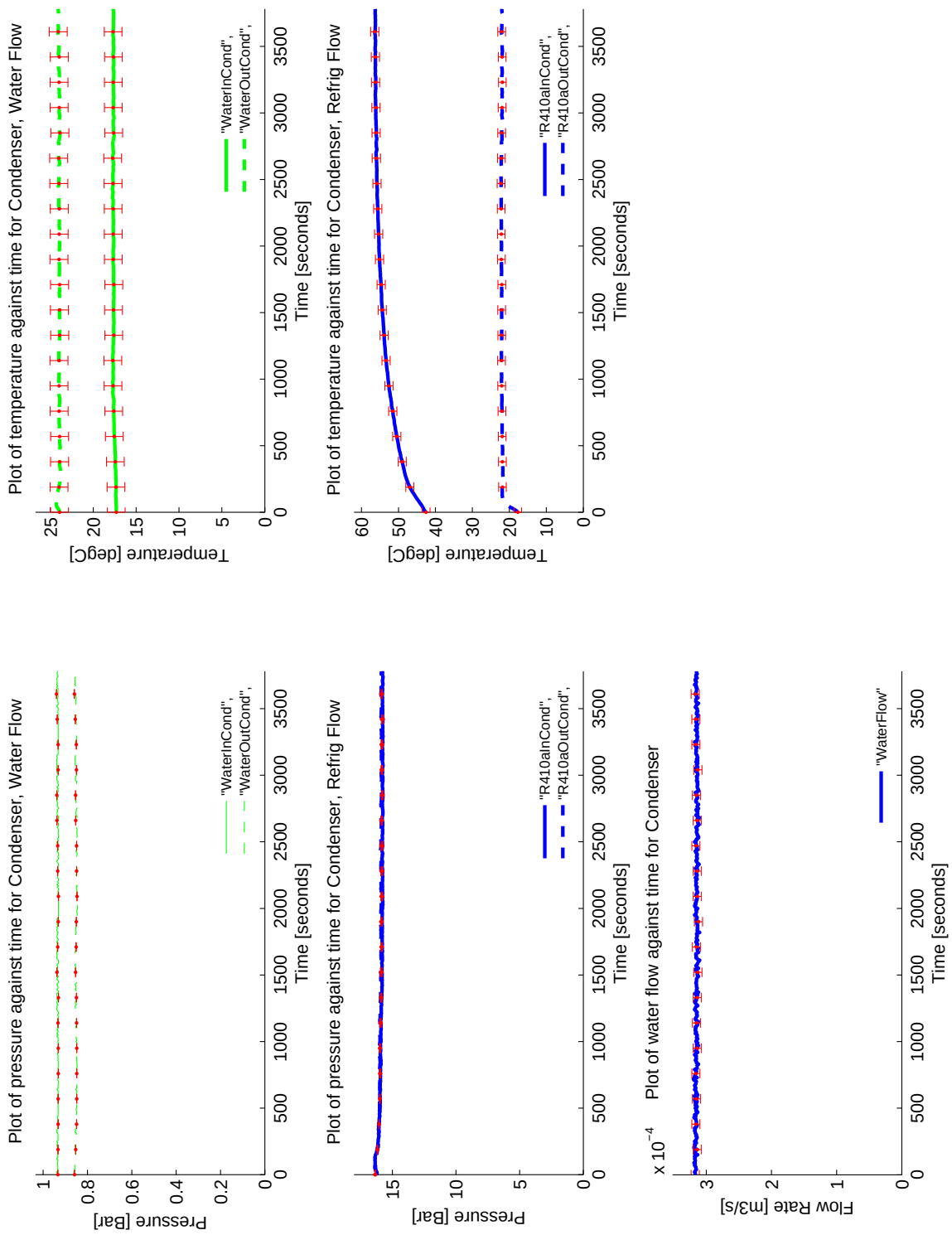

Figure 3.9: Condenser Data from GSHP with R410a working fluid. Error bars are shown in red

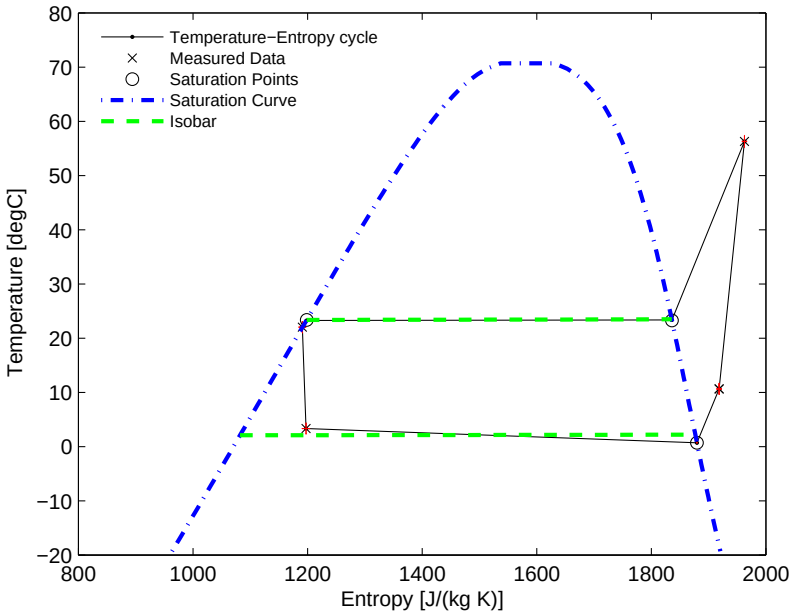

Figure 3.10: Temperature against entropy plot of GSHP with R410a working fluid. Error bars are shown in red

data points specific enthalpy is calculated from measured temperatures and pressures, using REFPROP.

Figure 3.11a shows that the pinch point in the evaporator occurs at the refrigerant inlet. Therefore, the heat transferred into the cycle is limited by the temperature of the refrigerant entering the evaporator. Also, the amount of heat energy transferred into the cycle defines the amount by which the refrigerant is superheated.

In the condenser the pinch point is at the vapour saturation point of the refrigerant, as shown in Figure 3.11b.

In both of these heat exchange plots, the heat source and sink streams are not well matched. This is shown on the figures by the large area between the two heat streams in each plot. Better matching of the heat source and sink stream would allow more heat transfer into/out of the cycle. As shown in these T-H plots the pinch point location determines the amount of heat transferred in to and out of the cycle, and therefore the cycle performance.

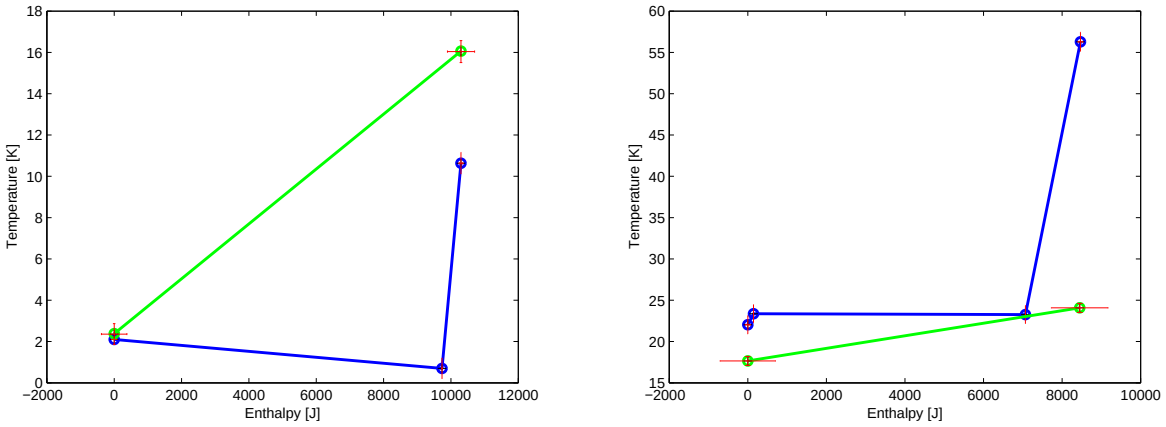

(a) Evaporator (b) Condenser

Figure 3.11: Temperature-Enthalpy plots of the heat exchangers with R410a

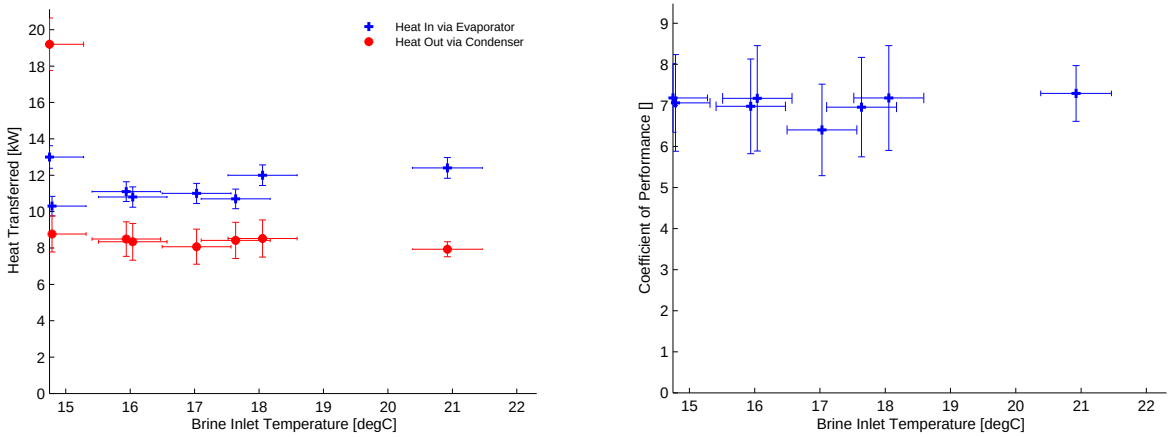

(a) Heat Transfer (b) Coefficient of Performance

Figure 3.12: Heat Transfer and COP against Brine Inlet Temperature for R410a

Heat Transferred and Coefficient of Performance

Figure 3.12a shows the heat input to and output from heat pump calculated form the data collected over a range of brine inlet temperatures. Each case uses data from steady state operation of the heat pump. There are no dramatic differences in heat exchange across the evaporator and the condenser at difference brine inlet temperatures. This is because the location of the pinch point in both the heat exchangers remains at the same locations for each brine inlet temperature, consistent with Figure 3.11.

In general the heat into the cycle increases with brine temperature and the heat output

of the cycle decreases slightly. The coefficient of performance remains reasonably constant at around 7, as shown in Figure 3.12b. This is because although the heat out decreases with increase in brine temperature, the compressor work also decreases. As COP is the ratio of heat output to compressor work, as given in equation 3.4, the COP of the heat pump remains sensibly constant with brine temperature.

3.5.2 Zeotropic Working Fluid

The GSHP was run at a range of different brine inlet temperatures resulting in different cycle performance with the zeotropic fluid R407c in a similar manner to the previous tests carried out with R410a. The results of the heat pump performance with R407c substituted for R410a are described in the following section.

Raw Data

Figures 3.13 and 3.14 show the pressures, temperatures and flow rates logged in the evaporator and condenser. The data were logged over a period of approximately 1 hour, with a steady brine inlet temperature of approximately 20.1 +/- 1.04 $°C$.

Figure 3.13 shows the evaporator data. This figure shows, at steady state, the temperature of the refrigerant increases by 2.75 $°C$ with a pressure drop of 0.39 bar over the evaporator (measured at 3000 seconds). The volumetric flow rate of the brine is measured as 0.000199 +/- $6.23x10^{-6}$ m^3/s.

Figure 3.14 shows the data logged for the condenser. At 3000 seconds, in steady state operation, the refrigerant decreases temperature by 25.46 $°C$ temperature drop and 0.042 bar pressure decrease. The water flow rate is measured to be 0.000242 +/- $6.23x10^{-6}$ m^3/s.

Thermodynamic Cycle

Figure 3.15 shows the Temperature-Entropy plot for the heat pump cycle with working fluid R407c. This is produced using the data shown in Figures 3.13 and 3.14. Saturation points are calculated using measured pressures at the nearest point in the cycle using REFPROP. This plot shows that the cycle is similar to the cycle with R410a as the

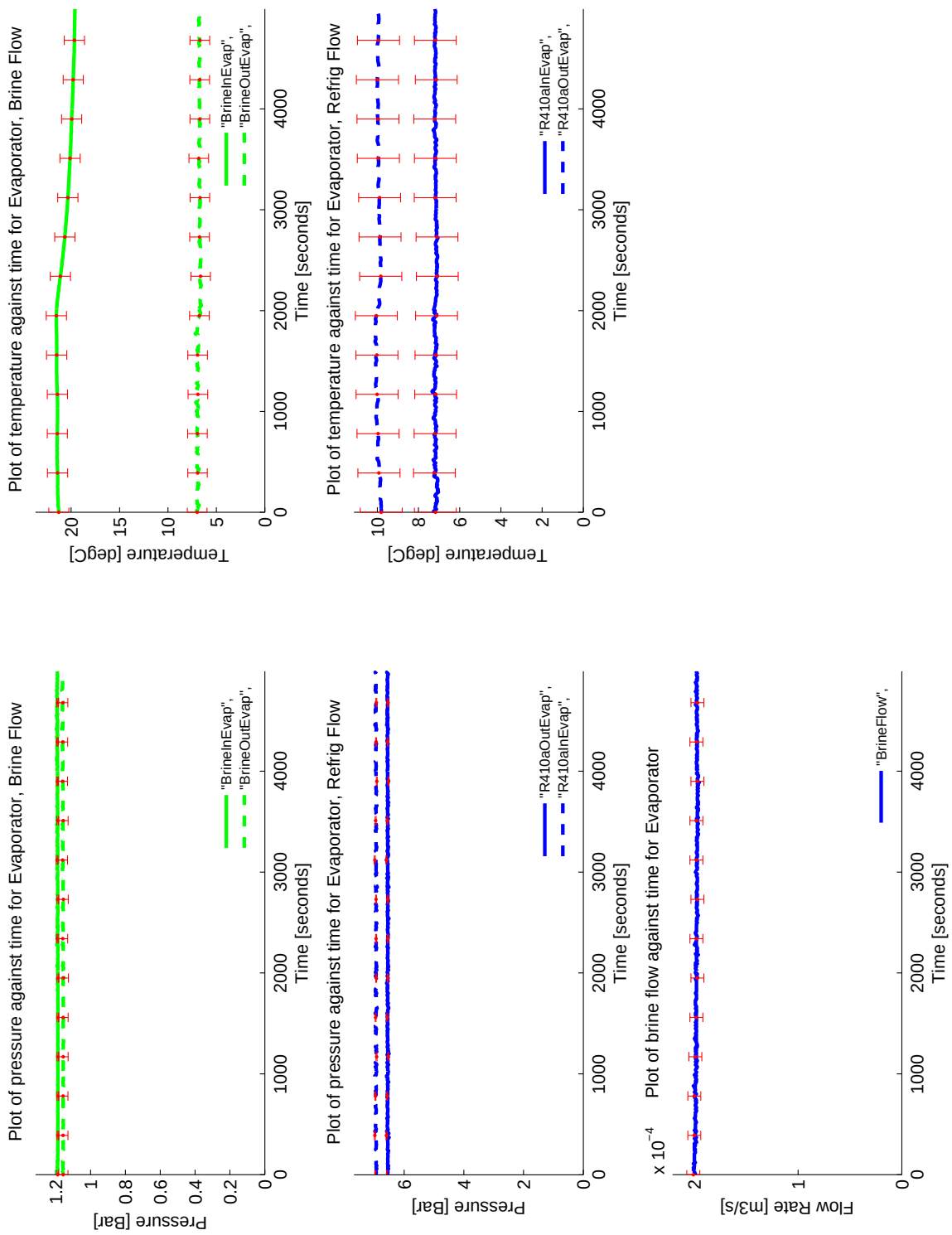

Figure 3.13: Evaporator data from GSHP with R407c working fluid. Error bars are shown in red, every 20 data points

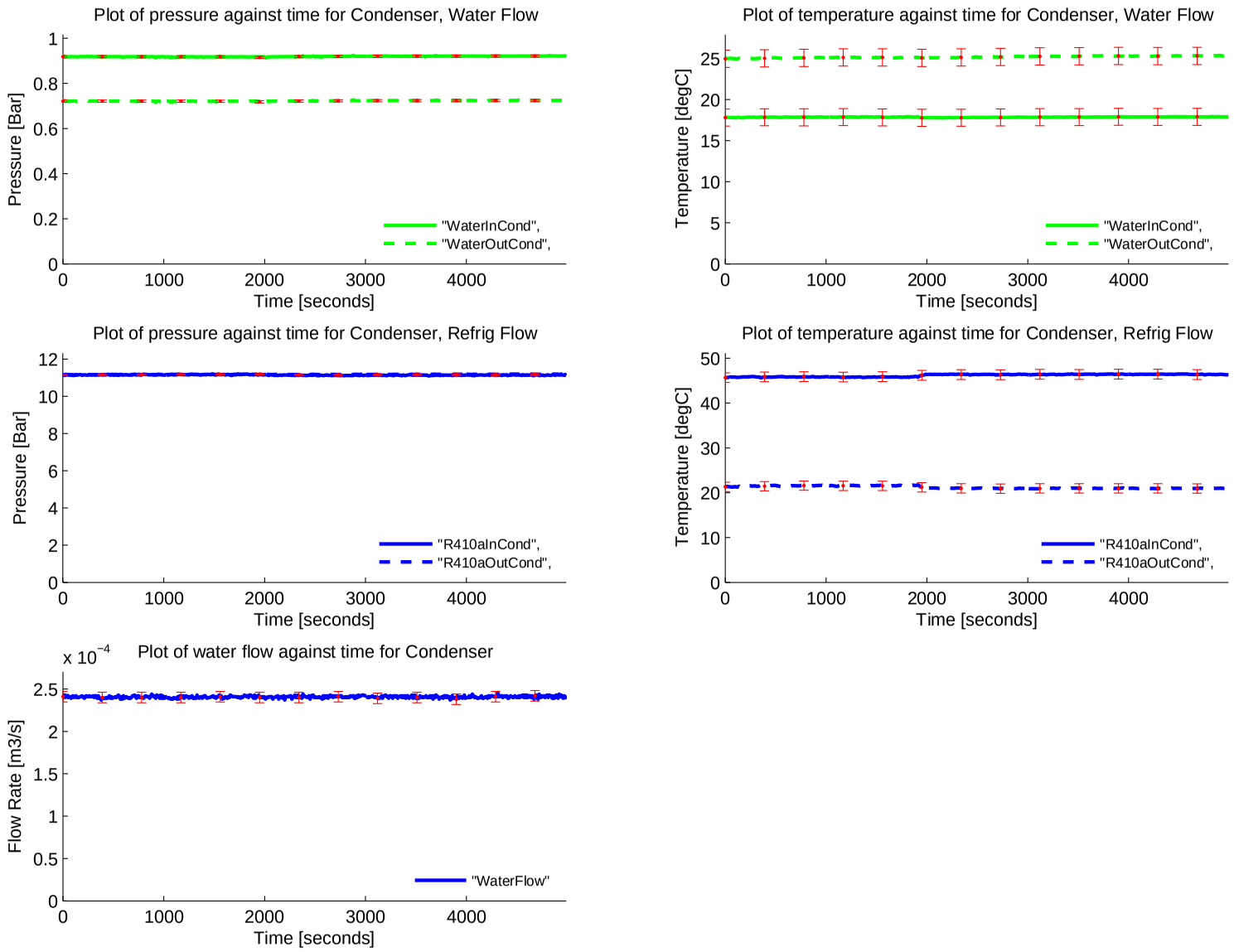

Figure 3.14: Condenser Data from GSHP with R407c working fluid. Error bars are shown in red, every 20 data points

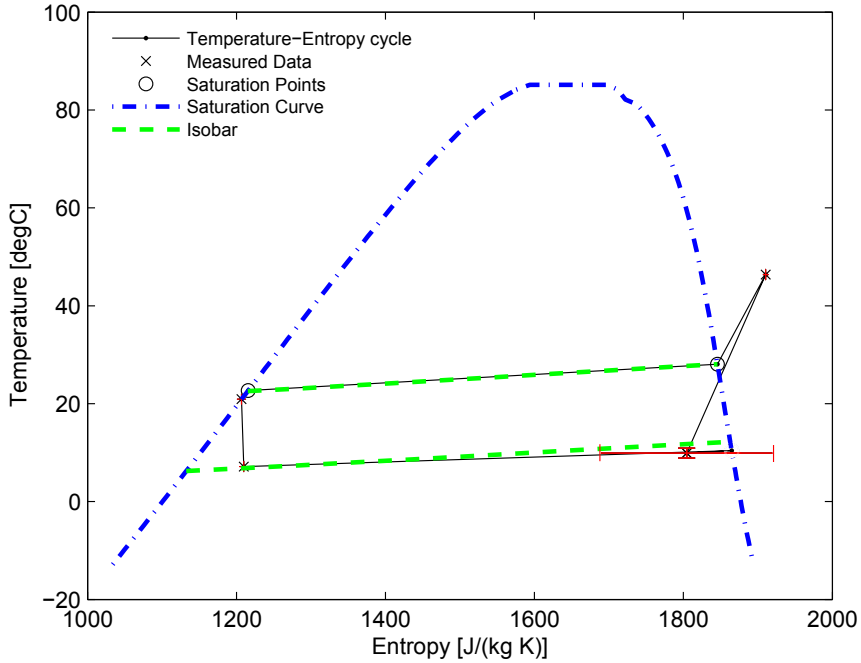

Figure 3.15: Temperature against entropy plot of GSHP with R407c working fluid. Error bars are shown in red

working fluid. The evaporation process starts with the working fluid as a liquid/ vapour mixture as with R410a, but it remains in a mixed state and does not become superheated. The error bars on this point are large because the error associated with the temperature measurement is +/- 1.02 °. This magnitude of change in temperature for the working fluid in a mixed state has a big effect on in the specific entropy of the working fluid, so the associated error is large.

The compression stage increases the temperature and pressure of the refrigerant and the working fluid becomes superheated during this process. The green dashed lines show isobars calculated at the inlet pressure to each heat exchanger. As with R410a this shows the effect of the small pressure drop in the condenser is negligible. The larger pressure drop over the evaporator, causes the temperature change during phase change to be smaller that that predicted for a constant pressure by 1.84 $°C$. This may negate some of the benefit of using a zeotropic mixture and so the heat exchange processes is investigated via Temperature-Enthalpy plots in the next section.

Heat Exchange

Figures 3.16a and 3.16b show plots of temperature against enthalpy for the evaporator and condenser with R407c using the same data as shown in Figure 3.15. These plots are calculated in the same way as described in section 3.5.1. The data used is taken at 3000 seconds.

The pinch point is at the refrigerant inlet for the evaporator which is the same as for R410a, Figure 3.16a. The temperature profiles of each side of the evaporator do cross over near the inlet to the evaporator, left hand side of the plot. This is not physically possible. It is assumed the error due to overlapping fluid streams is due to experimental uncertainty with the measurements and this is consistent with the magnitude of the error bars for these data.

In the condenser, the pinch point has moved in comparison with the results obtained using R410a, see Figures 3.11b and 3.16b. The pinch point is now at the refrigerant exit of the condenser so, in this case, the heat transferred is constrained by the inlet temperature of the water in the condenser. The pinch point temperature difference in the condenser plot with R407c is significantly larger than shown in the condenser plot for R410a at 3.07 $^{\circ}C$.

In general, both streams appear better matched in comparison to the heat exchanger plots for R410a as shown in Figure 3.11. For example, in the evaporator, if one was to imagine an azeotropic fluid, instead of the zeotrope R407c, the blue line would be horizontal, representing a much poorer temperature profile match. Therefore it might be expected that a larger amount of heat transfer would occur in the heat exchangers using R407c compared with R410a. However, by comparing graphs 3.17a and 3.12a it can be seen that this is not the case, this is explored in the next section.

Heat Transferred and Coefficient of Performance

Figure 3.17 shows plots of both heat transferred in the evaporator and condenser and COP against brine inlet temperature for all data set gathered using the working fluid R407c.

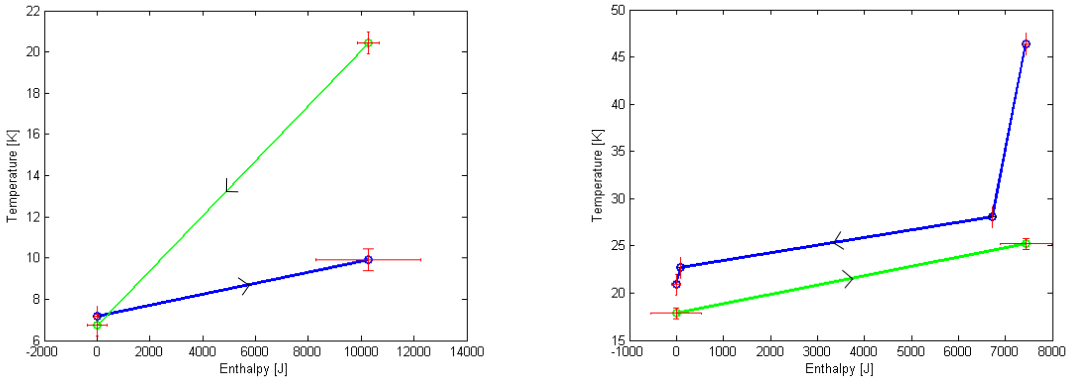

(a) Evaporator (b) Condenser

Figure 3.16: Temperature-Enthalpy plots for heat exchangers with R407c

There are large error bars in these plots, particularly on the COP plot, due to the large number of measured data points where the state of the working fluid falls in the fluid vapour/liquid mixture region. The errors propagated through the calculation of working fluid mass flow rate and compressor work results in the much larger error bars in Figure 3.17b than was the case for the R410a COP data in Figure 3.12b.

The trend shown in the plot of heat exchange against brine inlet temperature for R407c is similar to that shown in Figure 3.12a for R410a. The heat transferred into the cycle tends to increase with brine inlet temperature. However, heat transferred out of the heat pump appears to remain reasonably constant, where as for R410a heat output appeared to decrease with brine inlet temperature.

Generally, the magnitude of the heat transferred when R407c is used as the working fluid is lower than for R410a. By looking at the temperature enthalpy profiles for the data it is clear that the working fluid often does not vaporise completely in the evaporator. The pinch point does not prevent the fluid vaporising completely because it is located at the refrigerant inlet in all cases. This means the results confirm that the heat exchangers operating with R407c have a lower heat transfer coefficient than they do when R410a is used. The area of the heat exchanger would therefore need be increased to restore heat transfer to the same level as R410a if R407c is used.

The error bars on the COPs, Figure 3.17b are too large to draw any meaningful conclu-

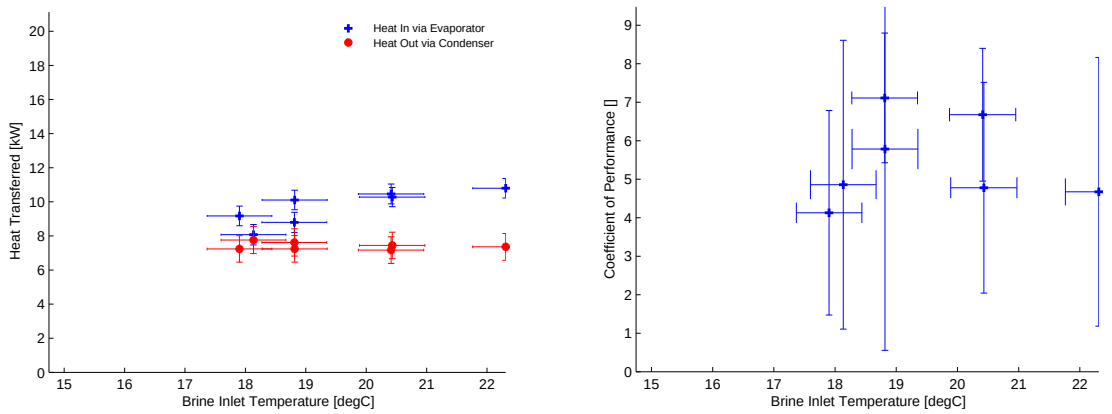

(a) Heat Transfer (b) COP

Figure 3.17: Plots of heat transferred and COP against brine inlet temperature for working fluid R407c

sions on the trend of these results. The central figures have a larger range, with generally lower values than for R410a which again suggests that heat exchanger performance is reduced when R407c is used in place of R410a.

3.6 Summary and Further Work

This chapter follows the experimental work for the thesis through rig design, construction and data collection. An assessment of literature and previous work from chapter 2 shows there is a need for experimental data on the phase change of refrigerant mixtures. Zeotropic mixtures have been shown, in Chapter 2 and literature, to provide a theoretical improvement in performance of thermodynamic cycles. However, experimental data shows measured performance improvement to be lower than theory would predict. The reason for this discrepancy is largely attributed to degradation of heat transfer coefficient for a zeotropic mixture during phase change, but this is not well understood.

For this study, it was recognised that heat exchangers could be tested with the same azeotropic and zeotropic working fluids as used in ORCs by adapting a commercially available GSHP, avoiding the need to buy a more specialised ORC system.

A suitable 5 kW ground source heat pump system was successfully instrumented and commissioned. This experimental rig was designed to allow the measurement of heat

exchange in both the evaporator and condenser. Instrumentation was specified to collect temperature and pressure data, via thermocouples and pressure transducers, at inlet and outlet of both heat exchangers in the heat pump cycle. Flow rate was measured via a turbine meter for the non-refrigerant stream in each heat exchanger. Data were logged using DSW.

Tests were carried out with azeotropic and zeotropic working fluids. The results show that the heat pump cycle operates as expected with both fluids. The data were used to determine Temperature-Entropy plots of the cycle behaviour and Temperature-Enthalpy plots of heat exchange in both the heat exchangers. The results clearly demonstrated how zeotropic fluids decrease the heat transfer coefficients in the heat exchangers compared with operating them with azeotropic fluids. Despite a better apparent match in the temperature enthalpy profile between the fluid streams in the heat exchangers with zeotropic mixture, the total amount of heat transferred and hence COP both decreased due to the poorer heat transfer coefficients with the zeotropic working fluid. The results are consistent with the findings of Lee et al. [9] and Gabrielli and Vlamming [11] etc. The following three recommendations are made for further experimental testing with this new test facility:

- The uncertainty in the results obtained from the test facility can be reduced significantly by installing a flow meter to directly measure the mass flow rate of the working fluid in the heat exchanger. Without a flow meter on the refrigerant line the refrigerant mass flow rate had to be deduced through heat balances over the heat exchangers. While this was an appropriate method, the calculated mass flow rates carry large uncertainties that could be reduced by direct measurement.

- The zeotropic working fluid tested was a mixture of three gases. A binary fluid mixture is needed in order to compare the experimental results with those from the heat exchange model described in Chapter 4 because of the limitations of REFPROP. This would allow detailed comparison to be made between experimental data and the theoretical modelling of the phase change process for a binary mixture, which

would address a gap in current literature. It is recommended that a zeotropic binary fluid mixture is sourced for future tests.

- Stratification within the underfloor water reservoir used with the test facility is considered to be a source of uncertainty in test conditions. Greater control over the heat pump heat source and sink would be available if any stratification in the water tank was measured and the water pipes could be adjusted to create different conditions for the heat pump to operate at. Hardware has been developed to measure stratification in the water reservoir and this should be implemented in future tests. A floating device, affectionately known as 'Jenny the jellyfish', was built, this is shown in Figure 3.18. This has 5 temperature sensors (DS18B20) which hang below the device capable of measuring the temperature at different depths within the tank. The temperatures are logged by a raspberry pi, a tiny computer, running from a battery inside a waterproof box. Floats on either side provided stability in the water and extra buoyancy, it was planned to attach hang the device on a line above the water so the position of the device could be fixed. A Bluetooth module was installed on the raspberry pi to allow remote communication with Jenny to a computer. Data were saved to an SD card locally and the Bluetooth communication allowed the user to view the most recent temperature logged by the sensors.

References

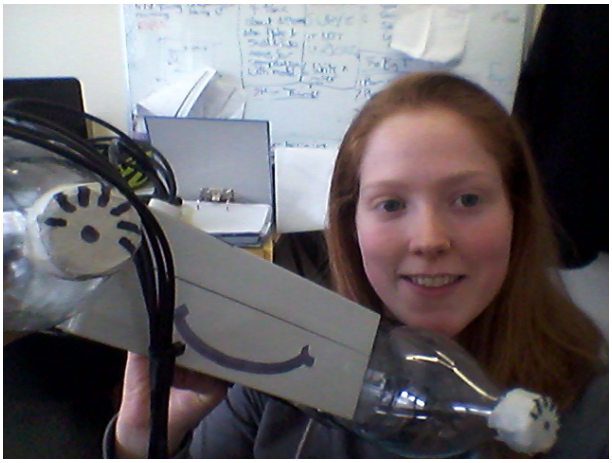

Figure 3.18: Floating bluetooth device for remote measurement and logging of temperatures in water

[1] M. Chys, M. van den Broek., B. Vanslambrouck., and M. D. Paepe, "Potential of zeotropic mixtures as working fluids in organic rankine cycles," *Energy*, vol. 44, pp. 623–632, 2012.

[2] F. Heberle, M. Preissinger, and D. Bruggemann, "Zeotropic mixtures as working fluids in organic rankine cycles for low-enthalpy geothermal resources," *Energy*, vol. 37, pp. 364 – 370, 2012.

[3] S. Lecompte, B. Ameel, D. Ziviani, M. van den Broek, and M. De Paepe, "Exergy analysis of zeotropic mixtures as working fluids in organic rankine cycles," *Energy Conversion and Management*, vol. 85, pp. 727–739, 2014.

[4] R. Radermacher, "Thermodynamic and heat transfer implications of working fluid mixtures in rankine cycles," *International Jounral of Heat and Fluid Flow*, vol. 10(2), pp. 90–102, 1989.

[5] X. Wang and L. Zhao, "Analysis of zeotropic mixtures used in low-temperature solar rankine cycles for power generation," *Solar Energy*, vol. 83, pp. 605 – 613, 2009.

[6] W. Wu, L. Zhao, and T. Ho, "Experimental investigation on pinch points and maximum temperature differences in a horizontal tube-in-tube evaporator using zeotropic refrigerants," *Energy Conversion and Management*, vol. 56, pp. 22–31, 2012.

[7] A. Chandra, *Refrigeration and Air Conditioning*. PHI Learning, 2010.

[8] F. Department for Environment and R. Affairs, "The eu ozone regulation: Legislative update and strategies for hcfc phase-out. information sheet rac 8: R22 phase-out," April 2012.

[9] M. Yilmaz, "Performance analysis of a vapor compression heat pump using zeotropic refrigerant mixtures," *Energy conversion and Management*, vol. 44, no. 2, pp. 267–282, 2003.

[10] D.-Y. Lee, Y. Ahn, Y. Kim, Y.-S. Chang, and L. Nam, "Experimental investigation on the drop-in performance of r407c as a substitute for r22 in a screw chiller with shell-and-tube heat exchangers," *International journal of refrigeration*, vol. 25, no. 5, pp. 575–585, 2002.

[11] J. Pannock, D. Didion, and R. Radermacher, "Performance evaluation of chlorine free zeotropic refrigerant mixtures in heat pumps–computer study and tests," *Electric Power Research Institute*, vol. 0, pp. 1 – 73, 1992.

[12] C. Gabrielii and L. Vamling, "Replacement of r22 in tube-and-shell condensers: experiments and simulations," *International journal of refrigeration*, vol. 20, no. 3, pp. 165–178, 1997.

[13] D. Sajjan, T. Karlsson, and L. Vamling, "Reasons for drop in shell-and-tube condenser performance when replacing {R22} with zeotropic mixtures. part 1. analysis of experimental findings," *International Journal of Refrigeration*, vol. 27, no. 5, pp. 552 – 560, 2004.

[14] T. Karlsson and L. Vamling, "Reasons for drop in shell-and-tube condenser performance when replacing {R22} with zeotropic mixtures. part 2: investigation of mass transfer resistance effects," *International Journal of Refrigeration*, vol. 27, no. 5, pp. 561 – 566, 2004.

[15] B. M. Fronk and S. Garimella, "In-tube condensation of zeotropic fluid mixtures: A review," *International Journal of Refrigeration*, vol. 36, pp. 534–561, 2013.

[16] F. Smit, J. Thome, and J. Meyer, "Heat transfer coefficients during condensation of the zeotropic refrigerant mixture hcfc-22/hcfc-142b," *Journal of Heat transfer*, vol. 124, no. 6, pp. 1137–1146, 2002.

[17] A. Cavallini, G. Censi, D. Del Col, L. Doretti, G. A. Longo, and L. Rossetto, "Condensation of halogenated refrigerants inside smooth tubes," *HVAC&R Research*, vol. 8, no. 4, pp. 429–451, 2002.

[18] M. Dobson and J. Chato, "Condensation in smooth horizontal tubes," *Journal of Heat Transfer*, vol. 120, no. 1, pp. 193–213, 1998.

[19] L. Silver, "Gas cooling with aqueous condensation," *Trans. Inst. Chem. Eng*, vol. 25, pp. 30–42, 1947.

[20] K. Bell and M. Ghaly, "An approximate generalized design method for multicomponent/partial condenser," in *AIChE Symp. Ser*, vol. 69, pp. 72–79, 1973.

[21] W. Richardson, "Revolution power." Personal Communications, 2015.

[22] I. H. Bell, J. Wronski, S. Quoilin, and V. Lemort, "Pure and pseudo-pure fluid thermophysical property evaluation and the open-source thermophysical property library coolprop," *Industrial & Engineering Chemistry Research*, vol. 53, no. 6, pp. 2498–2508, 2014.

Chapter 4

Understanding Heat Exchange with Zeotropic Mixtures

4.1 Introduction

Zeotropic mixtures have been shown, in theory, to improve the thermodynamic performance of organic Rankine cycles for some heat sources (see Chapter 2). However, the use of mixtures of working fluids instead of pure fluids will also influence other factors key to ORC system performance and design such as cost and size of plant [1–3]. Previous studies have identified that the heat transfer coefficient of zeotropic mixtures degrades (relative to that of the constituent fluids) during phase change and therefore larger heat exchanger areas are required for these fluids, than are needed for single fluids.

Chapter 3 described an experimental facility where heat exchange for both an azeotropic and a zeotropic working fluids was investigated. In this chapter, the mechanisms involved in phase change for a zeotropic mixtures and its effects on heat transfer coefficient are explored further by considering the available theoretical data and theoretical modelling.

The physical effect of a decrease in heat transfer coefficient is important to plant design because it can mean an increase, in both cost and area of the heat exchangers required for the same heat transfer. Size of plant is particularly important when implementing an Organic Rankine Cycle (ORC) fuelled by waste heat streams. In these scenarios, available

space is often limited due to the existing plant. As the evaporator and condenser are the largest components in the ORC cycle, it is these components that determine the maximum size of ORC that it is possible to install. It is therefore important to be able to minimise the size of the heat exchangers needed for each application.

In order to estimate the size of heat exchangers required, a reliable value for heat transfer coefficient between the fluid streams in the evaporator and condenser is needed. For zeotropes, this requires modelling of the phase change process in detail, because it is widely reported in the literature that the heat transfer coefficient of a fluid mixture is lower than that obtained from a linear interpolation of the pure component values. However, the reason for this is not well understood [4, 5]. During the phase change processes, the concentration of the mixture in the liquid and vapour phases changes according to the difference in volatility between the mixture components. It is this that causes the local heat transfer coefficient of the fluid mixture to vary during the phase change process. The changing concentration in liquid and vapour phase means modelling phase change for zeotropes is more complex than for pure fluids.

Typical methods for modelling the rate of heat transfer in heat exchangers are the Log Mean Temperature Difference (LMTD) and Number of Tranfer Units (NTU) methods. These methods are based on the same assumptions which include constant overall heat transfer coefficients and fluid stream heat capacities [2]. This is not the case for the phase change of fluid mixtures. An alternative method of modelling the local heat transfer coefficient along the heat exchanger is required in order to calculate the heat exchange area needed.

The available literature on quantifying the local heat transfer coefficient of binary zeotropic mixtures is reviewed in this chapter and a method for modelling this process is presented. The model is used to investigate the effect on heat exchanger size for ORCs.

The experimental results, presented in Chapter 3, are reviewed in the next section. This allows the global heat transfer coefficient for the heat exchangers in heat pump experiments for both R410a and R407c working fluids to be compared. A detailed model

of the condensation process for a fluid mixture is proposed based on methods available from the literature. The model could be used to calculate the required heat exchanger area for pure fluids and fluids mixtures, and used as an indicator of plant size to fully understand the implications of using zeotropic fluid mixtures as working fluid in ORCs.

4.2 What do the experimental results show?

4.2.1 Comparison of R410A and R407c UA value

The experimental results from Chapter 3 were used to compare the heat exchange and overall heat transfer coefficient for the two different working fluids tested under similar operating conditions.

The total heat transfer across the heat exchangers in the test rig described in Chapter 3 was calculated by measuring the temperature and pressure at inlet and exit of the heat exchanger and measuring the flow rate through them. Density and specific enthalpy were calculated from the measurements using REFPROP and total heat transfer was calculated according to the equation in 4.1. Heat transfer can also be expressed by the right hand of this equation, where ΔT_{LM} is the log mean temperature difference, U is the global heat transfer coefficient and A is the heat exchange area.

$$Q = \dot{V}\rho\Delta\dot{h} = UA\Delta T_{LM} \tag{4.1}$$

The heat transfer coefficient is the amount of heat energy transferred per unit of area for each degree of temperature difference. This quantity is a measure of how readily the fluid streams transfer heat energy between themselves, a high heat transfer coefficient is therefore desirable for heat exchangers.

It is not possible to reduce the data from Chapter 3 to just the heat transfer coefficient without high uncertainty, as this would require calculation of the heat exchange area for each heat exchanger, which is unknown and could only be roughly approximated. For the data taken from the heat pump rig, described in chapter 3, the heat exchanger area is the

same for both sets of data measured with the azeotropic (R410a) and zeotropic (R407c) working fluids. Therefore the comparison of the UA value used in this study is effectively a comparison of the difference in heat transfer coefficients.

In order to reduce the data to a UA value, the log mean temperature difference must be calculated according to equation 4.2. Where the data spans different phase conditions for the refrigerant fluid the saturation temperature is calculated from the pressure measured at the nearest location. Errors may be incurred from this approach, but in the absence of pressure measurements along the length of the heat exchanger, this is the best approximation that can be made for the current data.

$$\Delta T_{LM} = \frac{\Delta T_{IN} - \Delta T_{OUT}}{ln(\frac{\Delta T_{IN}}{\Delta T_{OUT}})} \tag{4.2}$$

For some of the data for R407c presented in chapter 3, the temperature profiles crossed over near the inlet to the evaporator (see Figure 3.16a. While the error bars associated with the measurements account for this error, it is not possible to make an appropriate assumption for how to adjust this data to allow the computations of UA values for these results to be made. Therefore, they are excluded from this analysis.

The error bars associated with the calculations are large due to error propagation. In particular the high uncertainty associated with data involving mixed vapour/liquid phases.

Figure 4.1 shows UA values calculated for the azeotropic and zeotropic data from Chatper 3 plotted against brine inlet temperature for R410a and R407c. By comparing UA values for the condensers for both R410a and R407c, in general the UA values are higher for R410a than R407c. Therefore, the heat transfer coefficient is generally higher for R410a than R407c. This means a larger area heat exchanger is required if R407c to achieve the same heat transfer at that measured with R410a.

In order to understand the lower heat transfer coefficient for R407c and its implications for heat exchanger design, a theoretical model capable of calculating the heat transfer coefficient of zeotropic mixtures is required. As reported in chapter 2, traditional models

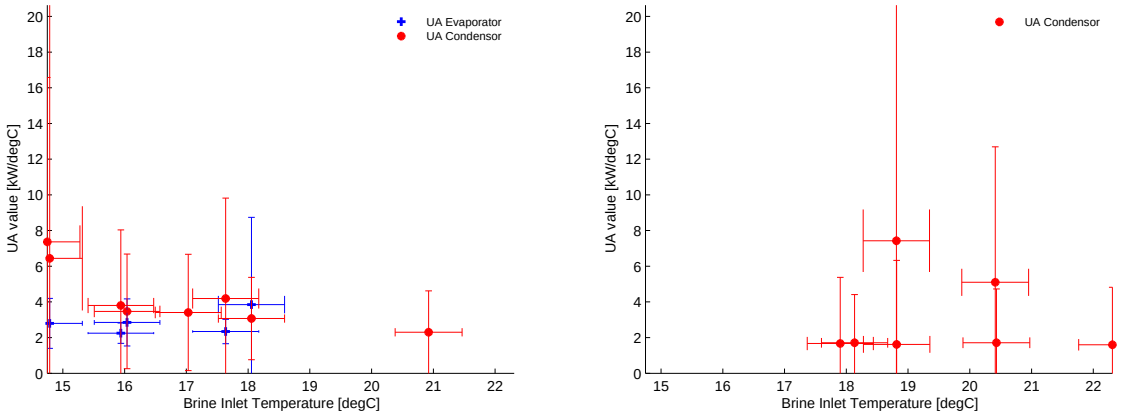

(a) R410a (b) R407c

Figure 4.1: Plots of UA value against brine inlets temperature

assume constant heat transfer coefficient during phase change, this is not always an accurate assumption for zeotropic mixtures and therefore a more sophisticated model is required.

4.3 Literature Review of Heat Exchange Models for Zeotropic Mixtures

Several studies calculate heat exchanger area as part of a combined thermodynamic approach to ORC design, for example [6, 7]. However, none of these studies can accommodate modelling zeotropic mixtures.

Zeotropic mixtures were initially proposed for use in vapour compression cycles for refrigeration and heat pump applications, [8–10], before later being proposed for use in ORCs [5]. Literature on the behaviour of zeotropic mixtures is more widely available for applications in vapour compression cycles than Organic Rankine Cycles, though for both cycles there is no evidence zeotropic mixtures have been adopted in any commercial systems. Interest in zeotropic mixtures comes not only from the potential improvement they offer for thermodynamic performance, but also because of the requirement to find alternative working fluids to CFCs and HCFCs, as these are phased out to comply with international agreements for reducing the use of fluids with high Global Warming Potential

(GWP) [5, 11].

It is widely reported that zeotropic mixtures exhibit a lower heat transfer coefficient relative to that of the pure constituent components during both evaporation and condensation processes, [4, 5, 11]. The degradation of the heat transfer coefficient is different for the evaporation and condensation processes and studies published do not agree on the precise reasons for this.

Radermacher [5] attributes heat transfer degradation during evaporation to loss of wall superheat and mass transfer resistance. Loss of wall superheat is the decrease the thermal gradient due to the evaporation temperature increasing during evaporation. This only applies in the case of a constant wall temperature. Mass transfer resistance arises from the non-uniform concentration of the mixture in each phase particularly near the liquid/vapour interface. During evaporation there is less of the more volatile fluid in the liquid near the interface. This slows the evaporation process as the more volatile fluid has to diffuse through the less volatile fluid before it can vaporise. However, Kedzierski [4] also identifies that there are several explanations for heat transfer degradation and although the above reasons are popular it cannot be confirmed that these are the only significant effects. Kedzierski [4] and Didion [11] both identify the nonlinear variation of thermodynamic and transport properties with composition may contribute to heat transfer degradation in both evaporation and condensation and Didion identifies that fluid property calculators, like REFPROP, are inadequate at capturing these non-linear effects. Although REFPROP has been updated since both Didion and Kedzierski's studies, and is therefore likely to be better at accurately capturing zeotropic mixture properties, it is not possible to quantify the accuracy of the equations of state employed by REFPROP [12].

The temperature, concentration and heat flux profiles of a zeotropic mixture during film condensation are shown in Figure 4.2. Fronk and Radermacher explain that as heat is removed from the fluid mixture the least volatile component condenses most readily. Therefore, locally at the vapour/liquid interface the concentration of the more volatile

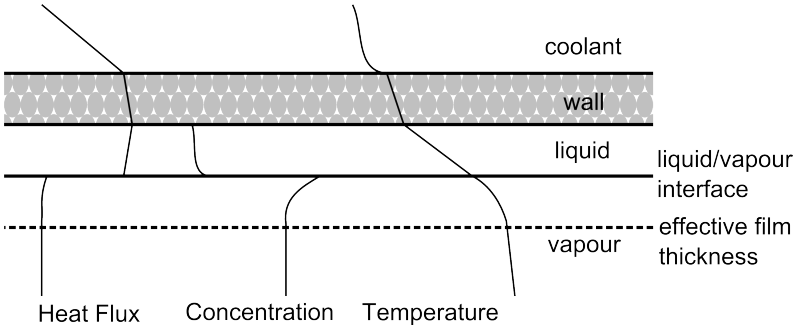

Figure 4.2: Temperature, concentration and heat flux profiles during condensation of a mixture

component is higher, as shown in Figure 4.2 [5, 13]. This results in a lower saturation temperature. Similarly the concentration gradient of the vapour portion means the more volatile component diffuses from the interface to the vapour bulk. So the concentration gradient causes a resistance to transfer of vapour into the liquid phase. The concentration at the interface determines the interface temperature, thus the heat and mass transfer effects in condensation of mixtures are strongly coupled [13].

Kedzierski [4] asserts that the local heat transfer coefficient is often calculated using the saturated equilibrium temperatures. However, if concentration gradients are present during phase change then temperature at the liquid/vapour interface will be higher than the equilibrium temperature and therefore the local heat transfer coefficient will be calculated incorrectly using the equilibrium temperature. This suggests that the apparent degradation in heat transfer coefficient could be due to inadequate experimental method as a key assumption is that the interface temperature is the equilibrium temperature. These studies highlight the high amount of uncertainty surrounding phase change of zeotropic mixtures - from the physical mechanisms that result in heat transfer degradation, to the inadequacy of both theoretical and experimental methods used to quantify the local heat transfer coefficient of a zeotropic mixture.

The larger heat transfer degradations occur for mixture compositions with larger temperature glides, which also have the greatest potential for improving thermodynamic performance. Similarly, glide and degradation in heat transfer coefficient decrease with

increase in pressure [5]. This means that for an ORC, the condenser, will suffer the largest decrease in heat transfer coefficient. Therefore, this chapter focuses on modelling the behaviour of zeotropic mixtures during condensation, in order to understand how to quantify the local heat transfer coefficient.

Modelling the heat transfer during phase change requires heat exchanger geometry, direction of fluid streams, orientation (i.e horizontal or vertical) and flow regime to be defined. Modelling strategies are published for all combinations of horizontal/vertical flow, for boiling/evaporation processes, inside/outside single tubes, tube bundles and plates and on smooth and enhanced surfaces, in co and counter current flows, [13–17].

In order to constrain the study, condensation inside smooth tubes is investigated in detail in this work as they represent common types of heat exchangers that are used in ORCs. For example, finned tube and shell-and-tube heat exchangers [13]. There are four main modelling approaches to in-tube condensation: conservation equation, non-equilibrium, equilibrium and empirical models.

Conservation equation models use transport equations for continuity, momentum, energy and species conservation for the liquid and vapour components of flow during condensation. These models are theoretically thorough, but they are expensive to solve and computationally demanding [13]. Consequently, there are not many studies published which use this approach for in-tube condensation.

Conversely, equilibrium and empirical methods are computationally much less intensive but less theoretically rigorous. In equilibrium models complete thermodynamic equilibrium is assumed throughout both phases, so this method fails to model the concentration gradients that influence the rate of vapour condensation at the liquid/vapour interface. Bell and Gauly, [18], and Silver, [19], first developed this technique, by assuming equilibrium at interface and by neglecting mass transfer effects. However, Bell and Ghaly argue that simplifying the physics of the mixture phase change process in this way will result in the heat transfer coefficient being under-predicted. This is partially compensated for by assuming that the sensible heat change of the saturated gas mixture must be conducted

across the gas film. Bell and Ghaly acknowledge their assumption is very conservative and will result in an over estimation of the heat transfer area required.

Webb et al. [20] present a study on the relationship between the Silver, Bell and Ghaly equilibrium method and the non-equilibrium method developed by Colburn and Drew [21]. The Lewis number, defined as the ratio of Schmit to Prandtl Number ($Le = \frac{Sc}{Pr}$), is used to compare the performace of the methods for different mixtures. Webb et al. found that the equilibrium method is only in agreement with the non-equilibrium method over a small range of Lewis number, 0.6 - 0.8. Furthermore at a Lewis number > 1 Webb reports the equilibrium method is unsafe, predicting a higher than actual heat transfer coefficient and therefore a lower heat exchange area than actually required. At Le < 1 the equilibrium method under predicts the heat transfer coefficient and therefore this method is considered conservative as it will over predict the required heat exchange area. Webb et al. point out that the overall agreement of the equilibrium method to the actual heat exchange area is helped because the Lewis number can vary from less than one to greater than one along a heat exchanger and therefore there is some over/under prediction of the heat transfer coefficient which will cancel out. Webb et al. propose a new correlation to improve the agreement of the equilibrium method and the non-equilibrium model, based on this work.

This study aims to quantify and understand the effect of zeotropic mixtures on required heat transfer area. Zeotropic mixtures fundamentally change the mass transfer process during condensation which cannot be modelled accurately via the equilibrium method. Given the lack of theoretical basis to the equilibrium method and its poor accuracy it will not be considered further in this work.

Similarly, empirical correlations have been developed for mixture condensation, for example Koyama et al. [22] who developed an empirical relation for the heat transfer coefficient of a mixture of R22/R114 in grooved horizontal tube heat exchanger. However, correlations of this type lack a physical basis and have extremely limited applicability, usually only for one mixture in a specific heat exchanger configuration. As it is necessary

to compare the performance of several fluids and fluid mixtures in this study, it is not appropriate to use empirical models.

A compromise between the over simplification of the equilibrium and empirical models and the complexity of conservation models is found in the non-equilibrium models. These models assume thermodynamic equilibrium at the liquid vapour interface and accounts for concentration gradients by calculating the bulk concentration of the liquid and vapour using coefficients for heat and mass transfer. There is a large amount of literature available on non-equilibrium models. One of the first such models was developed in a study by Colburn and Drew [21].

Colburn and Drew developed a set of equations to describe the heat transfer from the vapour to the liquid and from the liquid to the cooling stream. These are described in detail in section 4.4. In order to solve the equations, the heat transfer coefficient of the vapour, condensate film and coolant must be known in addition to the mass transfer coefficients for the liquid and vapour phase [21]. Subsequent studies using the Colburn and Drew non-equilibrium model method used various combinations for methods of calculating the heat and mass transfer coefficients.

Price and Bell [23] develop Colburn and Drew's system of equations into a model for a shell and tube condenser. The equations are solved at increments along the condenser, the algorithm for this, presented by Price and Bell, forms the basis for numerous studies employing the non-equilibrium model of mixture condensation. For example the following studies all use Price and Bell's method to model condensation inside smooth horizontal tubes [24–26].

Table 4.1 lists the various methods for calculating the heat and mass transfer coefficients used in these studies for application in the non-equilibrium method for modelling condensation in smooth horizontal tubes. Lu and Lee [26] and Cavallini [24] use the Friedel correlation [27] for pressure drop due to friction in pipes. Lu and Lee report an average pressure drop error of -3.2 %, with a maximum of 33 %; this seems a significant deviation and would in turn influence the heat transfer calculation.

Table 4.1 shows that there is a significant range of reported accuracies for the models used by Jin, Lu and Lee and Cavallini et al. This is due to the different methods used to calculate the heat and mass transfer coefficients. The non-equilibrium method can only be as accurate as the coefficients used to determine the mass and heat transfer. The range in accuracy shows there is still relatively poor understanding of how to quantify these values. However, all of the models summarised in Table 4.1 provide a reasonable estimate of the heat exchange area required, given that the primary requirement is to calculate heat transfer area for difference cycles, this method should be sufficient.

The non-equilibrium method, as presented by Price and Bell [23], assumes a fully annular flow regime. However, the local flow regime is likely to change significantly. Accommodating alternative flow regimes requires an alternative method for heat transfer calculation. Fronk [13] identifies the need for further research to enable heat and mass transfer coefficients in alternative flow regimes to be accurately predicted. However, Cavallini et al. [24], state that the model used in their study can be applied to the case of total condensation.

In summary, there is a huge amount of literature relating to the development of models to simulate phase change of mixtures. The primary reason there are so many studies is the requirement for different models according to the type of phase change, flow regime, orientation and geometry of heat exchanger. This study has chosen to focus on condensation as the degradation of heat transfer coefficient is larger for this process. Furthermore, condensation inside horizontal tubes is selected for further research as this is common for heat exchangers used in Rankine cycles. A review of available methods of modelling condensation shows the non-equilibrium method has a good physical basis whilst being less complex and computationally expensive than the conservation method. Equilibrium and empirical models were discounted due to their lack of physical basis. The non-equilibrium models review showed that reasonable agreement to experimental studies for heat exchanger area had been found by some workers.

4.4 Modelling method for heat transfer during for condensing zeotropic mixtures

As described in the literature review section 4.3, section 4.4 will focus on modelling the degradation in heat transfer for a fully annular condensing flow of refrigerant mixture inside a horizontal pipe. The non-equilibrium method, as described by Price and Bell [23], is selected with heat and mass transfer coefficients calculated according to the method used by Cavallini et al. [24].

The method presented requires the following assumptions:

- film condensation
- condensate is miscible
- vapour/liquid phases are in equilibrium at interface
- heat and mass transfer resistance is limited to the thin film shown in Figure4.2
- temperature and concentration do not vary outside of the thin film
- all heat and mass transfer occurs perpendicular to film.

4.4.1 Description of the Model

The non-equilibrium method for modelling heat exchange during a phase change process is essentially a method of performing heat and mass balances at increments along a heat exchanger. At each location the change in concentration, vapour quality, temperature and pressure are calculated and applied as inputs for the next stage along the heat exchanger. This model is described for a binary fluid mixture in this section; it can be extended to ternary mixture but this is more complex. A diagram of the model is shown in Figure 4.3.

The change in vapour quality as condensation progresses is calculated using the condensing molar flux of the fluid from the interface to the liquid film, is defined as $\dot{n}_t$ and

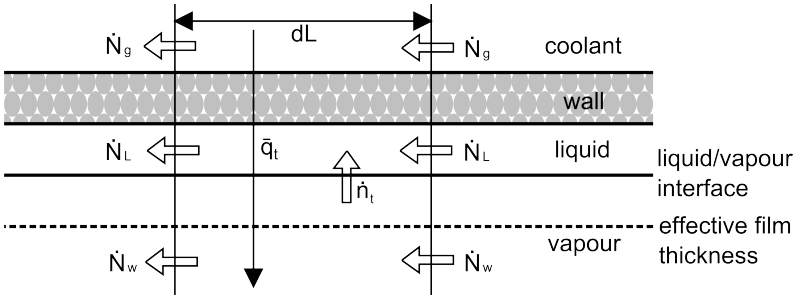

Figure 4.3: Mass and heat fluxes as defined in the non-equilibrium model for condensation of a mixture

shown in Figure 4.3. The condensing molar flux is the flow from the gas to the liquid film, perpendicular to the bulk direction of flow. The mass balance between the interface and bulk vapour is represented by equation 4.3.

$$\dot{n}_1 + \dot{n}_2 = \dot{n}_t = C_t \beta_G \ln\left(\frac{r_1 - \bar{y}_{1,int}}{r_1 - \bar{y}_{1,G}}\right) \tag{4.3}$$

Where r is the ratio of condensing components ($\frac{\dot{n}_1}{\dot{n}_t}$) and $\bar{y}_{1,int}$ and $\bar{y}_{1,G}$ are the molar fractions of the most volatile component at the interface and bulk vapour respectively. C_t is the total molar concentration:

$$C_t = \frac{P_G}{RT_G}. \tag{4.4}$$

β_G is the mass transfer coefficient within the vapour phase. This can be calculated from several different correlations. Here, Sherwood's correlation for turbulent flow is used [24], this is calculated from equations 4.5.

$$\beta_G = \frac{Sh_G D_{12}}{d_i} \tag{4.5a}$$

$$Sh_G = 0.023 {Re_G}^{0.8} {Sc_G}^{1/3}. \tag{4.5b}$$

$$D_{12} = \frac{9.2916 \times 10^{-4} T_G^{3/2} \left(\frac{M_1+M_2}{M_1 M_2}\right)^{1/2}}{P_G r_{12} W^{(1)}{}_{(1)} (1-\Delta)} \tag{4.5c}$$

Next, the heat balance between the heat flux from interface to cooling stream is formulated. The total heat flux added to the coolant water from the interface must be the sum of the sensible heat lost from the vapour and the latent heat associated with the amount of vapour condensed to liquid over the increment.

Latent heat flux (q_λ) is calculated from the individual components of the condensing mixture according to:

$$q_\lambda = \dot{n}_t \left(r_1 \tilde{h}_{LG1} + (1-r_1) \tilde{h}_{LG2} \right) \tag{4.6}$$

$\tilde{h}_{LG2}$ and $\tilde{h}_{LG1}$ are the molar latent heats calculated at T_i.

The sensible heat flux associated with the vapour phase is calculated by equations 4.7. The fraction $\frac{\eta}{1-e^{-\eta}}$ is the Ackerman correction factor, which accounts for the effect of mass transfer in the same direction as heat transfer. A similar equation can used without the Ackerman correction factor for sensible heat associated with the liquid film. The local transfer coefficient of the vapour component is calculated via the Dittus Boelter equation, as shown in 4.8.

$$q_s = \alpha_G \frac{\epsilon}{1-e^{-\epsilon}} (T_g - T_i) \tag{4.7a}$$

$$\epsilon = \frac{\dot{n}_t \tilde{c}_P}{\alpha_G} \tag{4.7b}$$

$$\bar{c}_P = r_1 \tilde{c}_{P1} (1-r_1) \tilde{c}_{P2} \tag{4.7c}$$

$$Nu_G = 0.023 {Re_G}^{0.8} {Pr_G}^{0.3} \tag{4.8a}$$

$$\alpha_G = \frac{Nu_G \lambda_G}{d_i} \tag{4.8b}$$

The heat balance from the interface to coolant and from the interface to bulk gas can then be computed from equations 4.9. Where, $\bar{U}$ is the overall heat transfer coefficient and R_w is the tube wall conductive resistance. The local value for the overall heat transfer coefficient can be calculated from a variety of correlations, for example Cavallini and Zecchin, [30]. An alternative correlation is presented by Shah [28], which is more general and therefore more widely used. Cavallini et al. take the water heat transfer coefficient from their own measurements. As these are not available in this case and to allow the model more flexibility the Dittus-Boelter equation, equation 4.8, can be used to determine the local heat transfer coefficient on the coolant side. The model is constrained by the flow conditions that the correlations for heat transfer coefficients are valid for. Usually these relations are valid for a limited range of conditions. Table 4.2 details the bounds which apply to this model.

$$\bar{U}(T_i - T_c) = q_\lambda + q_s \tag{4.9a}$$

$$\bar{U} = \frac{1}{\frac{d_i}{d_e \alpha_c} + R_w + \frac{1}{\alpha_i}} \tag{4.9b}$$

The change in concentration of each of the phases in the binary mixture and the change in molar flow rate of the vapour and liquid phases are calculated from the condensing molar flux rate and the concentrations. The relations used are shown in equations 4.10, ΔA is determined by the increment length and heat exchanger geometry. These are combined to allow the new concentration and vapour molar quality to be calculated according to equations 4.11.

$$\Delta \dot{N}_g = -\dot{n}_t \Delta A, \quad \Delta \dot{N}_l = \dot{n}_t \Delta A, \tag{4.10a}$$

$$\Delta \dot{N}_{1,g} = -r_1 \dot{n}_t \Delta A, \quad \Delta \dot{N}_{1,l} = r_1 \dot{n}_t \Delta A \tag{4.10b}$$

$$\tilde{z}_{1,c} = \frac{\dot{N}_{1,l} + \Delta\dot{N}_{1,l}}{\dot{N}_l + \Delta\dot{N}_l} \tag{4.11a}$$

$$\tilde{Q} = \frac{\dot{N}_g + \Delta\dot{N}_g}{\dot{N}} \tag{4.11b}$$

Finally, the change in bulk gas and cooling water stream temperatures are calculated from equations 4.12. While, the pressure drop along the heat exchanger for both streams is calculated using the Friedel model, [27]. The next section discusses how these calculations can be implemented in an algorithm.

$$\Delta T_g = -\frac{\frac{\alpha_g}{e^{\epsilon}-1}\Delta A(T_g - T_{int})}{\dot{N}_g \tilde{c}_{p,g}} \tag{4.12a}$$

$$\Delta T_c = -\frac{\tilde{U}\Delta A(T_{int} - T_c)}{\dot{m}_c c_{p,c}} \tag{4.12b}$$

4.4.2 Algorithm

The model described by Cavallini et al. simulates a single tube in a shell heat exchanger. It has the potential to be developed for more complicated heat exchanger geometries at a later stage if required. The inner diameter of the tube, wall thickness and inner diameter of the shell are required as inputs to define the geometry of the heat exchanger. Similarly, the input variables required are the temperature, pressure, mass flow rate and composition of both streams entering the heat exchanger.

Figure 4.4 shows the algorithm used to implement the condensation model described in section 4.4.1. When the condensing fluid entering the condenser is superheated the model computes the single phase heat transfer using the Dittus-Boelter equation until the wall temperature is calculated to be less than the dew point of the condensing fluid, the point at which condensation begins.

At the beginning of each calculation the pressure of each stream, temperature of bulk vapour and coolant and the vapour quality are known based on the values calculated at the previous location. To solve the heat balance, equation 4.9, there are three unknown

variables, T_i, $\dot{n}_t$, r_1, and two equations to solve, i.e. 4.9 and 4.3. Therefore the first step in the method is to estimate the interface temperature, T_i, of the refrigerant as the bubble point of the mixture from the mixture composition and vapour quality, this calculation is done using REFPROP. Once the interface temperature is known, the concentration of the liquid portion, $\tilde{y}_{1,I}$ can be calculated from the assumptions that the vapour/ liquid phases are in equilibrium at the interface and the concentration does not vary outside of the thin film. Similarly, the concentration of the bulk vapour can be calculated from the conservation of mass. Then, the molar specific heat capacities and latent heats can be calculated. These calculations are done in REFPROP, molar latent heats are calculated at the interface temperature while the molar specific heat capacities are calculated at $(T_G + T_I)/2$.

The program solves the equations for r_1 iteratively. Once r_1 has been adjusted to satisfy the heat balance relation, the change in quality, concentrations, temperatures and pressure are computed for the increment along the heat exchanger, ΔL. The model stops stepping along the heat exchanger once the fluid becomes subcooled, although this criteria could be adjusted to another vapour quality or target exit temperature for the condensing fluid.

4.5 Further Work

The ultimate objective would be to carry out experiments of a binary zeotropic fluid mixture using the test facility described in Chapter 3, and to use this test data to validate a heat exchanger model based on the algorithm described in Section 4.4.2.

Further work is needed to identify and qualify a supplier of an appropriate binary zeotropic gas mixture for the tests, as discussed in the previous chapter.

Also the software model of the heat exchanger needs to be available. The algorithm described in Figure 4.4 was coded using MATLAB in the present study. First attempts to run the model identified that assigning suitable values to T_i and defining heat transfer coefficients for the very thin liquid layer as condensation first starts to occur in the heat exchanger, both presented modelling challenges which have not been resolved in the

current work. This is therefore another area for future investigation.

4.6 Summary and Conclusions

At the beginning of this chapter, experimental data from the Ground Source Heat Pump (GSHP) test facility described in Chapter 3, was used to determine the global UA values for the heat exchanger. The UA value for working fluids R410a (near azeotropic) and R407c (zeotropic) were compared. The global UA value for R407c is lower than that for R410a, this indicates R407c had a lower heat transfer coefficient than R410a. Therefore a larger heat exchanger would be required, to have the same heat exchange with the zeotropic mixture compared to that with R410a.

The data presented shows that there is a need to be able to calculate the heat transfer coefficient for zeotropic mixtures, in order to understand the potential impact of heat exchanger size for ORC systems. A literature review has been presented of various modelling approaches. A modelling scheme was selected to model the case of a zeotropic mixture condensing in a horizontal single shell and tube heat exchanger.

The insight gained from trying to implement even a very limited model, as described in section 4.4, of a simple heat exchanger with binary mixtures does show this is a complex problem. To build a program that could capture the change in heat transfer coefficient during phase change, that is flexible enough to inform plant design for different waste heat source would require a significant extra study. As discussed previously, a different model would be required for each mechanism of phase change and heat exchanger geometry; additionally the correlations used to calculate coefficients for heat and mass transfer have limited applicability depending on the flow conditions. Developing a model to inform plant design with zeotropic mixtures is a much larger undertaking than initially imagined at the start of this study. There is a need to model zeotropic mixtures accurately in thermodynamic cycle simulations, this is a major piece of work for the future.

References

	Heat Transfer Resistance		Mass Transfer Resistance		Validation Study	Mean deviation of heat transfer
Study	h_{liq}	h_{vap}	k_{liq}	k_{vap}		
Lu and Lee 1994 [26]	Shah 1979 [28]	Gnielinski 1976 [29]	Fick's Law	Reynolds analogy	R114/R12 concentrations: 0.5/0.5 - 0.9/0.1	-5.6 %
Cavallini 2002 [24]	Cavallini and Zecchin 1974 [30]	Dittus Boelter	∞	Sherwood correlation	R135/R236ea, concentrations: 0.3/0.7, 0.46/0.54, 0.64/0.36. Mass velocities: 400, 750 kg/m^2s	8.7 %
Jin et al. 2003 [25]	Shah 1979 [28]	omitted	Koyama et al. 1998 [31]	Lamourelle and Sandell 1972 [32]	R134a/R112 concentrations $\approx$ 0.35/0.65, 0.65/0.35, 0.85/0.15 Mass velocities $\approx$ 200, 300 kg/m^2s	10.3 %

Table 4.1: Heat and mass transfer coefficients applied to the non-equilibrium method of modelling condensation inside smooth horizontal tubes

Constraints		
$0.8 \leq$	Pr_L	≥ 20
$5000 \leq$	Re_{LO}	≥ 500000
$0.1 \leq$	Q	≥ 0.9
	Re_L	≥ 1200
$10 \leq$	ρ_L/ρ_G	≥ 2000
$0.01 \leq$	μ_G/μ_L	≥ 0.1
$0.01 \leq$	Ph_L	≥ 0.2
$15 \leq$	$\frac{\frac{G}{\rho_G}}{gD^{0.5}}$	≤ 4000
$25 \leq$	$Ph_L(\frac{\rho_L}{\rho_G})$	

Table 4.2: Flow condition boundaries for the heat transfer correlations used in the condensation model for binary zeotropic mixtures [24]

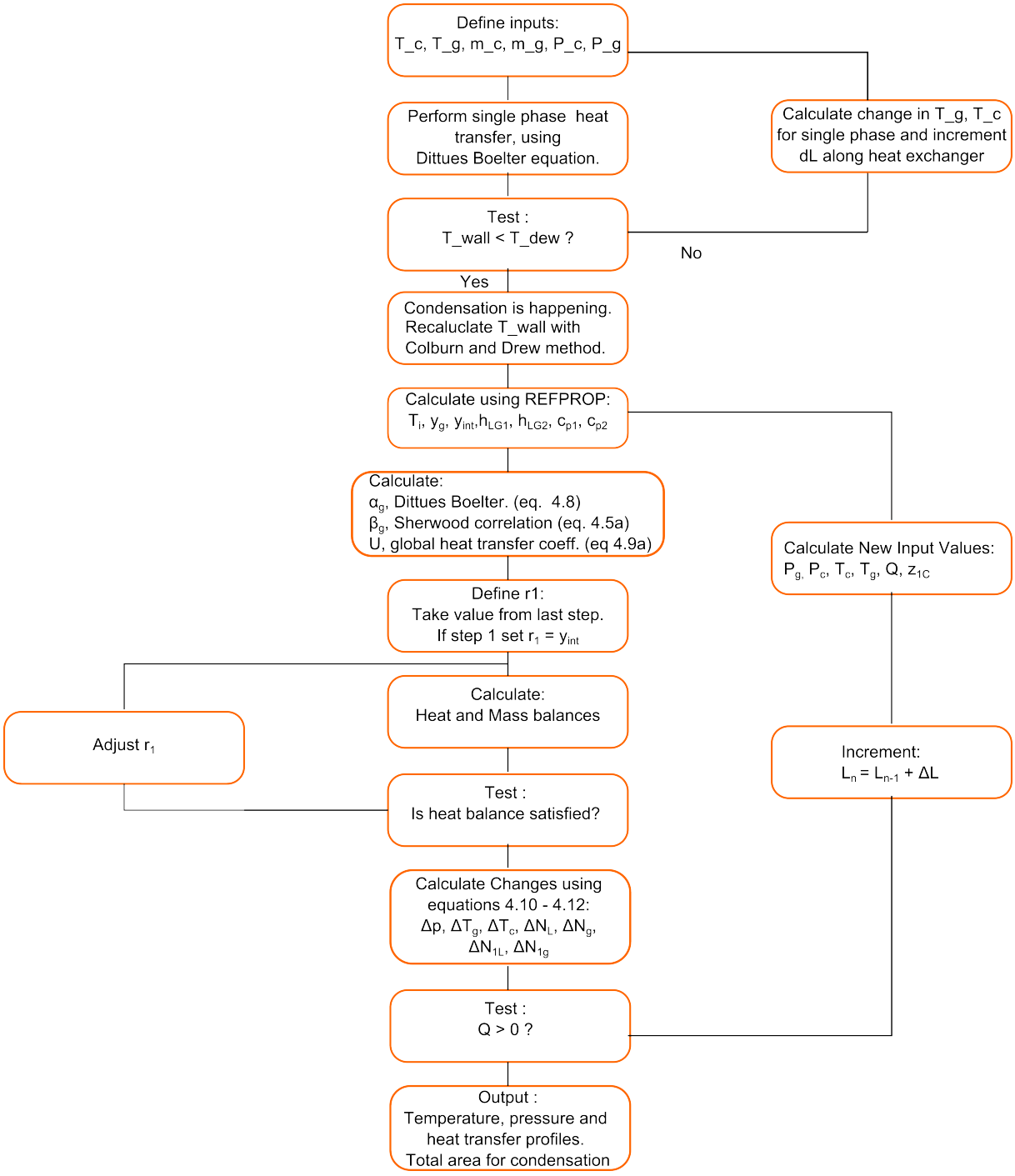

Figure 4.4: Algorithm for non-equilibrium model of condensation

[1] F. Heberle, M. Preissinger, and D. Bruggemann, "Zeotropic mixtures as working fluids in organic rankine cycles for low-enthalpy geothermal resources," *Energy*, vol. 37, pp. 364 – 370, 2012.

[2] M. Chys, M. van den Broek., B. Vanslambrouck., and M. D. Paepe, "Potential of zeotropic mixtures as working fluids in organic rankine cycles," *Energy*, vol. 44, pp. 623–632, 2012.

[3] S. Lecompte, B. Ameel, D. Ziviani, M. van den Broek, and M. De Paepe, "Exergy analysis of zeotropic mixtures as working fluids in organic rankine cycles," *Energy Conversion and Management*, vol. 85, pp. 727–739, 2014.

[4] M. A. Kedzierski, J. H. Kim, and D. A. Didion, "Causes of apparent heat transfer degradation for refrigerant mixtures," in *28th National Heat Transfer Conference*, vol. 197, (San Diego, California), pp. 149 – 158, ASME, August 1992.

[5] R. Radermacher, "Thermodynamic and heat transfer implications of working fluid mixtures in rankine cycles," *International Jounral of Heat and Fluid Flow*, vol. 10(2), pp. 90–102, 1989.

[6] L. Pierobon, T.-V. Nguyen, U. Larsen, F. Haglind, and B. Elmegaard, "Multi-objective optimization of organic rankine cycles for waste heat recovery: Application in an offshore platform," *Energy*, vol. 58, pp. 538–549, 2013.

[7] S. Quoilin, S. Declaye, B. F. Tchanche, and V. Lemort, "Thermo-economic optimization of waste heat recovery organic rankine cycles," *Applied Thermal Engineering*, vol. 31, no. 14, pp. 2885–2893, 2011.

[8] A. Rojey, C. Meyer, B. Choffe, J. Jacq, L. Asselineau, and J. Vidal, "Heat pump operating with a fluid mixture," *New Ways to Save Energy*, vol. 0, pp. 242–251, 1980.

[9] K. P. Murphy, "New refrigerants for automotive air conditioning," *SAE Technical Paper*, vol. 2, no. 1, pp. 1–8, 1971.

[10] R. Jakobs and H. Kruse, "The use of non-azeotropic refrigerant mixtures in heat pumps for energy saving," *International Journal of Refrigeration*, vol. 2, no. 1, pp. 29–32, 1979.

[11] D. A. Didion, "The influence of the thermophysical fluid properties of the new ozone-safe refrigerants on performance," *International Journal of Applied Thermodynamics*, vol. 2(1), pp. 19 – 36, 1999.

[12] E. W. Lemmon, M. L. Huber, and M. O. McLinden, *NIST Standard Reference Database 23: Reference Fluid Thermodynamic and Transport Properties - REFPROP*. National Institute of Standards and Technology, Standard Reference Data Program, Gaithersburg, 9.0 ed., 2010.

[13] B. M. Fronk and S. Garimella, "In-tube condensation of zeotropic fluid mixtures: A review," *International Journal of Refrigeration*, vol. 36, pp. 534–561, 2013.

[14] S. Grauso, R. Mastrullo, A. Mauro, and G. Vanoli, "Co2 and propane blends: Experiments and assessment of predictive methods for flow boiling in horizontal tubes," *International Journal of Refrigeration*, vol. 34, pp. 1028–1039, 2011.

[15] D.-S. Jung, M. McLinden, R. Radermacher, and D. Didion, "A study of flow boiling heat transfer with refrigerant mixtures," *International Journal of Heat and Mass Transfer*, vol. 32, no. 9, pp. 1751–1764, 1989.

[16] M. Wettermann and D. Steiner, "Flow boiling heat transfer characteristics of wide-boiling mixtures," *International Journal of Thermal Science*, vol. 39, pp. 225 – 235, 2000.

[17] A. Cavallini, G. Censia, D. D. Cola, L. Dorettia, G. Longob, L. Rossettoa, and C. Zilioa, "Condensation inside and outside smooth and enhanced tubes: a review of recent research," *International Journal of Refrigeration*, vol. 26, pp. 373–392, 2003.

[18] K. Bell and M. Ghaly, "An approximate generalized design method for multicomponent/partial condenser," in *AIChE Symp. Ser*, vol. 69, pp. 72–79, 1973.

[19] L. Silver, "Gas cooling with aqueous condensation," *Trans. Inst. Chem. Eng*, vol. 25, pp. 30–42, 1947.

[20] D. Webb, M. Fahrner, and R. Schwaab, "The relationship between the colburn and silver methods of condenser design," *International journal of heat and mass transfer*, vol. 39, no. 15, pp. 3147–3156, 1996.

[21] A. P. Colburn and T. B. Drew, "The condensation of mixed vapors," *Transactions of American Institute of Chemical Engineers*, vol. 33, pp. 197 – 215, 1937.

[22] S. Koyama, A. Miyara, H. Takamatsu, and T. Fujii, "Condensation heat transfer of binary refrigerant mixtures of r22 and r114 inside a horizontal tube with internal spiral grooves," *International Journal of Refrigeration*, vol. 13, no. 4, pp. 256–263, 1990.

[23] B. C. Price and K. J. Bell, "design of binary vapour condensers using colburn-drew equations," *AIChEJ Symposium Series*, vol. 70, pp. 163 – 173, 1974.

[24] A. Cavallini, G. Censi, D. Del Col, L. Doretti, G. A. Longo, and L. Rossetto, "Condensation of halogenated refrigerants inside smooth tubes," *HVAC&R Research*, vol. 8, no. 4, pp. 429–451, 2002.

[25] D. Jin, J. Kwon, and M. Kim, "Prediction of in-tube condensation heat transfer characteristics of binary refrigerant mixtures," *International journal of refrigeration*, vol. 26, no. 5, pp. 593–600, 2003.

[26] D. C. Lu and C. C. Lee, "An analytical model of condensation heat transfer non-azeotropic refrigerant mixtures in a horizontal tube," in *ASHRAE Conference Procedings*, vol. 100, 1994.

[27] L. Friedel, "Improved friction pressure drop correlations for horizontal and vertical two-phase pipe flow," in *European two-phase flow group meeting, Paper E*, vol. 2, p. 1979, 1979.

[28] M. M. Shah, "A general correlation for heat transfer during film condensation inside pipes," *International Journal of heat and mass transfer*, vol. 22, no. 4, pp. 547–556, 1979.

[29] V. Gnielinski, "New equations for heat and mass-transfer in turbulent pipe and channel flow," *International chemical engineering*, vol. 16, no. 2, pp. 359–368, 1976.

[30] A. Cavallini and R. Zecchin, "A dimensionless correlation for heat transfer in forced convection condensation," in *Proceedings of the Sixth International Heat Transfer Conference*, vol. 3, pp. 309–313, 1974.

[31] S. Koyama, J. Yu, and A. Ishibashi, "Condensation of binary refrigerant mixtures in a horizontal smooth tube," *Thermal science and engineering*, vol. 6, no. 1, pp. 123–129, 1998.

[32] A. P. Lamourelle and O. C. Sandall, "Gas absorption into a turbulent liquid," *Chemical Engineering Science*, vol. 27, no. 5, pp. 1035–1043, 1972.

Chapter 5

The Full Picture: A Tale of Money, Power, and Available Space

5.1 Introduction

Investigating the use of zeotropic mixtures in ORCs has shown that there may be a thermodynamic benefit, but also that the heat exchanger area required is likely to be larger than for pure fluids for the equivalent heat loads. So, whilst an improvement in performance may be possible by using zeotropic mixtures this may also come at a price in terms of a larger and more expensive system. When designing an ORC system the thermodynamic performance, system size and capital cost of the equipment must be understood in order to find the most optimised ORC system design for a given application, see Figure 5.1. In this chapter, the relationship between these factors is explored further and some generic conclusions are drawn concerning optimal system design.

Several studies have identified optimal ORC system design is not purely a function of thermodynamic performance. For example [1–3]. These studies present a technoeconomic evaluation of ORC systems. However, in waste heat recovery scenarios space is often limited and a system design may be constrained by the available footprint for the ORC unit.

Zabek et al. [3] present an analysis of an ORC system operating on a hot brine source

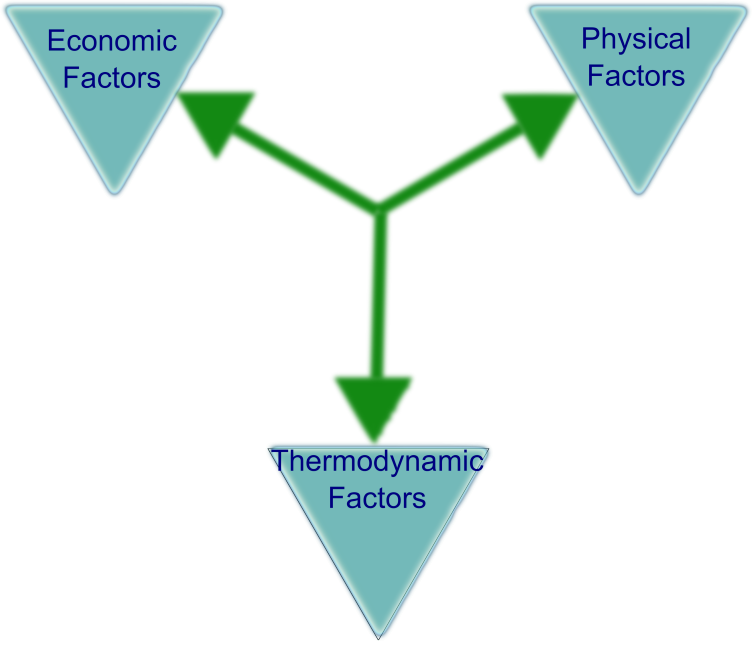

Figure 5.1: Three groups of factors which influence ORC system design selection

from an oil platform off the west coast of the USA. The study presents power output and UA value for various ORC configurations. Zabek et al. show that increasing heat exchanger size can increase power output, but at a potentially lower cycle efficiency.

In this chapter the characteristics of the coproduced hot brine stream from the Eider field are used as an exemplar around which to discuss system size, power and cost optimisation. The Eider field coproduces brine at 107 °C and peak production rate, using a 12 month average, is 160 kg/s. The condensing stream is assumed to be sea water at a temperature of 5 $°C$ and a mass flow rate five times that of the hot brine flow. This is an arbitrary assumption, ensuring the sea water volume does not constrain the heat transfer in the condenser. The model and assumptions are the same as those used earlier in Chapter 2.

The organic working fluid selected for this work was R134a. It was selected because, out of the range of working fluids considered it had a wide range of potential operating pressures and a similar power output to the other fluids used in the ORC model, as shown in Figure 2.8. Calculations were carried out for a range of TIPs and ORC working fluid mass flow rates as previously in Chapter 2, the TIP range is restricted to 0.01

$P_{crit} \leq TIP \geq 0.8P_{crit}$. The lower limit is selected to ensure the condenser vacuum was practically achievable and the upper limit of the TIP is set to limit error incurred by fluid properties uncertainty near the critical point (P_{crit}), in accordance with Heberle et al. [4]. Similarly, the working fluid mass flow rate (m_o) is limited to 0.4 $m_s \leq m_o \geq 2.5m_s$, where m_s is the mass flow rate of hot brine, to keep the quantity of working fluid within practically manageable limits.

5.2 Size and Scaling

Understanding the footprint of a potential ORC plant is important as the size available for an ORC will likely be limited. Various sources of waste heat will have different space limitations. For example, the footprint available when recovering industrial waste heat is dependant on the existing plant on the site. Similarly, the size of plant available for recovering hot brines offshore is dependant on the area available on the platform. Global UA and specific power are calculated as indicators of plant size and balance respectively. The global UA value is derived from the equation for heat transfer:

$$Q = UA\Delta T_{LM} \tag{5.1}$$

The UA value is the product of the heat transfer coefficient and heat exchange area. The total UA value is an indicator of the size of the heat exchanger required to achieve the heat transfer demanded for each ORC application. Thus, an understanding of how the ORC might scale with work output is possible by comparing how power output changes with UA value for different power cycle configurations. Specific power is the power per unit mass flow rate of working fluid in the power cycle

Figures 5.2, 5.3 and 5.4 present contour plots of work output, global UA value and specific power output with ORC configuration (TIP and working fluid mass flow rate) from data generated from simulations using the ORC model described in Chapter 2.

In Figure 5.3 the distribution of UA value for the heat exchanger according to ORC

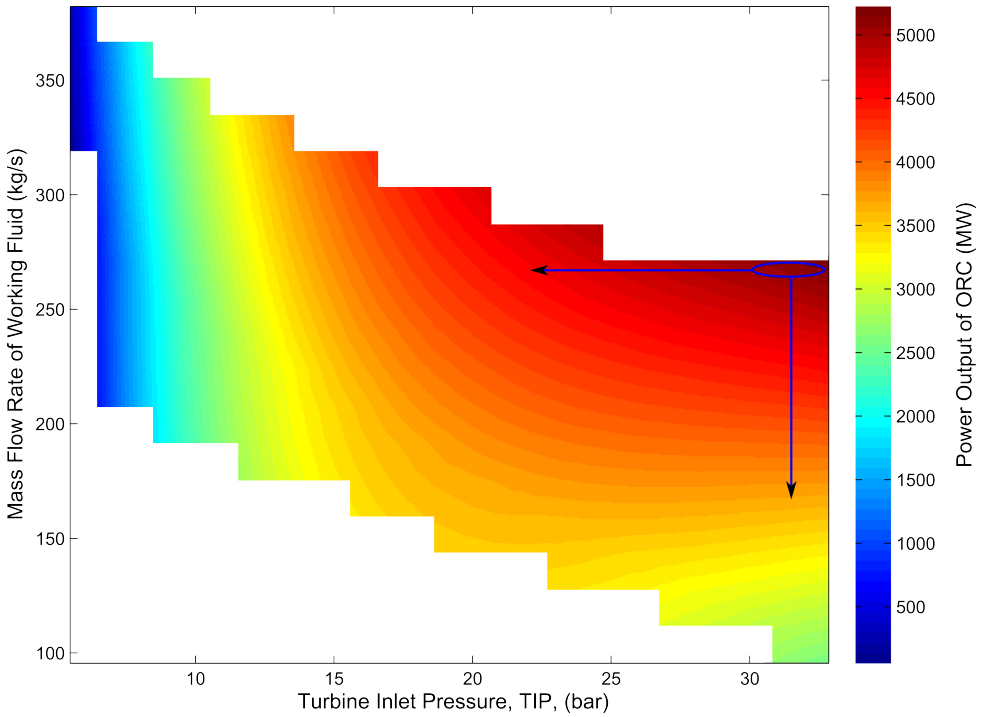

Figure 5.2: Power output as a function of ORC mass flow rate and TIP for the Eider field. The working fluid is R134a

configuration (TIP and working fluid mass flow rate) is shown. Figure 5.3 shows that the maximum UA value, and therefore the lowest heat exchange area requirement, does not occur at the same location as maximum power output, shown by Figure 5.2. This is because power output is a function of both cycle efficiency and heat input into the cycle. In this case, the maximum heat input into the cycle will occur when the UA value is largest but the ORC cycle configuration here is less efficient, resulting in maximum power output is occurring at a different UA value. From Figure 5.3 it is clear that by decreasing the mass flow rate from the location of maximum power output the UA value decreases rapidly and therefore the size of the heat exchanger would decrease significantly. Conversely, starting from the location of maximum power output and decreasing the turbine inlet pressure results in a gradual increase in UA value and therefore heat exchanger size.

Figure 5.4 shows the variation of specific power with TIP and ORC working fluid mass flow rate. Optimising for the specific power gives the best balance between size of plant and power output. At a low specific power there is a low power output per kg of working fluid so this represents a large system. Similarly a high specific power represents a smaller

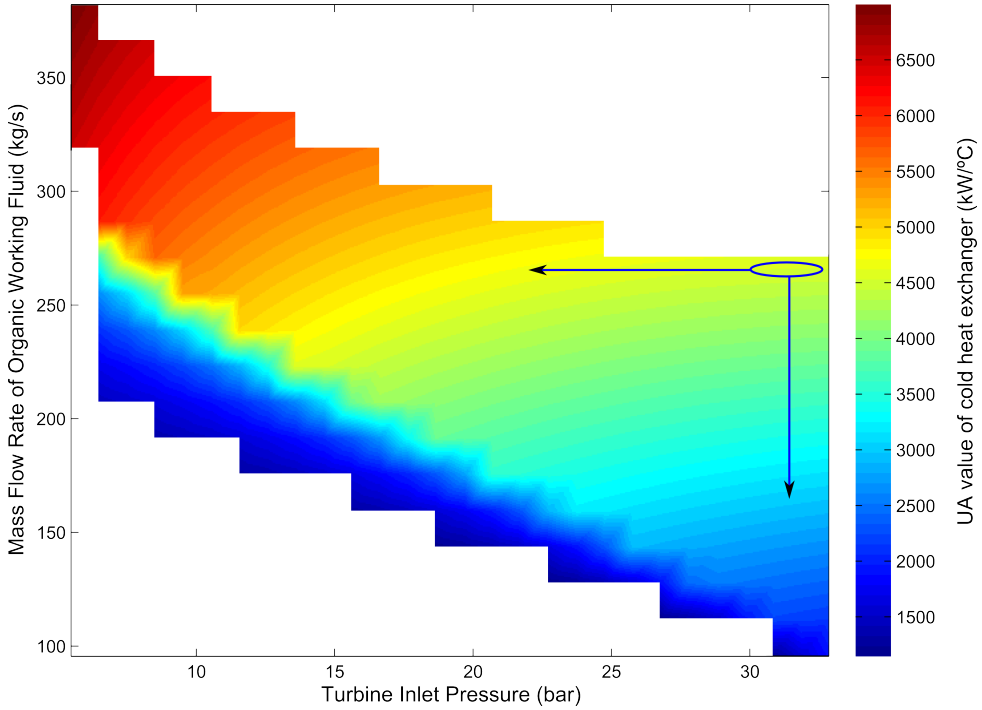

Figure 5.3: UA value as a function of ORC mass flow rate and TIP for the Eider field. The working fluid is R134a. Ellipse indicates area of maximum power output.

system. Figure 5.4 shows at maximum power output the specific power is quite high, but not at the maximum value calculated. The specific power decreases rapidly with mass flow rate of organic fluid but remains reasonably constant for decreasing TIP.

Figures 5.3 and 5.4 show that the power output of the ORC can be designed to scale with the heat exchanger area and system size. For example starting from the position of maximum power output, indicated by the ellipse in Figure 5.2, the power output can be decreased by lowering the mass flow rate in the cycle, this is indicated by the vertical arrow. Decreasing the mass flow rate, results in a higher specific power and lower UA value (Figures 5.3, 5.4). So the heat exchanger area needed and hence plant size will decrease with the power output. However, should the TIP be reduced, indicated by the horizontal arrow, the required UA value will increase and specific power will decrease a little, meaning that the size of the ORC system and heat exchanger area would be larger for a smaller power output. Care should be taken when designing ORC systems to avoid this scenario unless it offers an evaluated cost saving. Regions on all the maps (Figures 5.3, 5.4) with no data are outside the operating limits of the ORC. These limits

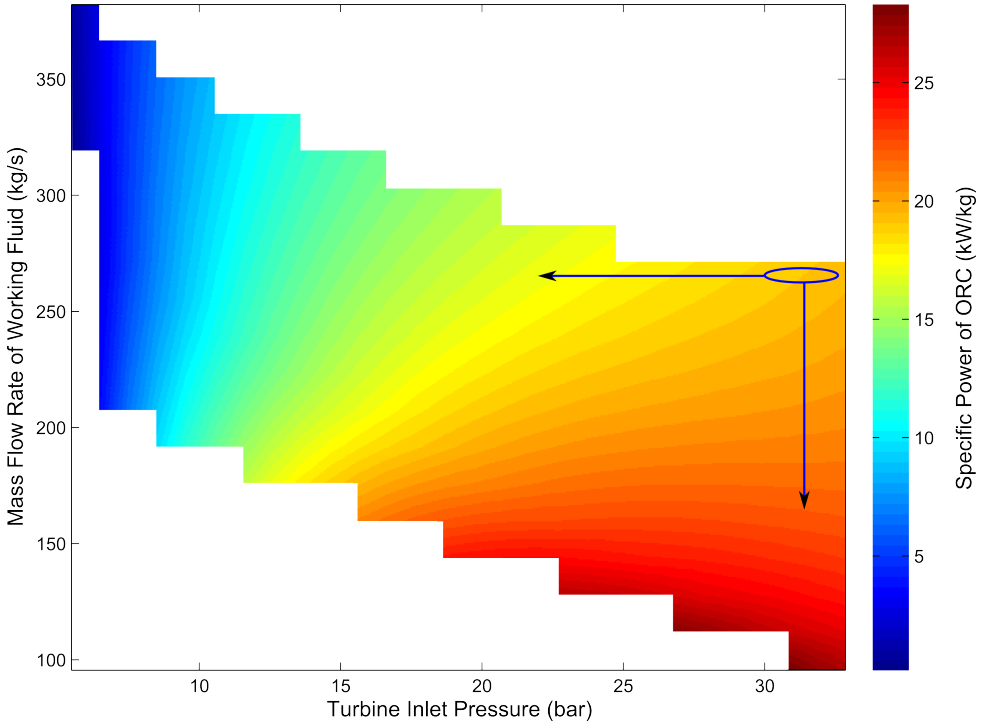

Figure 5.4: Specific power as a function of ORC mass flow rate and TIP for the Eider field. The working fluid is R134a. Ellipse indicates area of maximum power output.

are determined by the model and thermo-physical limits of the working fluid, which were described in Chapter 2.

To optimise an ORC power plant design, the power output should be maximised while cost is minimised. Minimising cost effectively means minimising the UA value, to minimise heat exchanger size, and maximising specific power, to produce maximal power per unit mass of ORC working fluid. Figs. 5.2, 5.3 and 5.4 show maximum work output, minimum UA value and maximum specific power occur at different ORC configurations. Therefore an ORC system design will have to be a compromise between power, size and cost.

5.3 Money

For an ORC power generation system to be economically viable the cost of installation, operation and maintenance, over an acceptable payback period, must be less than the existing levelised cost of generating electricity that the ORC would be replacing.

The ORC system will have a high initial capital cost, but as the fuel is often free (as is the case for waste heat or geothermal sources) there are low/zero fuel costs after

Base load power output	17 MW_e
Base load efficiency	32.20 %
Heat rate at base load	0.1060 therms/kWh (0.0112 GJ/kWh)
50 % load efficiency	25%
Heat rate at 50 % load	0.1990 therms/kWh (0.0210 GJ/kWh)
Turbine speed	3600 rpm

Table 5.1: Siemens SGT-500 turbine characteristics [6]

installation. In contrast, using the existing gas turbines clearly has no initial capital outlay, but a significant continual fuel and maintenance cost. Whether or not a platform will continue to produce, will partly rely on the fuel costs to be less than the income from the oil produced. To understand the feasibility of an ORC system versus continued use of gas turbines the cost of each scenario over time must be evaluated.

Nguyen et al. [5] report that an exemplar North Sea platform meets its power demand by using 3 Siemens SGT-500 gas turbine units. Typically, two turbines would be running at 50 % load while the third is on standby or maintenance. The cost of the gas supply is estimated using the characteristics of the SGT-500 turbines as shown in Table 5.1.

The capital cost of an ORC power system is estimated to be 3000 €/kW as used by Quoilin et al. [7]. This is an estimate for a MW-scale fully installed geothermal type system including the ORC plant and all process integration. The power requirement of North Sea oil and gas platforms varies from approximately 10 MW to several hundreds of MWs [8]. In this study, the financial evaluation is carried out for a power requirement of 10MW, as this is representative of the power requirement of a typical North Sea platform and the size an ORC power plant fuelled by hot brines could supply. Using 3000 Eur/kW the estimated cost of ORC capable of supplying 10 MW of power would be Eur 30 million.

The amount of gas required to produce 10 MW for a year via SGT-500 turbines operating at 50 % load is 18.4 million therms per year ($19.4x10^5$ GJ/year). Most North Sea platforms are supplied with gas to fuel the gas turbines via a pipeline. Therefore, the cost of gas to a platform is equal to the wholesale gas price [8].

The UK Department of Energy and Climate Change (DECC) fuel price projections 2013 [10] for natural gas have been used in this study, these are shown in Figure 5.5.

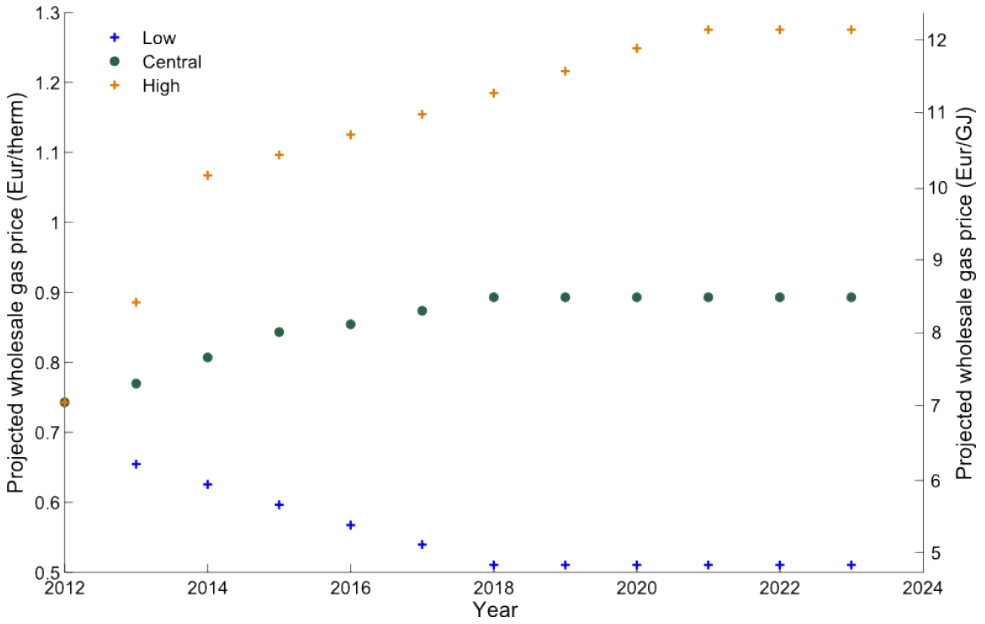

Figure 5.5: DECC 2013 natural gas price projections, figure taken from [9] data from [10]

Price projections are inherently highly uncertain, however the DECC projections are the best data available to use in this study. The DECC fuel price projections have been used to estimate the annual cost of gas required to continually supply 10 MW via gas turbines for a year. The estimated cost of both a 10 MW ORC power system and gas supply to power existing turbines have been combined in Figure 5.6 to show the cash flows for each scenario. From the cash flow model it is not immediately clear which scenario, continued use of gas turbines or adoption of ORC power plants, would cost the least over time.

A discounted cash flow model was used to calculate the present value of the gas cost in future years. The Discount Present Value (DPV) was calculated according to equation 5.3.

$$DPV = \frac{FV}{(1+d)^n} \tag{5.2}$$

FV is the future value of the gas cost, this is calculated using the projected gas price as shown in Fig. 5.5, n is the number of years from the present and d is the discount rate. The discount rate accounts for the time value of money, here it is set at 10 % in accordance with Aboody [11].

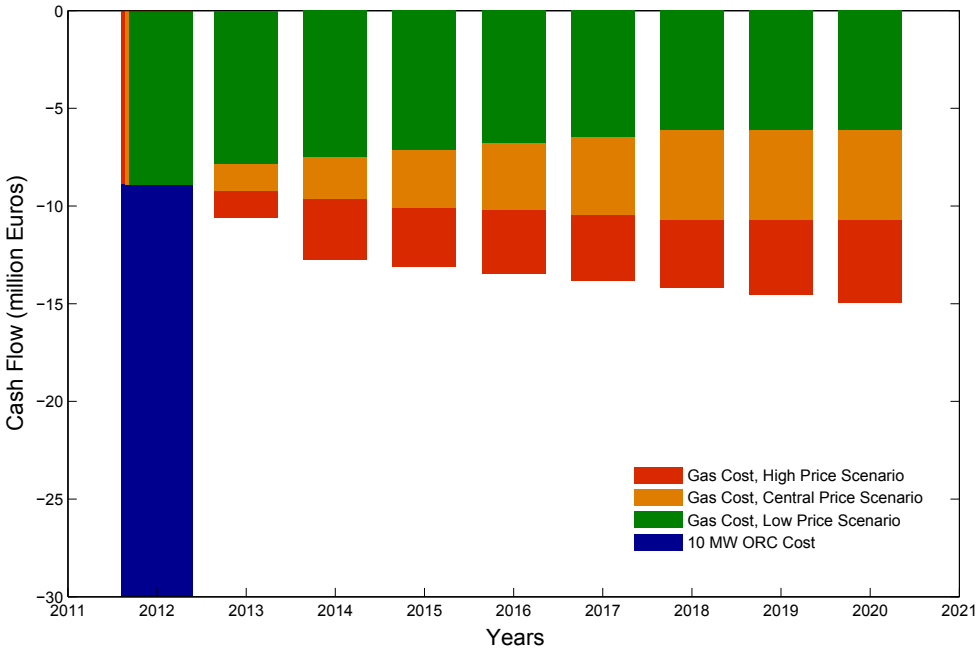

Figure 5.6: Cash flow for ORC and gas turbine scenarios, taken from[9]

DECC gas price scenario	Payback time (years)
Low	4.53
Central	3.63
High	3.09

Table 5.2: Payback time of a 10 MW ORC based on DECC gas price projections taken from [9]

The effective payback period of the ORC was then found by calculating how many years worth of gas, using DPV, is equivalent to the capital cost of the ORC. The effective payback time was calculated using the low, central and high gas price projections, shown in Figure 5.6. The results are shown in Table 5.2. The payback time for all three scenarios is encouraging. The maximum payback predicted time is 4.53 years for the low gas price scenario. This is particularly important in the North Sea where oil and gas reserves are depleting and therefore the forecast shut down date of many platforms in the North Sea may only be a matter of a few years. This is shown in Figure 5.7 by the 'decline' region of a typical well life.

However, the different gas price scenarios do show that gas price has a strong influence on the payback time. The payback time is 24.8 % longer in the low gas price scenario and 14.9 % shorter in the high gas price scenario relative to the central gas price projection.

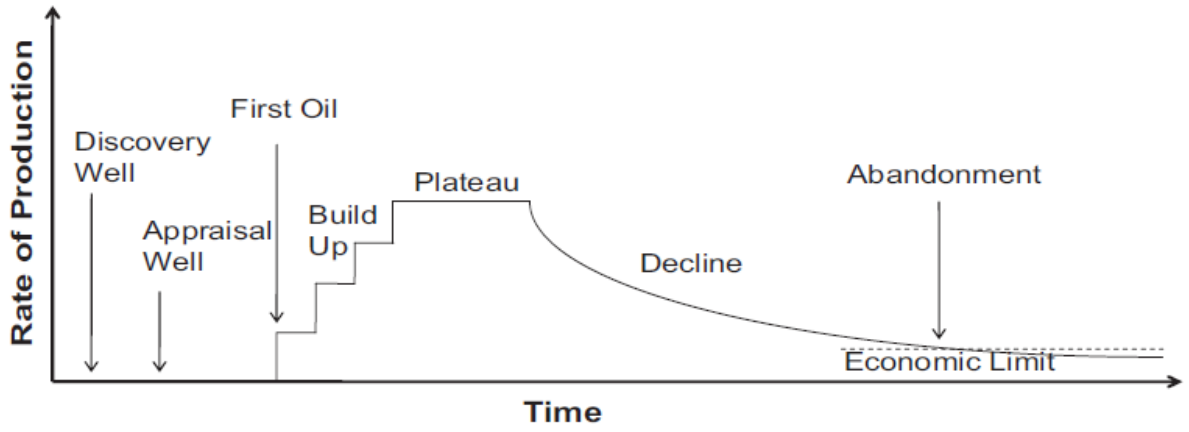

Figure 5.7: Stylised production cycle of an oil field taken from [12]

Uncertainty in effective payback time often means investments are less attractive. But in this case all the payback times are small (less than 5 years). Additionally, power production via ORC protects the platform operation from the influence of fluctuating gas price, as the platform could continue operation through periods of high gas price production where previously production would have been stopped until the gas price fell.

The number of active wells has remained fairly constant over the decades since North Sea production began in the 1970s. This is in part because the design of the platforms typically underestimated both the field performance and field longevity. Individual wells have been abandoned, but most of their host well slots have been used for sidetrack wells to target new areas of unswept oil. Even now, as the fields mature, it is likely that payback time will be less than well abandonment rate. Moreover, if the coproduced water generates value then in future wells could produce to even higher Water to Oil Ratio (WOR)s and the economic production life of wells extended.

CO_2 emissions associated with the gas turbine exhaust will incur additional expense above the fuel cost for the well operator. Norway has very clear levies on GHG emissions and therefore is used as a case study here. The Norwegian carbon tax is 200 Norwegian Krone, NOK, (€24) per tonne of CO_2 [13]. The CO_2 emissions from gas combustion is defined as 2.34 tonne CO_2 per 1000 Sm3 (where Sm3 is standard metre cubed) by Statistics Norway [14]. So the cost, due to the carbon tax to produce 10 MW via gas

turbines is €2.02 million per year. This is 23 % of the cost of gas (as calculated for 2012). Therefore, in Norway, CO_2 emission levies are a significant additional cost and will reduce the payback time of an ORC power system further relative to the values given in Table 5.2.

5.4 Summary

In this chapter, the relationship between thermodynamic performance, system size and capital cost of an ORC system have been considered. These variables must each be understood in order to find the most appropriate ORC system design for a particular application.

The characteristics of the hot brine produced by the Eider field, has been used as an exemplar to understand the relationship between money, thermodynamic potential and power plant size. The financial analysis carried out indicates a payback time for a 10 MW ORC based on a discounted cash flow model. The payback time based on DECC low gas price projections is 4.53 years while payback time based on high gas price projections is reduced to 3.09 years. Payback times would decrease even further if the cost of emitting GHG is taken into account in the project evaluation. Therefore, ORC power plants have the potential in terms of both financial cost and power output to fulfil significant proportions of power demand on the North Sea wells.

References

[1] L. Pierobon, T.-V. Nguyen, U. Larsen, F. Haglind, and B. Elmegaard, "Multi-objective optimization of organic rankine cycles for waste heat recovery: Application in an offshore platform," *Energy*, vol. 58, pp. 538–549, 2013.

[2] S. Quoilin, S. Declaye, B. F. Tchanche, and V. Lemort, "Thermo-economic optimization of waste heat recovery organic rankine cycles," *Applied Thermal Engineering*, vol. 31, no. 14, pp. 2885–2893, 2011.

[3] D. Zabek, J. Penton, and D. Reay, "Optimization of waste heat utilization in oil field development employing a transcritical organic rankine cycle (orc) for electricity generation," *Applied Thermal Engineering*, vol. 59, pp. 363–369, 2013.

[4] F. Heberle, M. Preissinger, and D. Bruggemann, "Zeotropic mixtures as working fluids in organic rankine cycles for low-enthalpy geothermal resources," *Energy*, vol. 37, pp. 364 – 370, 2012.

[5] T.-V. Nguyen, L. Pierobon, B. Elmegaard, F. Haglind, P. Breuhaus, and M. Voldsund, "Exergetic assessment of energy systems on north sea oil and gas platforms," *Energy*, vol. 62, pp. 23 –36, 2013.

[6] "SGT-500 Industrial Gas Turbine," 2011. accessed 27/01/14.

[7] S. Quoilin, M. Van Den Broek, S. Declaye, P. Dewallef, and V. Lemort, "Techno-economic survey of organic rankine cycle (orc) systems," *Renewable and Sustainable Energy Reviews*, vol. 22, pp. 168–186, 2013.

[8] A. J. Cavenagh, "Statoil." Personal Communications, 2013.

[9] A. Auld, A. Berson, and S. Hogg, "Organic rankine cycles in waste heat recovery: a comparative study," *International Journal of Low Carbon Technology*, vol. 8 (suppl 1), pp. i9–i18, 2013.

[10] "Decc 2013 fossil fuel price projections," 2013. accessed: 27/04/2014.

[11] D. Aboody, "Recognition versus disclosure in the oil and gas industry," *Journal of Accounting Research*, vol. 34, pp. 21–32, 1997.

[12] C. Adams, A. Auld, and J. Gluyas, "From hydrocarbons to heat: Evolution of offshore onshore oil wells to geothermal systems," *IN PREP*, vol. 0(0), pp. 1 – 15, 2015.

[13] P. Sopher and A. Mansell, "Norway, the world's carbon markets: A case study guide to emissions trading," tech. rep., IETA and EDF, May 2013.

[14] T. Sandmo, "The norwegian emission inventory 2011," tech. rep., Statistisk sentralbyra (Statistics Norway), 2011.

Chapter 6

Applicability of Organic Rankine Cycle (ORC)s for geothermal applications

6.1 Introduction

The influence of different ORC system configurations with pure fluids and fluid mixtures have been evaluated in earlier chapters in terms of potential work output, physical size of plant and system cost. In this chapter these metrics are used to evaluate the applicability of ORCs fuelled by three different geothermal sources of heat.

Geothermal energy is defined as energy derived from the Earth due to the radioactive decay in the Earth's crust and heat from the Earth's core. At the surface, heat flow is approximately 50 mW/m^2, comprised of 10 mW/m^2 heat from the core and 40 mW/m^2 due to radioactive decay [1]. Globally geothermal energy resources are significant; $140 \times 10^6 EJ$ of geothermal energy is theoretically extractable [2]. This is classified into three categories, see Table 6.1. High temperature geothermal resources are most commonly exploited as this heat can be converted into electricity using the conventional power plant technologies shown in Table 6.1. Conversion to electricity is often preferable to the direct use of the heat, because electricity can be more easily transported to where

it is required and, if necessary, stored. Low temperature heat sources account for the majority of unexploited geothermal resource, [3]. It is often less economically attractive to use low temperature geothermal resources, as power output per well is lower than for high temperature resources and available heat recovery technologies can be too costly. Currently, ORC geothermal plants make up around 13 % of global installed geothermal capacity. The US is the leading market in terms of binary plants, followed by New Zealand. In this chapter, three low enthalpy sources of geothermal heat are explored, each in a different setting, to examine the potential for Waste Heat Recovery (WHR) using ORC systems compared to other types of heat recovery systems.

Geothermal energy, once recovered, can be a particularly attractive energy source for the following reasons. Firstly, it is a renewable resource with minimal green house gas emissions. Furthermore, high capacity factors ($> 90\%$) are associated with the generated heat or electricity making it appropriate to provide base load power generation, unlike other formas of renewable energy such as wind or solar. Finally, it can be considered a secure energy source as it is an indigenous resource. The benefits of using geothermal energy may be augmented further by considering the use of ageing and abandoned oil wells. These can become a liability for their owners but by repurposing them for geothermal energy extraction, owners/operators will be able to generate further revenue streams. Also, using existing infrastructure reduces the capital cost of geothermal plants, which is often cited as a barrier to deployment for geothermal energy systems.

It has been demonstrated in chapters, 2 and 4 that low temperature heat sources have the thermodynamic potential to generate useful amounts of mechanical work. The work described in this chapter aims to investigate to what extent can ORC technology add benefit to existing oilfield operations, energy security and meeting energy demand with renewable resources.

This chapter begins with the introduction and characterisation of the three sources of low temperature geothermal heat streams. These are then analysed and discussed in Section 6.4 with particular focus on potential power output, location considerations, size

Low Temperature $< 85°C$	Moderate Temperature $85 - 150°C$	High Temperature $< 150°C$
Direct use (heat)	Direct use (heat)	Flash steam plant
Heat Pump	Binary Power Cycles	Binary and Combined power cycles
		Dry Steam power plant

Table 6.1: Classification of geothermal energy and applicable technologies, as in [5]

constraints, influence of institutional culture, risk and finance. These factors are then combined to evaluate the applicability of ORCs for operation with the geothermal heat resources identified. Finally, some conclusions are presented in section 6.5.

Some work in this chapter has/will be published in the following peer reviewed jounral papers [4–7].

6.2 UK Geothermal Resource Potential

Most countries have some geothermal potential due to the Earth's geothermal gradient. The Geothermal Energy Association (GEA) has estimated that the global geothermal resource potential, for electricity production lie somewhere between 35 - 210 GW_e [2]. Although, the report indicates that the actual technical potential could be several times larger due to unidentified resources and Enhanced Geothermal Systems (EGS) technology. EGS has the capacity to enhance geothermal output by increasing the poductivity of geothermal targets. Furthermore, the magnitude of recoverable low-temperature geothermal energy is estimated to be 4.4 TW_{th}. Both of these numbers indicate geothermal energy has the potential to contribute significantly to global heat and power demand especially through the recovery and use of the low temperature low grade heat resource.

Geothermal resource is classified in temperature bands, different energy recovery technologies are employable in each band as shown in 6.1. Low temperature geothermal energy is generally used directly as heat or as a heat source for geothermal heat pumps. Lund [8] reviews the direct use of geothermal energy and states that 70.5 GW_{th} is currently recovered globally. This is a 45 % increase since 2010. Similarly, Bertani [9] reviewed the current uptake of energy conversion technologies to generate electricity from geothermal resources. This generally requires moderate to high temperature geothermal energy.

cdt]

Plant Type	Proportion by installed capacity	Proportion by number of plants
Back Pressure	1.43 %	4.25 %
Binary	14.16 %	46.73 %
Flash Technologies	61.75 %	38.73 %
Dry Steam	22.65 %	10.29 %

Table 6.2: Distribution of geothermal power generation technologies and number of plants. Data taken from [9]

Bertani suggests that 12.6 GW_e is now exploited, which is an increase of 16 % from 2010.

Bertani's study predicts that the increase in geothermal power generation will follow an exponential trend, and therefore estimates 21 GW_e could be produced from geothermal power plants by 2020. In an alternative study, the GEA review of global geothermal power production by Matek [3] predicts a sustained level of growth resulting in 17.6 GW_e by 2020. Both of these studies agree that the growth in electricity production from geothermal sources is due to an increased uptake of binary, or ORC, power plants, which are able to utilize lower temperature geothermal fluids than has been possible with the traditional dry steam or flash geothermal power plants. Table 6.2 shows the distribution of generation from geothermal sources by technology type and number of units. Binary plants contribute 14.16 % of power generated while accounting for 46.73 % of plants installed. The average output for a binary plant is 6.3 MW_e/unit.

By examining the global state of geothermal energy use, it is clear there is an increase in the uptake of ORCs which convert low to moderate temperature geothermal energy into electricity. However, Bertani [9] and Lund [8] both report no increase in uptake of geothermal energy for electricity or direct use in the UK. This study aims to understand why the global trend of significant increase in uptake of geothermal energy for heat and power is not reflected in the UK and in what UK settings ORC systems might be appropriate.

Deep geothermal research in the UK peaked during the 1980s in response to the fuel crisis of the 1970s. At this time expectations that geothermal energy could make a significant contribution to UK energy supply were low, with estimations of a 4 million

tonnes coal equivalent resource (0.042 EJ) [10]. However, two consecutive subsequent 4 year projects to investigate the geothermal potential of the UK concluded in 1997 that, geothermal energy has the potential to supply 421 EJ of heat with the possibility for some electricity production [11].

The geothermal potential of the UK is concentrated in two main geological settings. Firstly the *Hot Dry Rock* study investigated the geothermal potential of the radiogenic Carnmenellis granite in Rosemanowes quarry in Cornwall. The Carnmellis granite forms a continuous granite batholith which extends 9 km in depth and has a higher than average thermal gradient of 35 ° C/km [12]. Granite is generally impermeable and may therefore require hydraulic and thermal fracturing to create a reservoir that will allow water to be injected, geothermally heated and then returned to the surface. These systems are often referred to as Enhanced Geothermal Systems (EGS), the longevity of this type of system is unproven and this combined with the more complex well engineering required means that EGS systems still have a very limited uptake to date [5]. Ultimately, the Rosemanowes project was unsuccessful in implementing EGS technology and further development was abandoned as it was considered to be too expensive [13]. There are examples of working EGS systems in other countries, for example Soultz Sous Forets [14] and Landau [15].

An alternative geological setting, in the UK also explored in the 1980s are hot aquifers [16]. These are found in deep sedimentary basins with an insulating overburden. Temperatures at depths of 2 km or more can exceed that expected from a typical thermal gradient of 20 - 30 °C/km [5]. Two test bore holes were drilled in to the Sherwood Sandstone in the Wessex basin at Southampton and Marchwood. The Southampton borehole was subsequently developed into a geothermal scheme, whilst the Marchwood borehole was abandoned. The drilling of both boreholes was successful and they delivered similar downhole temperatures, 73.5 ° C for Marchwood and 76 ° C for Southampton. However, only Southampton was taken to commercial operation [17]. West [18] asserts that the Marchwood well was expected to produce water hot enough to supplement fuel for a nearby power station. The power station closed soon after drilling and with no other

local heat demand, the well was abandoned. The Southampton bore hole was taken forward as a scheme to supply hot water to various buildings in the city centre. Smith [16] reported in 2000 that there was no financial reason for investment in the Southampton project beyond the initial borehole, which was descried in the report as *marginal at best*. Smith [16] cites the following as determining factors that ensured the development of the Southampton scheme:

- City councils motivation to demonstrate commitment to sustainable development,
- Enthusiasm from the developers, Utilicom Ltd.,
- Co-operation between all stakeholders: public and private sector, City Council, Utilicom, European Union and U.K. Department of Energy.

Clearly in the case of Southampton, factors beyond quantitative measures such as resource and finance were critical in determining investment in the project.

These studies, which constitute the first wave of interest in geothermal energy in the UK, were generally considered disappointing by the UK Department of Energy. Despite demonstrating there is a significant low enthalpy geothermal resource in the UK, geothermal energy was regarded as a *resource for the future*, as fossil fuel prices meant that geothermal energy could not be recovered in a financially competitive manner [19]. Despite only the Southampton scheme being developed into a commercial project, the studies showed that difference in setting (i.e. local heat demand and institutional culture) contribute significantly to likelihood of a project being developed.

In recent years, interest in UK geothermal energy has been poised for a revival, but to date Southampton is still the only commercial deep geothermal system in the UK. More recently, two review studies into the feasibility of geothermal energy schemes have been published. Firstly SKM reviewed the potential for electricity generation from geothermal heat in a report commissioned by the Renewable Energy Association [20] published in 2012. Later, in 2013 the Department of Energy and Climate Change commissioned a report into the potential of deep geothermal energy in the UK [21].

Adams et al. [22] identified a need for more subsurface data (from new surveys or boreholes) in order to better understand the geology of the UK and the characteristics of that geology at depths relevant to the development of geothermal systems (i.e. greater than 1km). Estimates are very difficult to substantiate owing to the current limited data on reservoir characterisation [21]

A further source of geothermal energy not considered in many previous UK geothermal studies is hot brine produced as a by-product of the oil and gas industry. This can be from on-shore oil wells, as investigated by Adams et al. [5] or offshore, as studied by Auld et al. [4]. The idea of using coproduced water from producing oil wells or circulating water round abandoned wells as sources of geothermal energy is not new, but the potential is yet to be established [23]. Coproduced hot brines from the North Sea have been discussed previously, using the Ninian field, in Chapter 5. Further examples of coproduced hot brines are included in this chapter and are considered as a benchmark in comparison to the other sources of UK geothermal heat considered.

6.3 Low temperature geothermal energy sources are similar but different

Previous research has shown that the UK has geothermal energy reserves capable of fuelling ORC power systems for generating electricity [21]. However, only one geothermal scheme, which only uses the geothermal resource as heat, exists in the UK today. The review in the previous section shows that several factors, in addition to economic feasibility, influence the feasibility of a geothermal scheme and that there is renewed interest in recent years for developing geothermal schemes in the UK. In this section case studies of three geothermal energy sources indigenous to the UK are described. These case studies are used to assess the factors that govern the feasibility of electricity generation using ORCs, later in section 6.4.

Figure 6.1: Map of Southampton geothermal and commercial district heating scheme customers from [24]

Southampton - A Onshore Geothermal Well

The only operational geothermal scheme in the UK is located in the car park of *Toys 'r' Us* in Southampton city centre. The well head occupies a footprint of about 2 car parking bays, Figure 6.1. Hot water from the well is piped to the Southampton Energy Centre building, where it contributes to supplying a heat network. Once used, the cooled geothermal water is rejected into the Solent. Although the geothermal well is currently being refurbished, Cofely (who currently operate the scheme) supplied data relating to the construction of the well and flow and temperature data obtained when it was operational.

The well was drilled following the original UK geothermal resource investigation in 1981 [17]. The borehole was drilled into the Wessex basin to a depth of 1796 m. The targeted geothermal aquifer is the Sherwood Sandstone, at a depth of 1729 m to 1767 m. The brine rises naturally under hydrostatic pressure up most of the well and is pumped

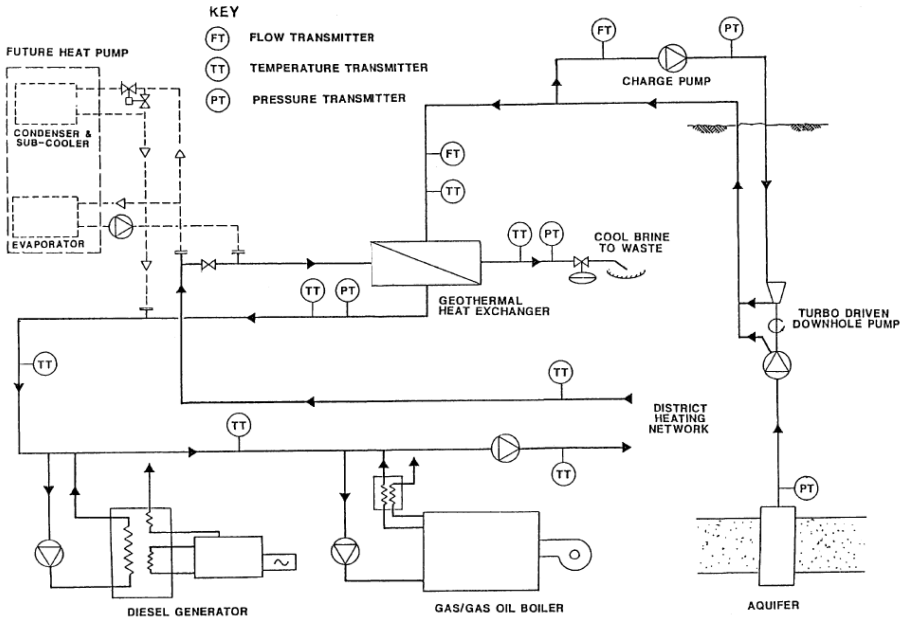

Figure 6.2: Schematic diagram of Southampton Geothermal Well and Heat Station [26]

out for the last 600 m via a turbo pump installed downhole. For simplicity, this scheme can be thought of as a *giant straw* [25].

Well testing revealed that the aquifer was bounded by faults, so water could not be reinjected into the aquifer once heat had been extracted. This means that the well may have a limited lifespan before extraction must be paused to allow the aquifer to recharge and water temperatures to recover. It was estimated that a pump rate of 10 - 15 l/s would give the well a lifespan of approximately 15 - 20 years, supplying water with a downhole temperature of 76 °C [16].

The hot water produced from the geothermal well supplies heat to a district heating system. As shown in Figure 6.2. The geothermal brine passes through a heat exchanger, where heat from the geothermal brine is transferred into water circulating round the heat network.

Initially, a limited district heating network was established in 1988 that solely used the heat supplied from the geothermal well. Over time, as demand grew, additional energy sources have been added, including gas Combined Heat and Power (CHP) units, in order to expand the network and provide heat to both residential and commercial customers

across the city. By 2011, the district heat network was supplying 70 GWh annually to more than 45 commercial customers and 800 residences, as shown in Figure 6.1 [24].

Given the city centre location of the borehole, there is no shortage of heat and electricity demand within a few meters of the borehole.

The then Department of Energy funded the drilling and test program of the well on behalf on the City Council. Further financial support was received from a European Communities scheme [27]. Later the City Council worked with Utilicom Ltd. to build the district heating infrastructure.

In a study by Smith [16], it is stated that the *economics of the proposal were marginal*. Rather it was the commitment of the council to demonstrate it's dedication to sustainable development and the culture within both the council and Utilicom, which made the project succeed.

Wytch Farm - Onshore Oil Extraction

Wytch Farm is the largest onshore oilfield in Western Europe. It was developed and produced by BP from the 1970s and is currently operated by Perenco. It is situated in South West England in the Purbeck District of Dorset near Poole, see Figure 6.3. The site operates discretely within an Area of Outstanding Natural Beauty over an area of approximately 18 km long by 3 km wide.

The field extends offshore to the east, toward Southampton. Like Southampton, the Wytch Farm oilfield exploits the Wessex basin, but extracts oil from three different reservoirs - the Sherwood, Bridport and Frome Sandstones. The Sherwood Sandstone is 150 m thick at Wytch Farm in comparison to 38 m thick at Southampton.

At its peak, between 1996 and 1998, the oilfield produced approximately 0.53 million m^3 of oil per month. However, peak total fluid production occurred in 2003, at approximately 1.45 million m^3 per month, with a water to oil ratio (WOR) of 4.8, as shown in Figure 6.4. Water is produced due to residual water within the oil leg and groundwater present within the aquifer beneath the oil bearing horizon [6]. As oil production has declined, water is injected to maintain reservoir pressure and promote oil sweep. Therefore the

Figure 6.3: Map of Wytch Farm, approximate well head sites taken from [28], and local energy demand

water produced is a mixture of injected and residual water from within the reservoir. At the end of the period shown in Figure 6.4, the water produced has risen to ten times the oil produced and is at temperatures of 61 °C.

As Figure 6.3, indicates Wytch Farm is in a rural location on the South coast of England where there is limited local energy demand. The nearest town with significant energy demand, for both heat and electricity, is Poole which is approximately 5 km away. The oilfield operations consume electricity, but have a negligible heat demand. Currently no geothermal energy recovery technologies are utilised at Wytch Farm and the coproduced water is reinjected into the oil field to continued oil production.

In this case, the exploration and subsurface work required for exploitation of the geothermal energy has already been completed as part of the oil operations. The exploration and drilling phase are the largest cost and risk factors for any geothermal project.

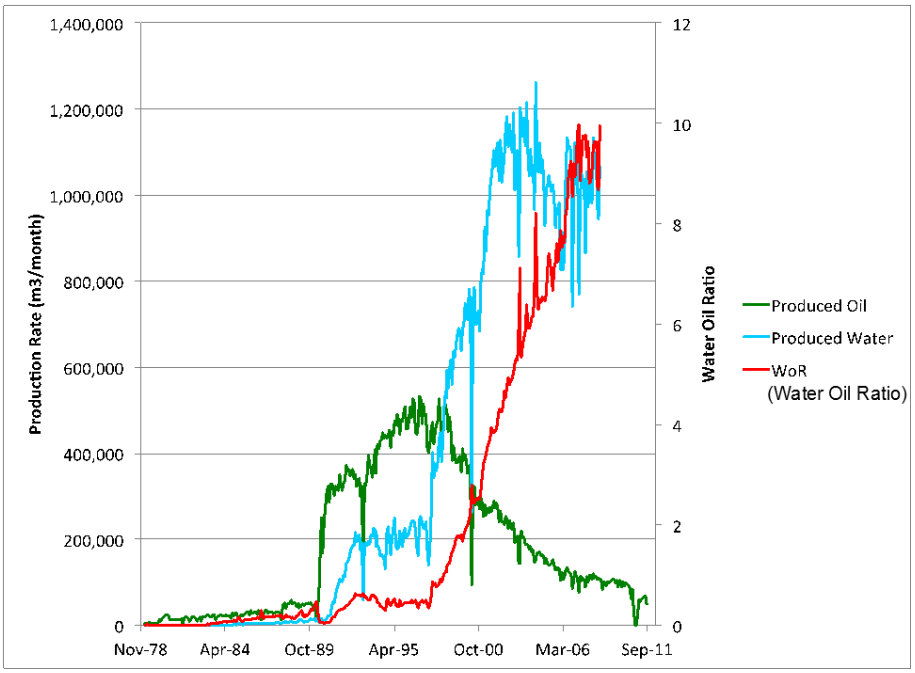

Figure 6.4: Production data for the Wytch Farm Oilfield taken from [6]

Exploitation of existing onshore oil and gas infrastructure for recovery of geothermal energy decreases the risk and cost associated with developing a geothermal project. Lower capital expenditure is required and the investment is more 'safe' meaning this should be a more attractive scenario to investors then building a geothermal scheme from scratch.

However, the impetus to begin exploiting the geothermal energy associated with the Wytch Farm hot brines must come from the company who operates the oilfield. Oil has a much larger value per unit mass than hot water and the oilfield will be operated to produce oil for profit, regardless of the volume of hot water produced. Exploitation of the thermal resource requires a change in mindset for the operating company into an area which they have no experience, expertise or even awareness of. This represents a significant hurdle to the recovery of geothermal energy. While using the geothermal heat may deliver an increase in profit in the future the initial effort for what may be perceived to be a small increase in overall profit for the field has prevented uptake so far.

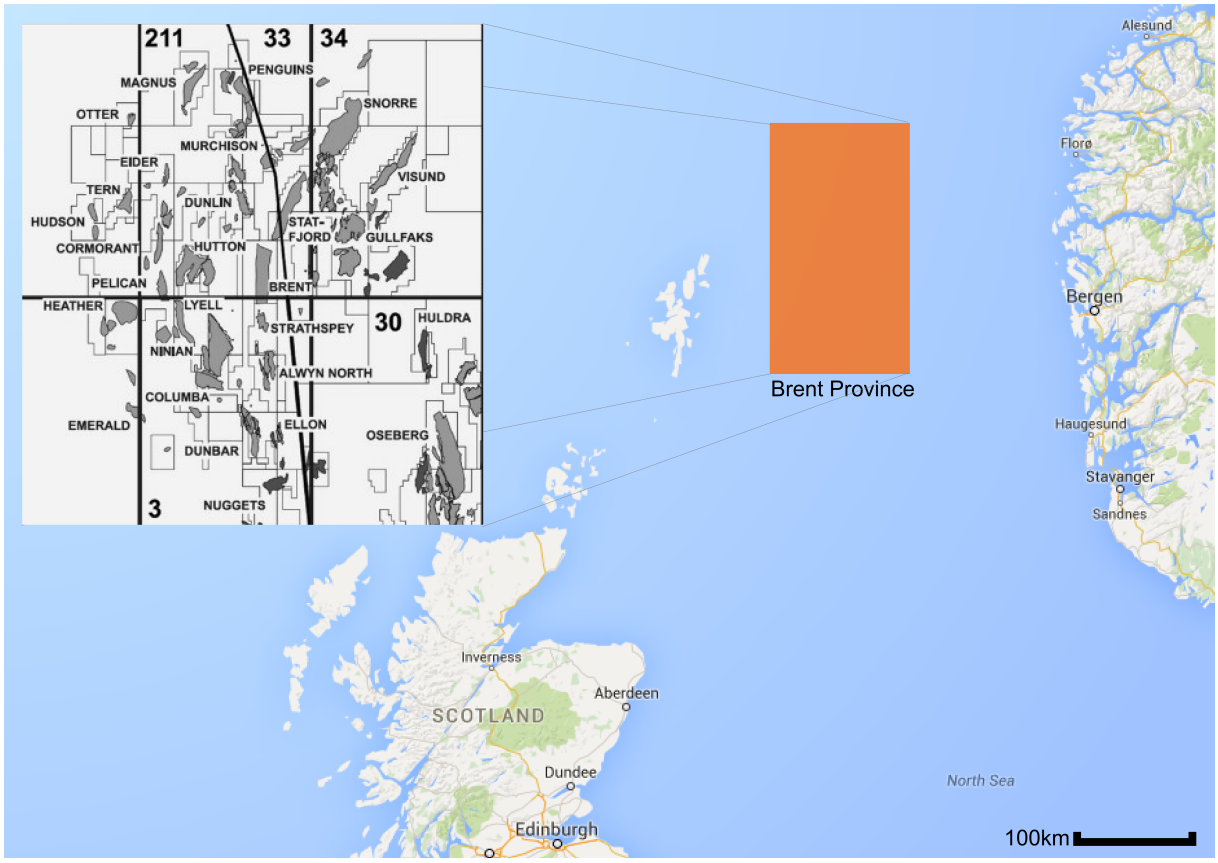

Figure 6.5: Map of Brent Province, North sea. Inset taken from [29]

Brent Province - Offshore Oil Extraction

The North Sea's Brent Province is located in the North Viking Graben, 150 - 300 km east and north east of the Shetland Isles in Scotland and the same distance west and north of Bergen in Norway, as shown in Figure 6.5. The water depth is around 150 m and the fields are typically large such that they have dedicated production platforms.

Most of the fields in this area were discovered and developed in the 1970s and consequently are all at a similar stage of exploitation; oil production is in decline and it is late in the fields life, see Figure 5.7. The development strategy in this area has typically been pressure depletion drive until a point just above the bubble point for the oil. After this, water injection is used to maintain production (Fig. 6.6). Water injection is a secondary recovery technique, whereupon water is pumped back into the reservoir. This increases pressure in the reservoir and displaces or *sweeps* remaining oil to the production well. In

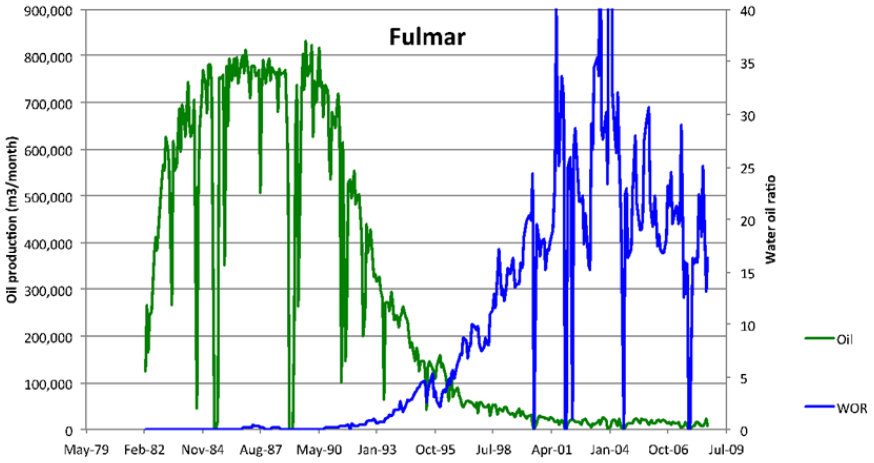

Figure 6.6: Monthly production profile for the Fulmar Field, Central North Sea, showing development of the water production as the field aged. WOR = water oil ratio

general, the proportion of water produced over the lifetime of the well increases, although this is controlled by the water injection pumps, hence the variability shown in Fig. 6.6.

The depth to top reservoir varies from field to field but typically is close to 3 km and as such the reservoir temperature is about 100 °C. This means that the water injected into the formation is heated to the reservoir temperature and therefore the coproduced water from water injection is hot. Currently fields produce about 10 times the quantity of water compared with that of oil and hence associated gas, see Fig. 6.6. Meaning typical flow rates of coproduced water are approximately 0.1 - 1 m^3/s at temperatures between 89 - 128 °C, see Table 6.3.

For the Brent province in most of the fields, the oil is light (35 ° API) and has a low gas oil ratio meaning that relatively little gas is exsolved when the oil is brought to surface. Sweep efficiency and hence the proportion of petroleum recovered varies as a function of reservoir quality (recovery degrades with burial depth). The average recovery from the Brent Province is about 50 % (5 - 65 %).

The gas produced by oil wells in the Brent province, although small in quantity is important as it is used to fuel gas turbines to meet the energy demand of the platforms. Because the gas required is now in short supply, and therefore less power is available, production rates (oil plus gas and water) are declining for many fields. Where gas produced is insufficient it may be imported via tanker. This makes the cost of electricity

significantly higher than it would be onshore.

There comes a point when the operating expenditure (OPEX) exceeds income. Before that point is reached, the field needs to be abandoned as there are costs associated with decommissioning a platform. Predicting when a platform might shutdown is very difficult as this is tied to the market price of oil and gas, a platform must be able to produce oil at less than market price. This makes for an uncertain future for operations in the the North Sea. For example, the recent drop in oil price has resulted in the mothballing of many North Sea operations as they cannot produce at a price which can compete in this market [30].

Much of the oil reserve in the Brent province remains in the ground. If geothermal energy could be recovered from the hot brines to produce electricity, some of the electricity demand of the platform could be met and therefore the operating life of the platform extended. The viability of this depends on the cost of electricity production via ORCs.

Typically the temperature of the North Sea water at the surface is 5 °C. The cool sea water available will improve thermal recovery from the hot brines, because sea water is much colder than the ambient sink temperatures usually available for power production, hence more heat can be recovered.

While there is local electricity demand, a high existing cost of electricity and ready geothermal supply implementation of an ORC system requires an institutional culture willing to look beyond the traditional methods of operating an oil and gas platform. This is a significant barrier for a oil and gas company which may not possess expertise in exploiting thermal resources.

6.4 Factors Affecting the Feasibility of Geothermal ORC Systems

In this section, the factors which influence the feasibility of using geothermal energy to produce electricity using ORCs. The factors are divided into three groups recoverable energy potential, economic factors and physical factors, as indicated previously in Chapter

5, Figure 5.1. The discussion is framed by the three case studies, described in the previous section (section 6.3). These are used to explore the influence of each the factor on the viability of projects.

6.4.1 Recoverable Energy Potential

In order to assess potential power generation from the case studies described, simulations modelling different heat supply characteristics were run using the model described in Chapter 2. Potential power production is only one half of the story, there must be local energy demand, which is considered in this section too.

Heat supply is characterised by mass flow rate and temperature of the geothermal brine supply as shown in Table 6.3. Geothermal brine is assumed to be pure water in the calculations. In reality the streams will be brines but the thermodynamic properties are very similar which makes water an appropriate assumption for an estimate of ORC potential. The heat sink is assumed to be water as well and the mass flow rate is set at 5 times the working fluid mass flow rate. The temperature of the heat sink is set as the average temperature of the sea water at each location. In the case of the North Sea this is 5 °C, but for Southampton and Wytch Farm 12.9 °C was used.

In the Brent Province, temperatures of coproduced hot brines typically range from 70 °C - 130 °C and simulations are run in 3 °C increments through this range. Hot brine mass flow rates have a larger range, a typical range is 1 kg/s - 1500 kg/s (543 - 815,158 Barrels of water per day (bwpd)), so simulations were run in increments of 75 kg/s. The ORC was modelled for each possible combination of heat source characteristics using the following ORC configurations, varying working fluid, TIP and mass flow rate, as described in Chapter 2. To create Fig 6.7 the ORC configuration which produced the maximum power output was selected and this power output plotted as contours against the heat source conditions. Potential power output is also modelled using peak volume data from specific wells in the Brent province as recorded in Table 6.3. These results are plotted as data points on Fig. 6.7.

The figure shows significant power output can be generated even with low temperature

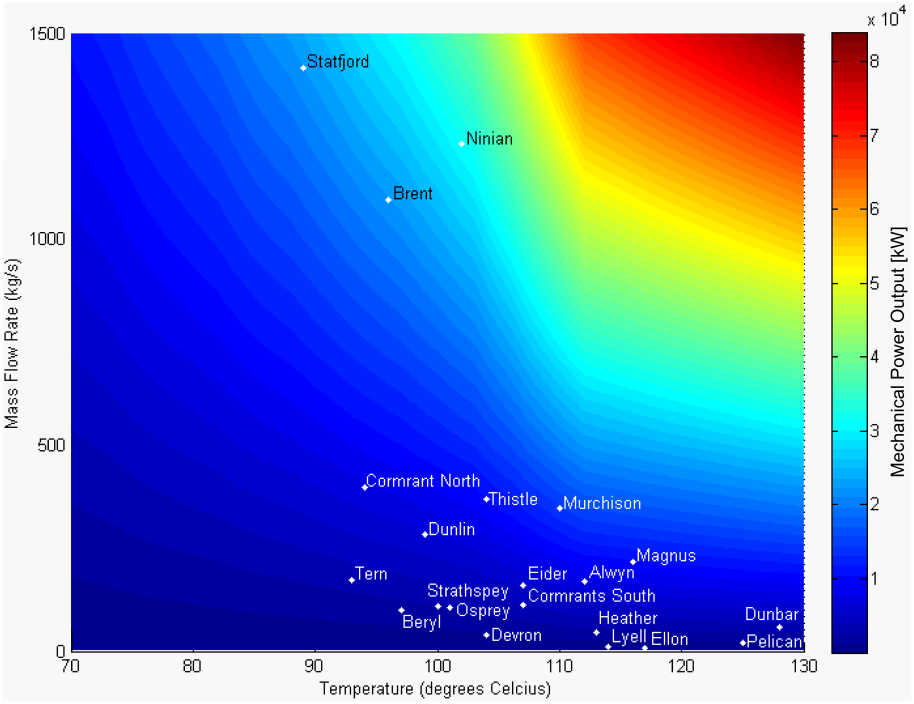

Figure 6.7: Potential power output of organic Rankine cycle fuelled by coproduced hot brines from the Brent Province taken from [31]

hot brine, due to the large flow rates that are available. This is evidenced by the Brent, Ninian and Statfjord fields. These fields have relatively low temperature coproduced brines but the large volumes produced mean they have the potential to produce the largest amounts of power. The model predicts that the Ninian field is able to produce the largest amount of power, 31 MW. In reality this size of system would require exceptionally large heat exchangers and the volume of organic fluid may so great as to be practically difficult or expensive to implement. However, this does indicate the potential of hot brines as an energy source. The Magnus, Thistle, Murchison, Brent, Ninian and Statfjord fields have the potential to generate more than 10 MW, while the majority of other sites are predicted to be capable of producing several MWs of power. This is a significant proportion of typical platform energy demand.

The potential power predicted by the model used in this work exceeds that predicted using similar data for the Brent field published by Younger et al. [32]. This is because Younger et al. assumed an arbitrary fixed temperature drop of 30 °C for each hot brine stream. The available heat input to the cycle is limited by this assumption and therefore

so is the possible power output.

The hot source in each simulation is modelled by a single temperature and mass flow rate and therefore the ORC selected is the optimum design. Off-design performance is not considered. The temperature of the hot brines will not fluctuate much because the temperature in the reservoir remains constant. The flow rate of the brine typically varies a lot but the application the ORC is expected to stabilise the production rate. This is because the mass flow rate of the brine is determined by the power applied to the pumps used to inject the cool brines into the reservoir. The power required by the injection pumps represents a significant proportion of a platforms power demand, typically requiring several MW_e. Currently operation is determined by the cost or availability of gas required to produce power to run them. Were an ORC to meet power demand, the mass flow rate of the hot brine can be held constant by supplying enough power from the ORC to the injection pumps. As a consequence using an ORC fuelled by hot brines to power the injection pumps will improve the stability of production.

In the case of Wytch farm, similar simulations were carried out. Typically coproduced brines from Wytch Farm have a temperature of 66 °C and a mass flow rate of 353 kg/s. This resource has both a lower temperature and lower flow rate than hot brines from the Brent Province, thus the potential power production via ORC is much less, just 1.69 MWe.

Despite the similar geological setting the hot brines produced at Wytch farm are slightly cooler than that produced at the Southampton geothermal scheme. Here the geothermally heated brine is 72 °C but the flow rate that can be produced is much lower, 10 kg/s. As a result the power production potential from Southampton is limited and simulations show an optimised ORC is predicted to produce just 65 kW of electricity, see Table 6.3.

In all cases, using the geothermal resource for power production must be balanced with the demand for electricity. Furthermore, each of the geothermal resources described in the case studies can be used to meet heat demand. Therefore the value of electricity production via an ORC should be considered against ability to supply heat, which similarly

depends on local demand.

As the Southampton geothermal scheme is located in the middle of Southampton city, there is high demand for both heat and electricity in close proximity to the well head, see Figure 6.1. This local heat demand means it is more economical to use the geothermal resource, (2 MW_{th}) in a district heating scheme, rather than to convert it to electricity in an ORC, which comes at an economic and thermodynamic cost.

In contrast at Wytch Farm, despite having a significant geothermal resource (35 MW_{th} or 1.69 MW_e) there is limited heat and electricity demand nearby. In a similar manner to the North Sea brines, converting the geothermal brine to electricity via ORC could subsidise power required for water injection pumps. Alternatively, heat or electricity could be supplied to Poole, but this would require transporting the energy over a distance of approximately 5 km. The costs of each of these scenarios must be balanced.

6.4.2 Physical Factors

Geology

There are two main geological factors that must be considered for the exploitation of geothermal energy. These are the reservoir temperature and the transmissivity at depth.

Firstly, the temperature gradient determines the temperature of the geothermal resource at depth. On average the geothermal gradient throughout the UK is 26 °C/km depth, however this does vary due to different geology as shown in Figure 6.8a [33]. This will determine the temperature of the geothermal resource that can be accessed. The depth to which a borehole is drilled is dependant on the geology at depth. Typical geothermal systems use two wells, one abstraction and one injection. The geology must allow fluid to flow from the bottom of the injection well to the bottom of the abstraction well, along this pathway the fluid is heated by the surrounding rocks. Therefore the geology selected must allow, or be engineered to allow fluid flow.

In the UK, there are two main geological settings identified as being appropriate for geothermal exploitation. These are buried radiogenic granites and their associated

marginal faults (e.g. Cornwall , the Lake District, the North Pennines and the Grampians) and sedimentary aquifers. These deep aquifers are Mesozoic and Palaeozoic basins which comprise of basal Permo-Triassic sandstones. The main onshore Mesozoic basins in the UK are shown in Figure 6.8b, these are the Wessex, Worcester, Cheshire and Eastern England basins in Britain and also Larne Lough and Neagh basins in Northern Ireland. The sedimentary aquifers are at depths greater than 1 km and have thicknesses ranging from a few tens of metres to hundreds of metres. Temperatures in the aquifers of up to 80 °C have been measured and it is thought that they could reach 100 °C in the deepest parts [34]. The case studies evaluated in this work and described in the previous section all target reservoir systems. Wytch Farm and Southampton both extract geothermally heated fluid from the Wessex basin, while the co-produced hot Brines from the North Sea come from various hydrocarbon reservoir systems in the Brent province.

These systems are naturally transmissive and do not require additional stimulation. Granite settings are not always naturally permeable and may require hydraulic fracturing in order to increase reservoir transmissivity and create pathways between the abstraction and reinjection wells. The subsurface in all of the case studies has been explored and therefore the local geology in each case is well understood. However, the Southampton borehole was drilled as part of an exploratory project and at the time of drilling the geology in this location was not as well understood as it is now.

Plant Size

A potential limitation of any geothermal system is the physical space available for a plant near the well head. Clearly in the case of the North Sea, plant size is limited by space available on the offshore platform. This has the potential to limit the power rating of any possible ORC system fuelled by coproduced hot brines. However, as the North Sea reserves have depleted, some platforms have been partially decommissioned leaving space available for additional plant. Platforms will have a maximum loading capacity and the mass of any additional equipment must be less this. However, this was not considered as part of the current study.

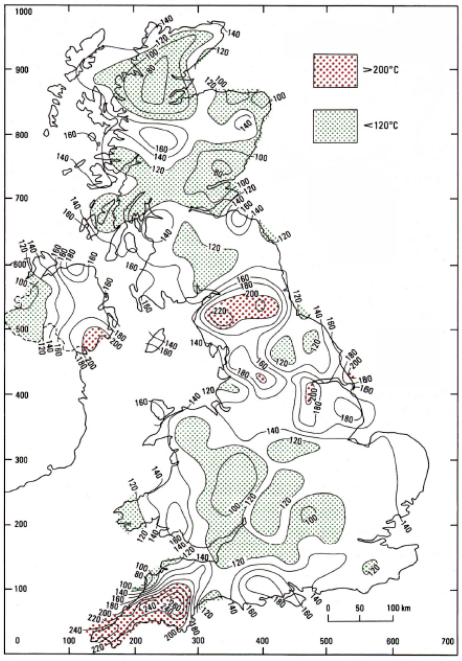

(a) Map of temperature at 7 km depth taken from [11]

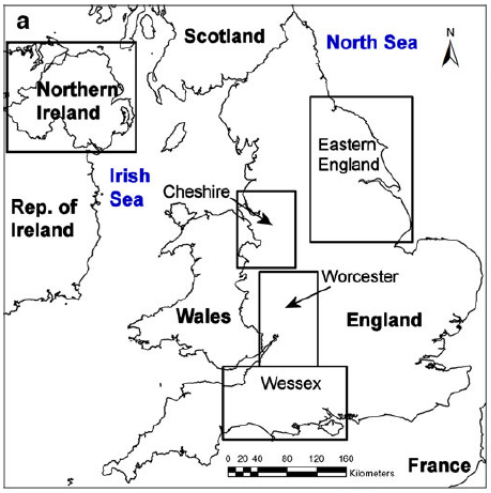

(b) Map of onshore mesozoic basins in the UK taken from [34]

Figure 6.8: Maps showing UK geothermal potential

Similarly both Southampton and Wytch Farm have space constraints. The Southampton well head is in the city centre, where available space is constrained by the high density of existing buildings. Wytch Farm is in an Area of Outstanding National Beauty (AONB) and is part of the Heritage Coast which has constraints requiring any development to have minimal impact on the landscape [35].

In each case, space may limit the size of the ORC system which can be installed.

6.4.3 Economic Factors

For an ORC power generation system powered by geothermal heat to be economically feasible, the cost of installation and operation and maintenance costs must be repaid over an acceptable period whilst being competitive with alternative methods of electricity generation. The economic scenario in each case is different and in each case different economic factors determine the feasibility or otherwise of a geothermally driven ORC.

In this section, the finance required to develop an ORC plant for each scenario is considered, together with the role of government subsidies and funding on project viability.

Finally, the influence of risk on each case is discussed and how institutional cultures influence the level of acceptable risk.

Finance

The cost of exploiting geothermal energy can be crudely split into: drilling and plant costs. Drilling cost is a huge part of the overall project cost. In 2013 the World Energy Congress (WEC) stated drilling rig rates and associated costs make up the single largest cost component of a geothermal plant (upwards of 55 %). A recent conversation with Kevin Mallin, Geolorn Ltd. [36], put drilling costs at *40 - 50 % of development costs*. Therefore, it is clear that there is a huge saving to be made by using coproduced hot brines, as in the case of the North Sea and Wytch Farm. In these cases an approximate figure of 3000 Eur/kW (3350 USD/kW) is used to calculate the capital costs [37]. Cost is not calculated for the Southampton scheme but an appropriate estimation would be between 2770 - 5540 €/kW (3000 - 6000 USD/kW) [36], i.e. up to twice the cost of scenarios where drilling costs can be excluded.

In all scenarios, the cost of electricity supply must be competitive with the local cost of electricity generation by other means over an acceptable payback period. At Wytch farm and Southampton this means electricity production via ORC would need to compete with the market cost of electricity from the national grid.

In the North Sea, local electricity demand is met by on-platform gas turbines and the economic landscape relating to power supply is more complex. This is described further in Chapter 5 section 5.3. Conventionally on-platform power is met by gas turbines. Once too little gas or diesel is produced by the platform to meet the power requirements, the gas has to be imported to allow the platform to keep producing. This is an expensive solution and the economically viable operating life of the platform becomes a function of the cost of importing gas against the profit from production [23]. An ORC plant powered by North Sea coproduced brine may extend the life of a well and therefore increase total oil recovered, as additional value is produced from the geothermal energy in addition to the oil. However, to be economical the remaining producing life of the well, including

geothermal energy recovery, must exceed the pay back period on the cost of plant to recover the geothermal energy. The marginal value of water will change with oil price. A higher oil price will mean a higher marginal value of the hot brine and this should be factored in to planning a hot brine fuelled ORC.

A Note on Drilling Costs:

Where the geology is uncertain, costs associated with drilling are significantly higher. In general, costs do not vary with different geology [36] but where the geology is unknown extra costs must be factored in.

Geothermal projects compete with oil & gas projects for the same drilling rigs, so a thriving oil and gas sector can end up meaning more expensive drilling costs for the geothermal sector [39]. In a report by Atkins, commissioned by Cornwall and the Isles of Scilly Local Enterprise Partnership, mobilisation of a drilling rig to site is estimated to be £1.3 million (approximately 2 million USD) See Table 6.4. Therefore the decline of oil and gas production in Europe, could bring with it a reduction in drilling costs which could help with geothermal exploration.

Subsidy and Grant Aid

Several mechanisms exist at government and EU level which can offset some of the cost of developing a geothermal scheme in the UK. Geothermal energy is an immature technology in the UK, even though it has been identified for some time that the UK has a significant low enthalpy geothermal resource, which can contribute to heat and electricity supply in a low carbon way.

Electricity generated via geothermal schemes in the UK currently qualifies for the following subsidies:

- *Contracts for Difference (CfD)* - A financial incentive for renewable electricity generation. These are contracts with the government, guaranteed for 15 years, to pay the difference between the market price for wholesale electricity and a strike price. The strike price is set as £145 / MWh for geothermal.

- *Offtaker of Last Resort (OLR)* - This is a guarantee renewable energy will be purchased. It is designed to reduced the risk profile for renewable energy, by providing a worst case scenario. It will typically be 10 % below the market wholesale cost, approximately 39 £/MWh (2015).

For context, if a geothermal scheme were to supply heat directly, rather than produce power, it would qualify for the Renewable Heat Incentive (RHI). This subsidy means a generator is paid £50 per MWh of heat produced.

Capital aid in the form of grants is available from the EU and the UK. Approximately 4.5 million pounds has been awarded by the UK government under the Regional Growth Fund (RGF) and the Deep Geothermal Fund between 2010 and 2015 [40]. This funding is split across 5 projects however the future availability of such grants is very uncertain due to the incumbent Conservative government's preference for cost effective energy generation, over renewable energy generation to meet climate change commitments.

There is a conflict between money paid out in subsidy and EU state aid rules. For projects which have received grant funding, unless it is repaid to the donor, the project would not qualify for subsidies. There are scenarios where the grant may be repaid through reduction of subsidy over a number of years, and in rare cases, repaying the grant might be avoided. This is a complex issue and there is no clear solution currently, as was acknowledged by Lord Jenkin in the House of Lords [41]. This complication causes additional delay and uncertainty to geothermal projects.

With regard to the geothermal case studies considered in this chapter, the new power plants at each site would qualify for CfD, OLR and RHI. Furthermore, the Southampton well was funded by a research grant in the 1980s. Subsidy of any energy technology is uncertain. Conversations with geothermal energy developers through Durham University [42] indicates that they only proceed with projects that are viable without accounting for subsidies, due to this instability. However, conversations with developers through DECC have revealed that their view is that projects are not viable without state aid. The reality probably lies somewhere between the two views, and certainly highlihgts the complexities

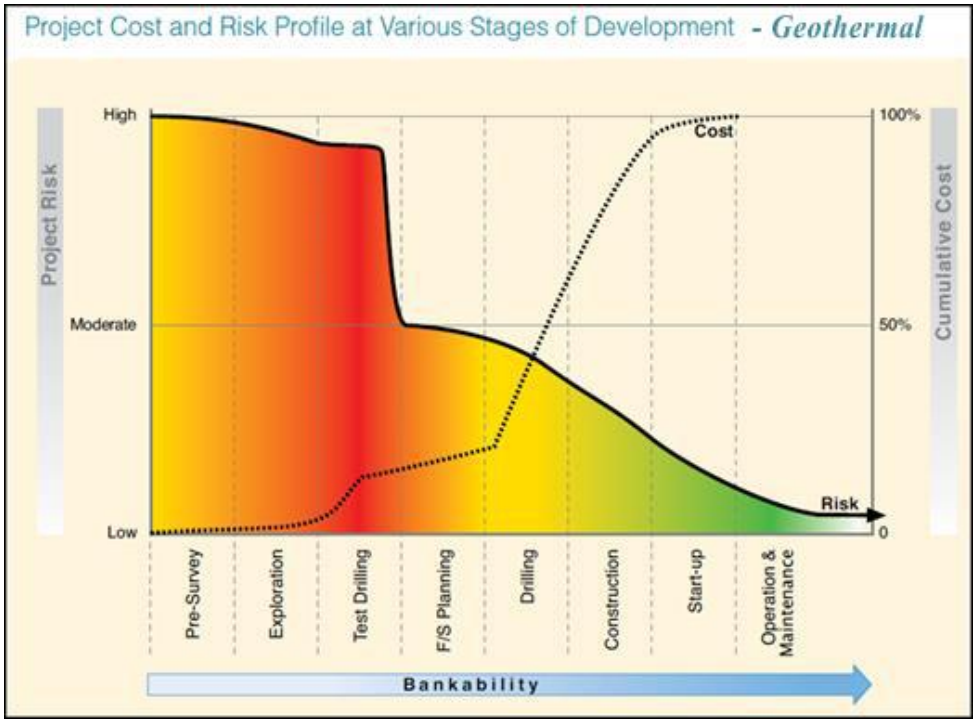

Figure 6.9: Risk profile associated with conventional geothermal projects [43]

in determining the economic viability of a geothermal project.

Risk

All of the criteria discussed above, represent different levels of uncertainty and this translates into different levels of financial risk to an investor. Figure 6.9 shows the different stages and magnitudes of risk in a geothermal project. Bankability, used in the Figure 6.9, is defined as the ability to attract financing from a commercial source.

As Figure 6.9 shows, the highest level of risk with any geothermal project is encountered during the research, exploration and test drilling phases. Geothermal energy resource identification and characterisation is a key source of uncertainty. However, more significant cost is associated with the test drilling phase.

Risks in drilling and test drilling include well failure due to factors such as loading from the surrounding rock formation, mechanical damage during well development, corrosion and scaling from geothermal fluids, thermal stress, metal fatigue and failure and expansion of entrapped fluids. Some of these risks may be reduced in a low enthalpy environment.

Another source of risk is poor fluid yields due to vertical and lateral heterogeneities in the rock. These factors mean the development and drilling phases of geothermal schemes carry a high amount of risk and account for the over half the cost of a project. This was the case for the construction of the Southampton geothermal scheme. Conversely, as the wells have already been drilled, in the case of Wytch Farm and the North Sea the drilling and construction risk does not exist because the borehole and exploration phases have already been carried out as part of the oil and gas exploitation activities.

Using an operational oil well reduces many of the upfront risks and costs associated with the research, development and drilling phases by using infrastructure that has been designed and proven to supply fluids over relatively long time periods. Although by using existing infrastructure there is less control over where it is sited. Repurposing existing wells is an effective strategy for de-risking the exploitation of geothermal resources [6].

Institutional Cultures

As identified in the discussion of risk, finance and geology the Southampton geothermal scheme represented a huge financial outlay with exceptionally high risk. Smith [16] acknowledged that the *economics of the proposal were marginal at best* with respect to exploiting the geothermal energy available from the well after drilling. Smith cites the enthusiasm from both the council and the utilities company involved in the developing the project, as the main drivers for bringing the project to fruition.

Conversely, in the case of both Wytch Farm and the North Sea sites, the operators are oil and gas companies. Exploitation of geothermal energy is a deviation and, might be perceived as a distraction from their core business areas. Similarly, oil and gas are high demand, high revenue products, therefore an oil and gas company is more likely to channel funds into exploiting oil and gas reserves, rather looking more holistically at the energy reserve they can access as a whole.

A further and non-trivial complication is that the oil and gas and geothermal industries use many different units to describe production. This makes comparison more difficult and means that cooperation between the geothermal and oil and gas industries are rarely

compared. Therefore the significance of the geothermal potential from oil and gas is not widely appreciated [7].

An institutional culture willing to overcome these types of challenges and with the willingness to deviate from core business practise, as was the case for the development of the Southampton scheme, is needed for geothermal schemes to go ahead for applications of the type considered in the test cases explored in this chapter.

6.5 Conclusions: Not all deep geothermal sources are equal

This chapter presented cases studies from three low enthalpy geothermal energy settings in the UK. These were: the Southampton geothermal scheme, co-produced hot brine from Wytch farm onshore wells, and co-produced hot brine from the North Sea wells. Each of these schemes were characterised in terms of energy available, local heat demand, geological and economic factors.

Factors which determine a geothermal ORCs feasibility were broken down into three categories: physical, economic and thermodynamic. These factors and the differences between each of the case studies have been discussed in detail.

In terms of potential supply and demand, the North Sea co-produced hot brine case has the largest potential power production via ORCs. In this case there is high electricity demand in the context of high cost of electricity offshore. It was calculated that the Wytch Farm geothermal brine could produce 1.69 MWe but local demand is limited. The Southampton case was calculated to have potential to supply only 0.65 MWe, the existing scheme serves as a district heating scheme.

In terms of physical factors, the geology of the Southampton borehole was very uncertain and unexplored at the time of drilling. This adds risk to exploiting the geothermal resource. However this is not the case for the other case studies as they have been well characterised from oil and gas activities.

Economic factors were considered in four areas: finance, subsidy, risk and institutional

cultures. In the case of coproduced brines, the capital cost of exploiting the geothermal resource is estimated to be 50 % less and the project risk is significantly reduced compared to cases where the drilling of the borehole has to be factored into the project. This makes the co-produced brines case appear more economically favourable. However, despite the apparently less favourable economics, the culture and willingness to see a geothermal project succeed by the stakeholders in the Southampton project means that this is the only deep geothermal project developed in the UK to date. The results of the discussion for each case study is summarised in Figure 6.10.

Should exploitation of deep geothermal energy via ORC be pursued in the UK? This chapter has shown that while there is the technical potential to do this, physical, economic and non-technical factors will drive the success or otherwise of geothermal ORC projects.

References

Name	Mass Flow Rate (kg/s)	Temperature (°C)	Max. Power Output (MW)
Brent Province			
Ellon	9.29	117	0.45
Lyell	11.25	114	0.52
Pelican	20.51	125	1.09
Devron	39.54	104	1.09
Heather	44.88	113	2.05
Dunbar	58.43	128	3.2
Beryl	100.88	97	2.1
Osprey	107.15	101	2.66
Strathspey	110.29	100	2.59
Cormorant South	111.94	107	3.67
Eider	159.22	107	5.22
Alwyn North (East)	168.71	112	7.58
Tern	173.17	93	3.15
Magnus	218.65	116	10.36
Dunlin	282.72	99	6.39
Murchison	346.46	110	14.1
Thistle	369.93	104	10.19
Cormorant North	398.72	94	7.57
Brent	1096.62	96	22.28
Ninian	1231.1	102	31.01
Statfjord	1417.43	89	22.56
Wytch Farm			
	363	66	1.69
Southampton			
	10.5	72	0.065

Table 6.3: Characteristics of hot brines used in simulations and power outputs calculated. For the Brent province mass flow rate data has been taken from DECC and temperature data from Gluyas and Hichens [29]. In the case of Southampton data was kindly supplied by Coefly and for Wytch Farm available data from DECC was used.

Cost of Demonstration Well	Cost (£)
Site access	150,000
Planning / Environmental / Permits	500,000
Infrastructure for Drilling site	1,000,000
Drilling well 1	5,700,000
Mob / Demob of drilling equipment	1,300,000
Testing per well	1,250,000
Reservoir engineering	1,500,000
Microseismic tests	700,000
Total	12,100,000

Table 6.4: Breakdown of cost of demonstration well taken from [38]

		Southampton	Wytch Farm	North Sea
Technical Factors	Recoverable Energy	~2 MWth, 65kWe	~35 MWth, 1.69 Mwe	~10s MW scale heat, ~MW scale electricity
	Local Demand	Large local heat and electricty demand	Some heat and electricity demand	Large local electricity demand
Physcial Factors	Geology	Aquifer (unexplored at time of drilling)	Aquifer, geological setting well explored.	Hydrocarbon reservoir, geological setting well explored.
	Available Plant Space	Limited by town centre location	Potentially limited by AONB status	Limited to platform space
Economic Factors	Finance	High Cap Ex.	No drilling cost. Plant capital and operational cost.	No drilling cost, plant capital and operational cost. High existing local electcity price to improve.
	Subsidy	Government grant. LEC, CfD, OLR. RHI (heat only)	LEC, CfD, OLR, , EU SIF. RHI (heat only)	LEC, CfD, OLR, , EU SIF. RHI (heat only)
	Risk	At time of drilling geoloical setting unkown. Subsidy change risk	Geological setting well explored. Subsidy change risk	Geoloical setting well understood but oil price influences viability to produce and therefore platform life. Subsidy change risk
	Instituational Culture	Council had a very strong drive to prove commitment to renewable energy	Oil and Gas operator not interested	Power shortage promotes some openess to innovative solutions

Figure 6.10: Summary of viability factors for ORC plant for each geothermal source

[1] D. J. MacKay, "Sustainability without the hot air," 2011.

[2] R. Bertani and J. Lund, "World energy resources: 2013 survey," Tech. Rep. 23rd Edition, World Energy Council, October 2013.

[3] B. Matek, "Annual us & global geothermal power production report," tech. rep., Geothermal Energy Association, February 2015.

[4] A. Auld, S. Hogg, A. Berson, and J. Gluyas, "Power production via north sea hot brines," *Energy*, vol. 78, pp. 674–684, 2014.

[5] C. Adams, A. Auld, J. Gluyas, and S. Hogg, "Geothermal energy the global opportunity," *Part A Journal of Power and Energy*, vol. 0, no. 0, pp. 1–8, 2015.

[6] C. Adams, A. Auld, and J. Gluyas, "From hydrocarbons to heat: Evolution of offshore onshore oil wells to geothermal systems," *IN PREP*, vol. 0(0), pp. 1 – 15, 2015.

[7] J. Gluyas, A. Auld, C. Adams, C. Hirst, S. Hogg, and J. Craig, "Geothermal potential of the global oil industry," *IN PREP*, 2015.

[8] J. W. Lund and T. L. Boyd, "Direct utilization of geothermal energy 2015 worldwide review," in *Proceedings World Geothermal Congress*, (Melbourne, Australia), April 2015.

[9] R. Bertani, "Geothermal power generation in the world 2010 - 2015 update report," in *Proceedings World Geothermal Congress*, (Melbourne, Australia), April 2015.

[10] "Britain to asses it's geothermal resources." Magazine article in New Scientist, July 1976.

[11] R. A. Downing and A. Gray, *Geothermal Energy, The potential in the United Kingdom*, ch. 10: Review of the Geothermal Potential of the UK, pp. 152 – 161. British Geological Survey, National Environment Research Council, 1986. ISBN 0 11 884366 4.

[12] R. Parker, "The rosemannows hdr project 1983 - 1991," *Geothermics*, vol. 28, pp. 603 – 615, 1999.

[13] P. MacDonald, A. StedMan, and G. Symons, "The uk geothermal hot dry rick r&d programme," in *17th workshop on geothermal reservoir engineering*, pp. 5 – 11, January 1992.

[14] R. Baria, J. Garnish, J. Baumgartner, A. Gérard, and R. Jung, "Recent developments in the european hdr research programme at soultz-sous-forêts (france)," in *Proceedings of the World Geothermal Congress*, vol. 4, pp. 2631–2637, 1995.

[15] R. Schellschmidt, B. Sanner, S. Pester, and R. Schulz, "Geothermal energy use in germany," in *Proceedings world geothermal Congress*, pp. 1–19, 2010.

[16] M. Smith, "Southampton energy scheme," in *Proceedings of the World Geothermal Congress, Kyushu-Tohoku, Japan*, pp. 695–697, 2000.

[17] I. F. Smith, *Geothermal Energy, The potential in the United Kingdom*, ch. 4: Mesozoic Basins, pp. 42 – 99. British Geological Survey, National Environment Research Council, 1986. ISBN 0 11 884366 4.

[18] I. West, "Geology of the wessex coast of southern england." Internet, 2015.

[19] R. A. Downing, *Geothermal Energy, The potential in the United Kingdom*, ch. 9: Engineering and Economic Aspects of Low Enthalpy Development, pp. 152 – 161. British Geological Survey, National Environment Research Council, 1986. ISBN 0 11 884366 4.

[20] S. L. Tim Jackson, "Geothermal energy potential in great britain and nornorth ireland," tech. rep., Renewable Energy Assocciation, May 2012.

[21] Atkins Ltd, "Deep geothermal review study," final report, Department of Energy and Climate Change (DECC), 2013.

[22] C. Adams and J. Gluyas, "Squeezing the barrel: Knowledge exchange adds value to oilfields in decline ne." NERC Innovation Awards: Project highlights and impact report.

[23] P. L. Younger, J. G. Gluyas, and W. E. Stephens, "Development of deep geothermal energy resources in the uk," *Proceedings of the Institution of Civil Engineers*, vol. 164(EN0), pp. 1–14, 2011.

[24] M. Smith, "Energy services cofely's approach to district energy," 2011.

[25] C. Hirst. Private Comms.

[26] Southampton Geothermal Heating Company, "Geothermal energy - southampton, demonstration project," final report, Commission fo the European Communities, 1989. ISBN: 92-826-0942-1.

[27] R. A. Downing, I. F. S. D. J. Allen, W. G. Burgess, and W. M. Edmunds, "Investigation of the geothermal potential fo the uk. the southampton (western exsplanade) geothermal well - a preliminary assessment of the resource," *Institute of Geological Sicences, Geophysics and Hydrogeology Division*, vol. 83, pp. 18 – 29, 1982.

[28] D. Knott, "Bp completes record extended-reach well." Internet, Januray 1998.

[29] J. G. Gluyas and H. M. Hichens, *United Kingdom oil and gas fields: commemorative millennium volume*, vol. 20. Geological Society, 2003.

[30] K. Stacey, "North sea oil producers face a perfect storm," *The Financial Times*, October 2015.

[31] A. Auld, A. Berson, and S. Hogg, "Organic rankine cycles in waste heat recovery: a comparative study," *International Journal of Low Carbon Technology*, vol. 8 (suppl 1), pp. i9–i18, 2013.

[32] P. L. Younger, J. G. Gluyas, and W. E. Stephens, "Development of deep geothermal energy resources in the uk," *Proceedings of the Institution of Civil Engineers*, vol. 164(EN0), pp. 1–14, 2011.

[33] J. Busby, "Geothermal prospects in the united kingdom," in *Proceedings World Geothermal Congress*, 2010.

[34] J. Busby, "Geothermal energy in sedimentary basins in the uk," *Hydrogeology Journal*, vol. 22, no. 1, pp. 129–141, 2014.

[35] Perenco UK, "Wytch farm, wareham and kimmeridge oilfields, aapplication to extend the opoperation life of the wytch farm, wareham and kimmeridge oilfields through the variation of existing planning conditions.," August 2012.

[36] K. Mallin. Personal Communications, September 2015.

[37] S. Quoilin, M. Van Den Broek, S. Declaye, P. Dewallef, and V. Lemort, "Techno-economic survey of organic rankine cycle (orc) systems," *Renewable and Sustainable Energy Reviews*, vol. 22, pp. 168–186, 2013.

[38] Arup, T. Briault, B. Laidlaw, and C. Lumsden, "Deep geothermal investment options appraisal," final report, Cornwall and the Isles of Scilly, Local Enterprise Partnership, September 2015.

[39] "World energy perspective cost of energy technologies," 2013.

[40] Department of Energy and Climate Change, "Policy paper, 2010 to 2015 government policy: low carbon technologies." Updated: May 2015.

[41] "Electricity capacity regulations 2014, motion to consider." Hansard, July 2014.

[42] C. Adams, "*Pers. Comms.*"

[43] M. Gehringer and V. Loksha, "Geothermal handbook: planning and financing power generation," *Washington DC: World Bank Group, Energy Sector Management Assistance Program. Accessed November*, vol. 6, p. 2013, 2012.

Chapter 7

Conclusions and Future Work

The power generation potential and challenges associated with the application of Organic Rankine Cycle (ORC) technology for heat recovery purposes has been evaluated in this thesis. The study has considered potential applications of ORCs for both waste heat streams and deep geothermal sources.

Theoretical models and an experimental test rig were developed with the aim of understanding the performance of ORCs driven by different heat sources and sinks and in different configurations. A discussion of the principal conclusions from the work, relating to the barriers and benefits of using ORCs, are presented below.

As discussed in Chapter 1, the ORC is a thermodynamic cycle capable of recovering heat into useful power with lower enthalpies than traditional steam Rankine cycles. The organic working fluids employed by ORCs, such as hydrocarbons (HCs), hydrochlorofluorocarbons (HCFCs), hhloroflurocarbons (CFCs), herfluorocarbons (PFCs), siloxanes, alcohols, hydrofluroehters (HFEs) and other refrigerant type compounds, have lower boiling points than water, so evaporation of these fluids can occur at lower temperatures and pressures.

Three potential sources of waste heat that could supply an ORC were used as case studies to draw conclusions on the potential energy recovery via ORC at different energy scales and with different working fluids, including zeotropes. The case studies were exhaust heat from an Internal Combustion Engine (ICE), industrial waste steam and hot

brine coproduced from oil production.

The three case studies were used as inputs to a theoretical model, developed as part of this study, which is capable of modelling the thermodynamic performance of ORC with both pure and zeotropic working fluids. The simulations showed that the optimal cycle configuration for recovered work output is strongly dependent on the T-H profile of the heat source fluid and therefore the position of the pinch point in the heat exchanger. By considering the gradient of both the T-H profile of the working fluid and the source heat stream general design principles for ORCs were developed. In summary, these rules are:

- Where the gradient of the source heat fluid T-H profile is steeper than that of the working fluid, cycle work output will increase with an increase in TIP.

- When the gradient of the source T-H profile is shallower than that of the ORC working fluid high TIP can result in a decrease in work output from the cycle.

The results showed that the conditions for maximum mechanical work output and maximum thermal efficiency of an ORC occur at different thermodynamic conditions. The maximum work output is delivered under conditions where there is the best balance between the heat input to the cycle (decreases with TIP) and thermal efficiency (increases with TIP).

ORC cycles powered by waste heat must be designed to operate in the region of the maximum work output, if possible, and avoid configurations that might cause the pinch point location to change and therefore the rate of heat taken into the cycle to decrease.

Simulations were also run using fluid mixtures. These results showed that there is a potential thermodynamic benefit from using fluid mixtures to increase heat input into the ORC. A potential heat increase of +14.26 % was calculated using a 0.5/0.5 Butane/ Pentane fluid mixture in the Ninian case. However, no benefit was predicted using Butane/ Pentane or Toluene/ Cyclohexane mixtures in the engine simulation test case. Simulation results show that this is because the cycle performance is dominated by the cycle efficiency.

Zeotropic organic fluid mixtures are not currently in common use in commercially available ORCs. If using a zeotropic mixture can increase the amount of energy recovered by an ORC, as the results presented in Chapter 2 suggest they can, then this will make installing an ORC plant a more attractive investment.

The theoretical result that zeotropic mixtures may provide a thermodynamic benefit for ORCs is consistent the with existing literature. However, studies published also report a decrease in heat transfer coefficient during phase change for zeotropic mixtures in comparison to that for pure fluids. A decrease in heat transfer coefficient represents a penalty, because a larger heat exchange area, and therefore larger and more expensive heat exchanger, is required for the same amount of heat transfer.

The next step in this study therefore was to try and evaluate the potential benefit or penalty of zeotropic mixture working fluids in heat exchangers. An experimental test facility based on a Ground Source Heat Pump (GSHP) was developed. A domestic heat pump system was modified to include additional instrumentation to measure the heat exchange process across the heat exchangers. Experimental data was collected using R410a, a near azeotropic working fluid that the heat pump was designed for, and R407c, a ternary zeotropic refrigerant mixture, over a range of heat source temperatures.

The experimental results showed that the heat pump cycle worked as expected for both fluid mixtures. The data captured the zeotropic behaviour of R407c showing significant glide during phase change and improved matching of the temperature profile in the heat exchangers compared to R410a. The data showed that the pressure drop measured over both heat exchangers influences the magnitude of the glide. In the evaporator the pressure drop means the glide during phase change in decreased, in comparison to a constant pressure. Whereas for the condenser the pressure drop augments the size of the glide. Therefore when designing an ORC with a zeotropic mixture the pressure drop across the heat exchangers must be taken into account in order to fully understand the heat exchange processes.

Heat transferred and COP were plotted against brine inlet temperature for each work-

ing fluid. This showed that heat into the cycle tends to increase with brine inlet temperature, while heat out has a decreasing trend for R401a and is generally constant for R407c. Comparison of UA values, calculated from the condenser data, for both R410a and R407c, showed generally higher UA values for R410a compared to R407c. Therefore, the heat transfer coefficient is generally higher for R410a than R407c. This means a larger area heat exchanger is required for the same overall heat transfer if R407c is used to replace R410a.

A theoretical model capable of calculating the heat transfer coefficient for zeotropic mixtures is needed in order to understand the implications on ORC system design of lower heat transfer coefficient with zeotropic mixtures. The published literature includes models capable of simulating the heat transfer for zeotropic mixtures, but a different model is required for each heat exchanger configuration, fluid condition, mechanism of phase change and orientation. Therefore, a program that is flexible enough to inform plant design using zeotropic mixtures would required many different models to be available.

One suitable heat transfer model for condensation of binary zeotropic fluid mixtures was suggested in this study. The aim in future work would be to validate this model by comparing results with experimental data obtained using the test facility developed in this study. This was not possible in the current work because of the qualification and lead-time associated with procuring suitable binary zeotropic mixtures for use in the test facility.

Ultimately, a general modelling strategy is needed for heat exchangers with multi-component zeotropic fluid mixtures. This is a major piece of work for the future.

The size of ORC plants was investigated using the global UA value derived from the modelling simulations. This allowed an understanding of the relative size of heat exchangers required. The characteristics of the hot brine produced by the Eider oil field were used in Chapter 5 an exemplar to explore the relationship between money, thermodynamic potential and size in ORC plant design. The results showed that ORC plants can scale to size or financial constraints. Additionally, financial analysis was used to calculate a pay-

back time for a 10MW ORC based on a discounted cash flow model. The payback time, based on a comparison with power generation via gas turbine for the platform yielded pay back times of between 4.53 and 3.09 years. Therefore, ORC power plants have real potential in terms of both financial cost and power output to fulfil some of power demand on existing North Sea platforms providing an opportunity for life extension.

In depth cases studies of three low-enthalpy deep geothermal energy settings in the UK were investigated in the final chapter of the thesis. These were: the Southampton geothermal scheme, co-produced hot brine from Wytch farm onshore oil well and co-produced hot brine from the North Sea wells. Each of these schemes were characterised in terms of energy available, local heat demand, geological and economic factors. The feasibility of developing these deep geothermal sources to supply ORC systems was discussed in terms of physical, economic and thermodynamic factors. Economic factors were considered in four areas: capital finance, subsidy, risk and institutional cultures. In the cases of coproduced brines, the capital cost of exploiting the geothermal resource is estimated to be 50 % less and the project risk is significantly reduced, compared to applications were drilling of the borehole had to be included in the project. This makes the co-produced brines case appear more economically favourable than the other cases studied. However, despite the apparently less favourable economics, the culture and willingness to see a geothermal project succeed by the stakeholders in the Southampton project, means that this is the only geothermal project in the UK to date.

Should exploitation of deep geothermal energy via ORC be pursued in the UK, chapter 6 illustrated that while there is the technical potential to do so, physical, economic and non-technical factors has historically driven the success or otherwise of projects.

This study has identified clear pieces of work for future studies. The experimental rig should be upgraded in the following ways:

- a flow meter should be installed in the refrigerant line of the GSHP. This will mean more accurate data can be collected as the flow rate of the refrigerant can be directly measured rather than inferred from the data as in this study.

- The equipment developed to measure water stratification should be used to allow heat pump operating conditions to be easily repeatable.
- A binary fluid supply should be found so data can be collected and compared to the theoretical models described.

This study has discussed the thermodynamic, physical and economic factors which contribute to the feasibility or otherwise of ORC systems. In order to translate this holistic strategy into a tool for ORC design, the existing thermodynamic model should be combined with models for heat exchange, applicable to zeotropic mixtures, to predict system size and for detailed financial assessment.